UNCLASSIFIED

AD NUMBER

AD872334

NEW LIMITATION CHANGE

TO

Approved for public release, distribution unlimited

FROM

Distribution authorized to U.S. Gov't. agencies and their contractors; Administrative/Operational Use; JUL 1970. Other requests shall be referred to U.S. Army, Frankford Arsenal, Philadelphia, PA 19137.

AUTHORITY

FA D/A ltr, 14 Nov 1974

THIS PAGE IS UNCLASSIFIED

AD No.
DDC FILE COPY

Project Themis

First Annual Technical Progress Report

"Environmental Sensitivity of Structural Metals : Liquid Metal Embrittlement"

Illinois Institute of Technology, Chicago, Illinois

Period Covered

June 25, 1969 - June 24, 1970

Submitted by:

Paul Gordon, Department of Metallurgical Engineering, Program Manager
Norman N. Breyer
James W. Dally
Darryl L. Albright
Lawrence J. Broutman
William R. Warke
Earl Zwicker
Russell D. Larsen

IIT

DDC
RECEIVED
AUG 6 1970
A

Contract Number:
DAAA-25-69-C0608

Submitted July 1970 to :

U. S. Army
Frankford Arsenal
Tacony and Bridge Streets
Philadelphia, Pennsylvania 19137

This publication or any portion thereof may not be reproduced without specific authorization from the Commanding Officer, Frankford Arsenal , ATTN: Chief, Metallurgy Research Laboratory, Philadelphia, Pa. 19137. However, DDC is authorized to reproduce the publication for U. S. Government purposes.

The information in this publication has not been cleared for release to the public.

DDC AVAILABILITY NOTICE

Qualified requestors may obtain copies of this publication directly from DDC.

Foreign announcement and dissemination of this publication by DDC is limited.

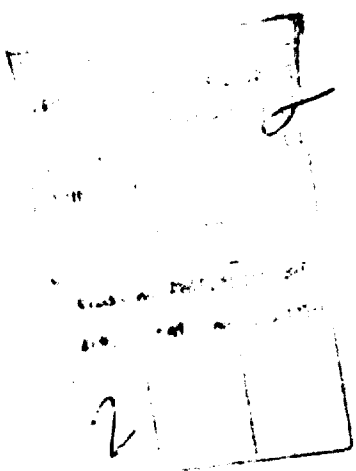

FIRST ANNUAL TECHNICAL PROGRESS REPORT

PROJECT THEMIS

"ENVIRONMENTAL SENSITIVITY OF STRUCTURAL METALS: LIQUID METAL EMBRITTLEMENT"

Period Covered

June 25, 1969 - June 24, 1970

Submitted by :

Paul Gordon, Department of Metallurgical Engineering, Program Manager

Norman N. Breyer

James W. Dally

Darryl L. Albright

Lawrence J. Broutman

William R. Warke

Earl Zwicker

Russell D. Larsen

Contract Number:

DAAA-25-69-C0608

...rials and each ...viduals may be

Submitted July 1970 to :

U. S. Army
Frankford Arsenal
Tacony and Bridge Streets
Philadelphia, Pennsylvania 19137

ABSTRACT

This is the first annual technical progress report on a research program on liquid metal embrittlement (LME). The phenomenon of LME is being investigated on levels from the atomic through bulk specimen and structural properties, and is being considered from both experimental and theoretical viewpoints. The research is aimed at elucidating the three important aspects of LME, namely, the mechanism by which embrittlement takes place at a crack, or potential crack, site, the mechanism by which the embrittling species is transported to this site, and the various metallurgical, physical, and mechanical factors which have a significant influence on the severity of the embrittlement.

Eleven specific investigations are underway, in various stages of progress, with the first two topics aimed primarily at an understanding of the transport mechanism in LME, the second five at the embrittlement mechanism, and the next three at mechanical and metallurgical factors influencing the embrittlement. The last topic is an effort at a new theoretical approach to LME.

1. Embrittlement by Solid Metals

Chief Investigator: W. R. Warke
Associate Investigator: P. Gordon
Graduate Student : J. C. Lynn

Purpose: To investigate "liquid" metal embrittlement below the melting point of the embrittler.

Progress: A high temperature dual-range extensometer has been received. The system for testing, including a Baldwin testing machine, a split furnace and temperature controller, temperature recorder, high temperature extensometer and stress-strain recorder, has been set up, calibrated and is now in operation.

The base line (unembrittled) elevated temperature tensile properties of the 4140 steel to be used throughout this study have been determined and are shown in Fig. 1 . A peak, due to dynamic strain aging, was observed in true fracture strength around 550°F. The reduction of area increases gradually from 55% at room temperature to 75% at 800°F.

Embrittlement by the solid metals, lead (99.9999%), cadmium (99.9999%) and tin (99.999%), respectively, has been studied using surface wetted tensile specimens. The soldering technique for wetting the embrittler to the specimen surfaces was the same as that employed by Warke.[1] The soldering temperatures were 675°F, 665°F and 500°F for lead, cadmium and tin, respectively. Tensile tests were run from room temperature to the respective melting points (618°F, 610°F and 450°F). Elevated temperature tensile properties for these three cases (Pb, Cd and Sn) are shown in Figs. 2, 3 and 4, respectively. Both the true fracture strength and reduction of area decrease drastically with increasing temperature.

The embrittlement is revealed more clearly by the decrease with increasing temperature of the normalized true fracture strength and the normalized reduction

of area, Figs. 5, 6 and 7, where the normalized true fracture strength (or reduction of area) is the ratio of true fracture strength (or reduction of area) for a specimen with an embrittler soldered on the surface, to that of a base specimen heat treated to the same strength level (i.e., Fig. 1) . When these normalized true fracture strengths and reductions of area are plotted against homologous temperature (test temperature divided by the respective melting point of the embrittler, temperatures are in degrees absolute), Fig. 8, it can be seen that these embrittlers (Pb , Cd and Sn) become effective when the test temperature reaches approximately three quarters of the respective melting points. Although there is some scatter in the data, it seems that cadmium embrittlement is more severe than lead embrittlement, and lead embrittlement is more severe than tin embrittlement, with respect to homologous temperature. This tendency is consistent with the vapor pressures of the embrittlers (cadmium has the highest vapor pressure and tin has the lowest vapor pressure). The fact that the ratios appear to approach a single value at the melting temperature (see Fig. 8), seems to indicate that the severity of the embrittlement proceeds at a decreasing rate as temperature increases to the respective melting points (H. T. = 1). In other words, there may not be much difference between these three embrittlement couples once the embrittler is molten.

The fractures of the base specimens, typical of those in high strength steel,[2] were initiated fibrously in the center of the specimen and propagated outward catastrophically. The appearance of the fracture surfaces of the surface wetted specimens indicated that the fracture was initiated from the surface where the embrittler was adhering to the specimen. The embrittled region, perpendicular to the loading axis, increased with increasing temperature and near the melting point looked shiny. The remainder of the fracture surface was usually dominated by shear fracture,

inclined at 45° to the loading axis. The given test temperature was that at the start of the tensile test. Some heating due to straining was observed and often raised the specimen temperature 20 to 25°F before fracture. Those specimens exhibiting shiny fracture origins were found to have been heated to the melting point of the embrittler in this way. Secondary stable micro-cracks near and parallel to the primary fracture were also observed in several severely embrittled specimens.

Future Plans: Elevated temperature tensile tests will be continued with other potential embrittlers wetted on the specimens. Other ways of putting the embrittlers on the specimens will be studied, as well. Stress rupture machines will be ordered in the near future. Quantitative studies of the embrittlement will be possible once the activation energy of the embrittlement has been obtained by delayed failure tests.

2. Combined Influence of Strain Rate and Temperature on LME

Chief Investigator: J. W. Dally
Associate Investigator: N. N. Breyer
Graduate Students: B. D. Agarwal and
K. L. Johnson

Purpose: To study strain rate-temperature effects aimed at delineating the transport mechanism in LME agent in producing brittle fracture of a normally ductile material. Several of the more important of these parameters include: the state of stress, alloy composition, metallurgical structure, strength level, composition of LME agent, temperature and strain rate. Of these parameters, the temperature and strain rate appear to jointly affect the fracture behavior in the presence of an LME agent. It is believed that these two parameters are directly related in the control of the transport phenomena where the LM is maintained in close proximity to the fracture front.

The combined influence of strain rate and temperature on fracture in the presence of an LM environment has been previously examined on a limited basis by other investigators. Rostoker[3] has reported the results of a series of tests conducted with tensile sheet specimens of aluminum alloy 2024 T 4 wetted with a mercury amalgam containing 3% zinc. The results of these tests shown in terms of per cent elongation as a function of test temperature with strain rate as a parameter are given in Fig. 9 . It is evident that the aluminum alloy is embrittled for all the strain rates considered; however, the temperature at which a significant level of ductility is regained increases with strain rate. Indeed, the transition temperature (brittle to ductile) has been expressed as

$$T = A \log \dot{\epsilon}^{o} - B \qquad (1)$$

where the constants A and B depend upon the elongation considered to represent the transition from brittle to ductile fracture.

Another study with aluminum alloy 2024 T 4 wetted with mercury was conducted by Barclay and Rhines[4] where tensile specimens were impacted at room temperature to obtain loading rates varying from about 50 to 1200 in/sec. Their results, shown in Fig. 10, indicate that embrittlement occurs over the entire range of loading rates; however, the difference in the reduction in area between LM and air environment decreases as the loading rates increase. The apparent decrease in embrittlement is attributed to the lack of time for crack initiation at high loading rates.

Several Russian investigators[5,6] have observed that embrittlement of Zn monocrystals coated with liquid Hg, Ga and Sn was markedly dependent upon strain rate $\dot{\epsilon}^{o}$ from 10 to 15 per cent/minute, all three liquids caused embrittlement (see Fig. 11), however, at lower strain rates of 10^{-1} to 10^{-3} per cent/min., the

ductility of wetted crystals was increased.

Later Kamdar and Westwood[7] disagreed with these observations and concluded that neither liquid Ga or Hg produced embrittlement in Zn single crystals (deforming principally by slip) over a variation in strain rate ranging from 1 to 100 per cent/min. These results are compared with the previous results in Fig. 11 . The discrepancies between the earlier observations and those of Kamdar and Westwood probably are due to damageinduced in handling the 1 mm diameter crystals used by the earlier workers. At high strain rates, these damage sites produce inhomogeneous deformation by introducing kink-bandsd formation in the crystal. Cracks nucleate from these kink-bands at relatively low strains. However, when the testing is performed at low strain rates sufficient time is available for relief of some of the damage and this results in the apparent plasticization affect referenced by the earlier investigators.

The effect of strain rate on the deformation behavior of both polycrystalline and single crystal materials in the presence of liquid metals does not appear to have been examined in any great detail. With single crystals, the effect of strain rate does not seem large. With polycrystalline materials, however, increasing strain rates appear to produce a reduction in susceptibility to embrittlement with higher brittle to ductile transition temperatures.

Introduction

It appears that a comprehensive study of the combined influence of temperature and strain rate on the transition from ductile to brittle failure is needed. The data obtained would give a measure of ductility (per cent reduction in area) and strength (ultimate and fracture strength) as functions of strain rate and temperature. Fracture surfaces and fracture times can be examined to gain some information

pertaining to the dynamic aspects of fracture and in particular the transport mechanism.

This report represents the results of the initial studies in this research task, where a series of experiments have been conducted with steel (AISI 4145) embrittled with 0.22 per cent lead internally distributed in the material. A second material examined was aluminum 2024 T4 which was embrittled by pure liquid mercury.

While the test program is not completed, sufficient data are available to prepare this preliminary report and to conclude that testing temperature and strain rate both significantly influence the mechanisms associated with liquid metal embrittlement.

Material Description

The steel used in this series of experiments was an AISI 4145 grade, cast by Inland Steel Co. in a split heat, with one half of the heat leaded and the other half free of lead. The chemical composition of each portion of the heat is presented in Table I.

Table I

Chemical Composition of AISI 4145 Steel

Alloying Elements	Internally Leaded	Non-Leaded
C	0.47	0.45
Mn	0.80	0.80
P	0.013	0.012
S	0.025	0.020
Si	0.22	0.22
Cr	0.96	0.95
Ni	—	—
Mo	0.17	0.16
Pb	0.22	—

A further examination of the lead composition was made by performing an electron probe analysis of the inclusions in the steel. This semi-quantitative analysis indicated that Zinc (0.3%), Antimony (0.2 to 0.3%), Tin (0.12%), Bismuth (0.6%) and Arsenic (0.1%) were present in the inclusions. The percentages given represent impurities in the lead. This steel was hot rolled from ingot form to 3 inch square billets and then subsequently hot rolled into 1 inch diameter rods. These rods were then rough machined into tension specimens 0.080 in. oversize and austenitized at 1525°F for one hour, oil quenched and tempered for one hour at 900°F. After heat treatment the tension specimens were finished machined. This heat treatment resulted in a nominal room temperature tensile strength of 215 ksi.

The aluminum used in this series of experiments was 2024-T4 produced by Reynolds Aluminum. This aluminum was obtained in the form of 5/8" diameter extruded rod. The chemical analysis of this aluminum alloy is presented in Table II. These rods

Table II

Chemical Composition of Aluminum 2024-T4

Copper	Silicon	Manganese	Magnesium
4.30	0.22	0.57	1.34

were machined into tension specimen and tested. The nominal room temperature tensile strength of this aluminum alloy was 76 ksi.

High purity Hg was obtained from the Bethlehem Apparatus Co. in 17.35 lb lots (Fed. Stock # 68:0-579-9426). This source material was processed from selected stock which was subsequently triple distilled in continuous stages under vacuum and controlled low temperature. After processing the Hg purity was in excess of 99.99% .

Experimental Procedure:

Test of uniaxial specimens of 2024 T-4 aluminum and internally leaded 4145 steel were conducted on a servo controlled hydraulically actuated test system. The testing system shown in Fig.12 consists of an electronic console, a loading frame and a hydraulic power supply. The hydraulic power supply provides up to 20 GPM of hydraulic oil at 3000 psi to the hydraulic actuator. The actuator (a 6 in.bore with an 8 in.stroke) provides a dynamic force up to 42,000 lbs with a maximum piston velocity of about 200 in/min. This maximum velocity is established by the 20 GPM capacity of the servo control valve which adjusts the flow of oil in the hydraulic actuator.

In operation, a linear positive ramp voltage is applied as a command signal to the servo-amplifier. This command produces a constant piston velocity when an LVDT transducer is used to provide the necessary feed back signal to the servo-amplifier. A typical example of the actuator displacement as a function of time is shown in Fig. 13 . By controlling the slope of the ramp command signal the piston velocity was varied from 0.016 to 160.0 in. min. Tests were conducted at piston velocities of 0.016, 0.160, 1.60, 16.0, 160 in/min. The ramp signals associated with the higher piston velocities were produced by a signal generator (HP type 3300A) and the lower piston velocities were produced by a curve following programmer (Research Incorporated Data Track).

The force on the specimen was measured by a load cell (10,000 lb capacity) and read out on a Y - t recorder for low piston velocities or a storage oscilliscope for high piston velocities. A typical example of a force-time record obtained from aluminum specimens is presented in Fig. 14 . These records were taken on each test and used to establish the force associated with the ultimate and fracture strengths and

the time required for initiation of yield and for complete fracture.

The strain rate reported for each test represents a value associated with the elastic response of the specimen. In this sense, the strain rate $\dot{\epsilon}_o$ may be computed from

$$\dot{\epsilon}_o = V/l_e \tag{2}$$

where V is the piston velocity

l_e is the effective gage length of the specimen

The effective length of the specimen was determined from the expression

$$l_e = \Delta l / \epsilon = Vt_y / \epsilon_y \tag{3}$$

where ϵ_y is the yield strain

t_y is the time required for yield.

Typical values of l_e associated with the steel and aluminum specimens were 6.5 and 5.0 inches respectively.

After yielding occurs, the strain rate computed by Eq (2) is much lower than the actual strain rate. This difference is due to the concentration of the deformation at the neck of the speciman which in effect reduces the effective gage length of the specimen by about an order of magnitude.

The post yield strain rate was examined by placing strain gages at the neck section of several aluminum specimens and recording the strain on these specimens in the post yield region. The gages were Micro-measurements Type EA-13-25088-120 and were placed circumferentially about the specimen to measure the transverse strain. A typical record showing the transverse strain as a function of time is presented in Fig. 15 . From this record it is evident that the strain rate after yielding is markedly

higher than the rate established during elastic loading. The strain rate during the elastic portion of this test (1.60 in/min piston velocity) was recorded as 0.1194 in/in/min while the strain rate observed in the post-yield region was determined to be 1.412 in/in/min Thus, the ratio of the plastic to elastic strain rates was 11.82 and this ratio was considered as constant for testing performed at higher and lower strain rates.

The temperature of the specimen was maintained with a single zone tube furnace and the temperature was measured at the neck section during each test with a #22 gage chromel-alumel thermocouple tied to the specimen. The output of the thermocouple was recorded on a strip chart recorder prior to and during the test. Due to the fact that the geometry of the tension specimen, as shown in Fig. 16, contained a minimum neck section the deformation area was highly localized and temperature gradients along the length of the tube furnace were not important.

Of more concern was the sharp increase in temperature recorded during the test. This increase was due to the heat generated as the specimen was plastically deformed. Temperature increases of 20 to 25°F which were encountered remained essentially constant, independent of the strain rate. It appears that the lack of variation of the temperature is due to the adiabatic generation of heat during the deformation process.

Results:

The results obtained by testing AISI 4145 leaded steel are shown in Figs. 17 to 20 where the fracture strength σ_f, the ultimate tensile strength σ_u, the proportional limit σ_{pl} and the per cent reduction in area are given as a function of test temperature for a specified strain rate. It is evident in all cases that the strength and ductility decreases monotonically with increasing temperature until a minimum

is reached corresponding to a temperature in the range from 600 to 850°F. For higher temperatures, the material regains its ductility and the fracture strength shows a marked increase.

Loss of ductility (defined as failures with RA less than 10 per cent) occurs over a temperature band which varies with strain rate as illustrated in Fig. 21. It is evident that the temperature band associated with embrittlement remains essentially the same (about 200-250°F) and that both the upper and lower temperatures associated with the embrittlement band increase with strain rate. The effective shift in the RA-temperature profile with strain rate is illustrated in Fig. 22 where it is evident that three decades of strain rate effectively translate the RA-temperature profile by about 150°F.

The effect of strain rate on the per cent RA is shown for testing temperatures of 75, 300, 450, 600, 700, 800 and 900°F in Fig. 23. It is clear that the strain rate has little influence at room temperature where the RA was constant at about 42 percent of at 700°F where the material exhibited very little plastic deformation. At all other temperature the effect of strain rate was pronounced.

The recovery temperature T_R (defined here as the temperature at which the material regains a RA of 40 percent) is presented as a function of log $\dot{\varepsilon}^o$ in Fig. 24. These results are similar to those reported previously by Rostoker et al where it was noted that the temperature-strain rate relation could be expressed as

$$T_R = A + B \log_{10} \dot{\varepsilon}^o$$

The constants A and B depend on the ductility. In this case where T_R was established at RA = 0.4 , the constants A and B were determined as:

$$A = 909°F$$

$$B = 43.6°F$$

The time necessary to complete each strain rate test is one measure of the dynamic aspects of the fracture process under LME conditions. The time to reach the load associated with the proportional limit t_{pl} and the time to reach the fracture load t_f are given in Table III. Also shown in this table is the time difference $\Delta t = t_{pl} - t_f$, the strain rate, test temperature and percent RA. Examination of these results shows that Δt is minimum whenever embrittlement occurs and RA is a minimum. Thetime difference decreases roughly in proportion to the strain rate being 5.5 seconds for $\dot{\varepsilon}^{o}$ = 0.0025 in/in/min to 50 millisec. for $\dot{\varepsilon}^{o}$ = 2.46 in/in/min. At the very high rates of loadings with time differences (which must be greater than fracture times) of 50 millisecs. average crack propagationrates exceeded 2 in/sec.

The results obtained with aluminum 2024 T4 correspond to both a liquid mercury and an air environment. In all cases, the results were compared to show the combined effect of temperature and strain rate under both environmental conditions.

Results showing the percent reduction in area as a function of temperature for both conditions are presented in Figs. 25 to 29. These results correspond to strain rates of 0.003, 0.03, 0.30, 3.00 and 30.0 in/in/min. In the presence of air, the RA increases monotonically with temperature increasing from about 30 percent at 75°% to 50 or 60 percent at 600°F with the larger value achieved at the higher strain rates. The results obtained for RA at strain rates of 0.003, 0.03 and 0.30 in/in/min with a liquid Hg environment show marked embrittlement for testing temperatures in the range from 75 to 400°F. However, at higher temperatures the aluminum recovers its ductility and exhibits a very sharp brittle to ductile transition. Indeed above the recovery temperature, the RA measured in the $(Hg)_L$ environment was consistently higher than that measured in air.

The influence of strain rate on RA is more clearly illustrated in Fig. 30 where

Table III

Time to Proportional Limit t_{pl} and Fracture t_f for 4145 Leaded Steel

$\dot{\varepsilon}_o$ = 0.0025 in/in/min

Temp (°F)	R. A. (%)	t_{pl} (sec)	t_f (sec)	Δt (sec)	Spec. No.
75	38.0	155.0	402.0	247.0	W - 1
310	25.5	160.0	350.0	190.0	W - 6
410	17.4	150.0	305.0	155.0	W - 7
500	14.1	144.0	277.5	133.0	W - 8
600	9.7	147.5	236.0	89.0	W - 9
700	5.5	142.5	147.5	5.5	W - 10
750	4.8	137.0	157.0	20.0	W - 3
800	62.6	125.0	472.5	347.0	W - 4
		$\dot{\varepsilon}_o$ = 0.025 in/in/min			
75	44.2	15.5	42.4	26.9	Z - 1
300	36.1	14.7	38.0	23.3	Z - 2
400	26.9	14.7	35.2	20.5	Z - 4
500	22.4	14.7	31.0	16.3	Z - 3
600	13.1	15.0	26.1	11.1	Z - 6
695	3.2	14.6	16.5	1.9	Z - 5
745	4.9	12.2	14.3	2.1	Z - 7
805	6.4	12.0	16.2	4.2	Z - 8
825	7.7	13.2	13.7	0.5	Z - 9
850	65.4	12.7	53.2	40.5	Z - 10
		$\dot{\varepsilon}_o$ = 0.23 in/in/min			
75	42.4	1.75	4.23	2.48	Y - 1
300	40.2	1.60	3.97	2.37	Y - 2
400	29.5	1.63	3.80	2.17	Y - 3
500	24.9	1.63	3.50	1.87	Y - 6
600	13.6	1.58	2.67	1.09	Y - 7
700	6.4	1.55	2.00	0.45	Y - 8
750	6.8	1.52	1.82	0.30	Y - 10
800	6.9	1.49	1.91	0.42	Y - 9
850	5.0	1.47	1.95	0.48	Y - 4
875	67.6	1.56	5.45	3.89	Y - 5
		$\dot{\varepsilon}_o$ = 2.46 in/in/min			
75	42.1	0.167	0.376	0.209	X - 1
300	40.2	0.150	0.370	0.220	X - 2
400	37.6	0.157	0.364	0.207	X - 3
550	22.3	0.155	0.305	0.150	X - 8
600	20.8	0.165	0.307	0.142	X - 9
700	3.3	0.145	0.205	0.060	X - 10
800	6.4	0.151	0.201	0.050	X - 11
875	6.5	0.145	0.196	0.051	X - 4
900	4.5	-----	-----	-----	X - 5
923	22.3	0.143	0.288	0.145	X - 6
940	71.4	0.135	0.474	0.338	X - 7

RA versus $\dot{\varepsilon}$ curves are shown for test temperatures of 75, 300, 450, 475 and 500°F. It is clear that the effect of increasing the strain rate is to markedly decrease the RA. This sharp loss of ductility with strain rate becomes more pronounced at the higher test temperatures.

Similar results for the fracture strength σ_f, as a function of temperature are given in Figs. 31 to 35. These results clearly indicate that the fracture strength is sharply reduced by the presence of liquid Hg over the temperature range from 75 to about 400°F. After the recovery of ductility, the difference in fracture strength between specimens tested in air and Hg is quite small.

While further tests must be conducted to complete this investigation, sufficient data has been taken to indicate that the recovery temperature T_R increasing with the log $\dot{\varepsilon}$ as indicated in Fig. 36. The general trend of the influence of strain rate on T_R in the 2024 T4 aluminum is similar to that noted for the 4145 leaded steel.

Future Work:

The current work with the aluminum will be extended to cover the temperature range from -75°F to room temperature. The loading frame will be modified with a cooling chamber replacing the furnace. Liquid nitrogen will be employed to establish temperatures down to -50° to -100°F so that the tests can be conducted with the aluminum at temperatures in the region where the Hg solidifies. These low temperature tests will include the five different strain rates from 0.003 to 30 in/in/min.

After the test program is completed the fracture surfaces of the aluminum specimens will be examined and an attempt made to classify the fracture zones. It is

anticipated that characteristics of the fracture surfaces can be related to temperature and strain rate in the presence of the embrittling agent or in air.

Finally an attempt will be made to interpret the results in terms of the existing fracture theories. It is anticipated that the strain rate dependence of the fracture stress will allow a choice between various transport mechanisms on the basis of their characteristic rates and activation energies.

Work will also be initiated on a related task where a series of experiments will be design to study crack propagation as affected by liquid metal environment. In the tests described to date (in relation to an embrittling environment) the liquid metal is in contact with the base material as the load is applied over relatively long loading intervals. This procedure is not adequate for measuring the time required for crack initiation since the effect of the time spent at stresses lower than the critical value can not be assessed. It is proposed to change this testing procedure and to apply a static load to a specimen and then dynamically apply the embrittling agent. With this approach the specimen (aluminum) in plate form would be loaded in uniaxial tension and the embrittling agent applied dynamically. The resulting crack patterns would be recorded by using a Fastax camera (both 8 mm and 16 mm models are available). The crack propagation rates are relatively low and consequently framing rates of the order of 1000 or 2000 frames/sec appear suitable for tracking the formation and development of the crack patterns and to establish initiation times.

The parameters which can be varied in tests of this type are almost unlimited. They include stress level, temperature, base material, embrittling agent, the quantity of the agent, the spatial distribution of the agent, the pressure of the agent, specimen size, and stress distribution.

3. The Effect of Structural Metal Purity on LME

Chief Investigator: W. R. Warke
Associate Investigators: P. Gordon, N. N. Breyer
Graduate Student: S. Dinda

Purpose: To study the effect of segregation of trace impurities to grain boundaries on the embrittlement in LME.

Introduction: Intergranular fracture is observed in both liquid metal embrittlement and temper embrittlement of steel. It has been well established[8-10] that the reason for the selection of an intergranular path for fracture in temper brittle steel is the segregation of trace impurities such as antimony, tin, arsenic, phosphorus etc. to the grain boundaries. In the present program, the effort will be made to evaluate the role of these trace impurities and their segregation to the grain boundaries in the liquid metal embrittlement of steel.

Recently, it was reported [11] that steel heat treated so as to be temper brittle was more susceptible to hydrogen embrittlement than the same steel without the embrittling treatment. The static fatigue life and the minimum stress for rupture were less for the temper brittle steel in the presence of hydrogen. In view of recognized similarities between hydrogen embrittlement and liquid metal embrittlement, these results are very encouraging and support the expectation that steel with segregated impurities in the grain boundaries will be more susceptible to embrittlement in presence of a liquid metal embrittlement.

Progress and Plans: Five ingots of 20 pounds each were received from the Research and Development Laboratory of General Electric Company, Schenectady. The base composition of the vacuum melted material is 0.40% C, 3.5% Ni and 1.7% Cr, and the special additions to the base steel are as follows:

1. Base composition, no addition
2. Base composition + 800 ppm Sb
3. Base composition + 500 ppm Sn
4. Base composition + 500 ppm As
5. Base composition + 500 ppm P

The ingots were soaked at 2075°F for one half hour and forged to 3/4 inch round bars. The bars will be drawn through die to an appropriate size for machining of tensile specimens. Materials from each ingot will be heat treated in accordance with procedures given in the literature and known to give unsegregated, unembrittled and segregated, embrittled states respectively. For the unsegregated condition, the material will be austenitized at 850 C (1562 F) for one hour, then quenched into oil, tempered at 625 C (1157 F) for one hour and water-quenched. For segregation of impurities to the grain boundaries, the water-quenched samples will be given an embrittling treatment which involves step cooling through the temperature range from 600 C to 350 C (1112 F to 662F).

Elevated temperature tensile tests will be carried out for the following four conditions:

a. Unsegregated, non-wetted
b. Unsegregated, wetted
c. Segregated, non-wetted
d. Segregated, wetted

Pure lead will be used as the embrittling liquid metal applied to the specimen surface. The results after elevated temperature tensile will be compared in each case and the role of these trace impurities in liquid metal embrittlement will be evaluated.

4. The Effect of Purity of the Embrittling Liquid Metal

Chief Investigator: N. N. Breyer
Associate Investigators: J. W. Dally, W. R. Warke
Graduate Student: K. L. Johnson

Purpose: This investigation is a study to characterize the effect of lead composition on the fracture behavior of externally wetted 4145 steel.

Introduction: One of the more intriging aspects of LME is its apparent specificity. It is often stated that certain liquid metals only embrittle certain solid metals. Furthermore, the additions of small amounts of impurity elements to a specific liquid metal embrittling agent can drastically affect the fracture behavior of the solid metal. The fundamental factors which determine whether or not a given liquid metal or liquid metal alloy will embrittle a particular solid metal, and the extent to which the embrittlement will be induced, are not understood.

This study was initiated in order to quantitatively determine the influence of changing the composition of a liquid metal embrittling agent (viz. Pb) on the fracture behavior of a high strength alloy steel. Binary alloys of lead with second element additions of tin, antimony and zinc are included in this study. An attempt will be made to understand the specificity of these additions to pure Pb in terms of their physical and atomistic characteristics.

Progress and Plans: Base line elevated temperature tensile (ETT) properties of 200 ksi nominal UTS non-lead 4145 steel, surface wetted with pure Pb, Pb-0.5% Zn, Pb-2% Sb, and Pb-9% Sn alloys (percentages are by weight) have been determined. Brittle-to-ductile recovery temperature differences as large as 300°F occur as the wetting metal composition is changed from pure Pb by the additions of the above element to the Pb. The ETT properties of specimen surface wetted with pure Pb and Pb-0.5% Zn are presented in Figs. 37 and 38 respectively. It can be noted that

the addition of 0.5% Zn to the pure Pb has shifted the brittle-to-ductile recovery temperature 100°F higher than that for pure Pb alone.

The systems Pb-Sb and Pb-Sn have been chosen for complete characterization for decreasing second element composition, down to trace element percentages. These systems were selected for two reasons: 1) both systems exhibit an initially high recovery temperature (250°-300°F above that of pure Pb), 2) a wealth of physical and thermodynamic data are available in the literature on these systems.

The system Pb-Sn has been completely characterized for second element (i.e., Sn) compositions of 9, 4, 1, 0.5, 0.1%. The ETT properties of 200 ksi nominal UTS non-leaded 4145 steel surface-wetted with the above alloys are shown in Figs. 39 thru 43. It can be seen that as the Sn composition of these Pb-Sn alloys increase from 0.1% to 9% the recovery temperature (that temperature at which the material regains a reduction in area of 40%) steadily increases. The effect of Sn in Pb on the LME of this material was found to follow the relationship

$$1/T_R = A \log_{10} (\%Sn) + B$$

Fig. 44 illustrate this relationship between the reciprocal of the absolute recovery temperature and the $\log_{10}$ (%Sn).

The effect of Sb on surface wetted Pb alloys is shown in Figs.45, 46 and 47 for 2, 1 and 0.1% Sb alloys of Pb respectively. Notice the marked deleterious effect which small Sb additions to Pb has on the LME characteristic of the 200 ksi nominal UTS alloy steel. For 2 and 1% Sb alloys, the brittle-to-ductile recovery temperature was greater than 975°F (above the original tempering temperature of the specimens). The Pb-0.1% Sb surface wetted alloy (Fig.47) produced a recovery temperature of 835°F. At the present time the Pb-Sb has not been completely characterized, however, new Pb-Sb alloys have been made and testing of these alloys is now underway. It is hoped that by completely characterizing the effect of these two binary systems, Pb-Sn and Pb-Sb, as the ETT behavior of a high strength steel, a better understanding of the specificity of second element additions to an embrittling agent can be gleaned.

5. The Specificity of Embrittling Systems

Chief Investigator: W. R. Warke
Graduate Student: F. A. Shunk

Purpose: To re-evaluate the present knowledge on this subject by a complete and critical review of the literature; ultimately, to develop further pertinent experimental evidence to fill in gaps, and to perform critical experiments to distinguish between available and proposed rationalizations.

Progress: The idea of specificity in liquid metal embrittlement (LME) appears to be derived from the conclusion of Rostoker et al.[12] that ".... liquid metal embrittlement is not general; the mating of specific couples is a necessary condition." This conclusion was based on the observations reproduced in Table I and on their literature survey. Attempts[12,13] to rationalize these observations have been, at best, only partially successful.

These rationalizations are phenomenological in character; to re-examine and re-evaluate them on a more fundamental basis suggests the need for an operational definition of non-embrittlement. In an obvious manner, one can proceed from a consideration of the embrittlement trough which is associated with LME; this trough is readily described. As the test temperature is increased, a gradual transition from ductile to brittle behavior --- as measured by the fracture stress and/or ductility at fracture relative to the same quantities when the specimen is fractured in air --- is observed (the onset of this transition is below the melting point of the test liquid in those cases[14-16] for which it has been reported). At some higher temperature, the fracture behavior is again identical with that in air; this reflects the high temperature side of the trough (brittle-to-ductile transition). Non-embrittlement is then defined as that condition where there is no change in the fracture behavior due to the presence

Table I

Behavior of Various Liquid Metals on Common Engineering Alloys[12]

Engineering Metal	Test Temperature (°F)												
	30	50	125	180	210	250	260	300	325	350	380	450	475
	Liquid Metal												
	Hg*	Ga	Na	In	Li	Se	Sn	Bi	Tl	Cd	Pb	Zn	Te
Al Alloys	E	E	E	E	N	N	E	N	N	N	N	E	
Mg Alloys	N	N	E	N	N	N	N	N	N	N	N	E	
Steel	N	N	N	E	E	N	N	N	N	E	N	E	E
Ti Alloys	E	N	N	N	N	N	N	N	N	E	N	N	N

* Hg - 3% Zn amalgam

E - embrittlement

N - nonembrittlement

of the test liquid as compared to the fracture behavior in air over a temperature range which includes the melting point (or liquidus) of the test liquid.

The first phase of the task of rationalizing specificity has been a literature search which has a two-fold objective. The first of these objectives is to up-date existing tabulations of couples which have been investigated while the second is to accumulate information on the test conditions under which embrittlement or non-embrittlement was obtained by the various investigators. This latter objective is of particular importance in classifying a particular couple as non-embrittling which is, of course, the basis of specificity.

For embrittlement to be observed, it is necessary that the test temperature be in the embrittlement trough. Data regarding how the ductile-to-brittle transition temperature (low-temperature side of the trough) is affected by test variables are meager. Much more is known about the brittle-to-ductile transition which occurs above the melting point (or liquidus) of the test liquid. The temperature of the upper transition is strongly influenced by (a) the grain size of the solid, (b) the strain rate of the test, and (c) the composition of the liquid and is influenced somewhat less by the composition and strength level of the solid. Thus, prior to defining a particular liquid/solid couple as non-embrittling, it is necessary to know (in terms of the above definition) that a brittle-to-ductile transition does not occur. Most recent investigators appear to recognize this requirement because very few "non-embrittling" couples have been reported since the appearance of the monograph by Rostoker et al.[12] All of the couples which have been claimed to be non-embrittling, as determined by the literature search, are summarized in Table 2 ; the limits to the claim of non-embrittlement are indicated in the footnotes to the table. Comparison with the definition of non-embrittlement shows (since most of these couples were reported as non-embrittling on the basis of testing at a single temperature above the melting point of the test liquid)

TABLE 2

Summary of "Non-Embrittling" Couples

P - element (nominally pure) C - commercial
A - alloy L - laboratory
E - also reported as embrittling

Solid \ Liquid		Hg P	Hg A	Ge P	Na P	In P	Li P	Se P	Sn P	Bi P	Tl P	Cd P	Pb P	Zn P	Te P
Bi	P			x[b]											
Cd	P	x[c]	x[c]												
Pb	P	x[c]													
Zn	P												E[c]		
Mg	CA		x[a]	x[a]	x[a]	x[a]	x[a]	x[a]	x[a]	x[a]	x[a]	x[a]	x[a]		
Al	P								x[c]						
	CA						x[a]	x[a]		x[a]	x[a]	x[a]	x[a]		
Cu	CP	E[c]		x[b]					x[c]				x[c]	x[c]	
Fe	P	x[a]	x[a]												
	LA	x[a]	x[a]												
	CA		x[a]	x[a]	x[a]			x[a]	E[a]	x[a]	x[a]		E[a]		
Ti	CA			x[a]	x[a]	x[a]	x[a]	x[a]	x[a]	x[a]	x[a]		x[a]	x[a]	x[a]

a) one test temperature

b) no published information

c) limited testing (known or inferred)

that most of these couples are not established as non-embrittling. A second group (unfortunately large) are reported as non-embrittling with no specific characterization of the testing conditions (although, in some cases, inferences may be drawn by referring to the tests with embrittled couples in the same work).

In addition to tests which are made outside of the temperature regime of the embrittlement trough, "non-embrittlement" may be observed if the test liquid does not wet the solid and/or if there is no sufficiently stable barrier to dislocation flow. The latter possibility is suggested by the observation of Nichols and Rostoker[17] that alloys are more likely to be embrittled than are pure metals. Furthermore, such a condition would be consistent with the above definition of non-embrittlement and simultaneously would give an operational definition of specificity. A definition of this type could be taken to imply that the liquid plays only a small role in LME (specifically with regard to the "bond-weakening" model) and even that specificity as a co-operative phenomenon between the embrittled and embrittler materials (as is usually [12,13] implied) is not a real aspect of LME. Of course, specificity resulting from a co-operative phenomenon may exist, but at the present time it must be considered as not established. The possibility that both "flow stress" and "co-operative" specificity occur also exists.

The literature search has yielded an up-dated listing of clearly established embrittlement couples; these couples are summarized in Table 3 . This table is organized on the basis of increasing melting points (of the base element in the case of alloys), the most significant aspect appears to be the seemingly random appearance of embrittling couples. This scatter would seem to exclude a simple relationship between embrittlement and some physical property.

In the rationalization of embrittling couples presented by Westwood et al ,[13]

TABLE 3

Summary of Embrittlement Couples

P - element (nominally pure) C - commercial

A - alloy L - laboratory

Solid \ Liquid		Hg		Cs	Ga		Na	In		Li	Sn		Bi		Tl	Cd	Pb		Zn	Te	Sb	Cu
		P	A	P	P	A	P	P	A	P	P	A	P	A	P	P	P	A	P	P	P	P
Sn	P	×			×																	
Bi	P	×																				
Cd	P		×	×	×	×					×											
Zn	P	×	×		×						×						×					
	LA		×																			
Mg	CA						×												×			
Al	P	×	×		×							×										
	CA		×		×		×	×			×								×			
Ge	P				×			×			×		×		×	×	×				×	
Ag	P	×	×		×	×				×												
	LA									×												
Cu	CP	×	×				×			×			×	×								
	LA	×																				
	CA	×	×					×	×	×	×(?)		×				×					
Ni	P									×							×					
	LA									×												
Fe	P																					×(?)
	LA	×	×							×												
	CA							×		×	×					×	×	×	×	×		
Pd	P									×												
	LA									×												
Ti	CA		×													×						

TABLE 4

Elemental Embrittlement Couples

A. Ordered by Pauling[18] Electronegativities

	Cs	Na	Li	Ga	Cd	In	Pb	Sn	Tl	Bi	Cu	Hg	Sb
Al				.1								.4	
Zn				.0			.2	.2				.3	
Cd	-1.0			-.1				.1					
Fe											.1(?)		
Ge				-.2	-.1	-.1	.0	.0	.0	.1			.1
Ni			-.8				.0						
Sn				-.2								.1	
Ag			-.9	-.3								.0	
Bi												.0	
Cu		-1.0	-.9							.0		.0	
Pd			-1.2										

B. Ordered by Gordy-Thomas[19] Electronegativities

	Cs	Na	Li	Cd	Sn	Hg	Ga	In	Cu	Tl	Bi	Pb	Sb
Al						.26	.28						
Cd	-.79				.07		.22						
Sn						.13	.15						
Zn					-.01	.12	.14					.27	
Ag			-.72			.10	.12						
Cu		-.87	-.86			-.04					.04		
Bi						-.08							
Fe									-.05				
Ge				-.32	-.25		-.10	-.08		-.04	-.04	.03	.08
Ni			-.97									.0	
Pd			-1.25										

it is suggested that embrittlement is associated with a small difference in electronegativity between the liquid and the solid. This criterion parallels the "non-existence of intermediate phases" criterion of Rostoker et al.[12] The couples in Table 3 which consist of (nominally) pure elements only are retabulated in Table 4 according to increasing electronegativity; the difference in electronegativities is recorded in the table. As suggested above, the scatter noted in Table 3 is still evident. The corresponding analysis of the intersolubility "rule" suggested by Rostoker et al. has not been completed but several exceptions are known and a similar random pairing is anticipated.

Future Work: The initial phase of the experimental work will be concerned with establishing a non-embrittling couple. The six elemental couples in Table 2 (Sn/Al, Hg/Cd, Hg/Fe, Ga/Bi, Ga/Cu, Pb/Cu) are the principal candidate couples.

The analysis of known embrittling couples in terms of both phenomenological and theoretical models will continue as will the literature search.

6. Direct Measurement of Surface Energies

Chief Investigator: E. Zwicker
Associate Investigator: P. Gordon
Graduate Students: R. Hudec, (A. Findeli)
Undergraduate Participation: 2 NSF supported physics undergraduates
2 unsupported physics undergraduates

Purpose: To measure surface energies by means of microbalance measurement of the force-distance curve when atomically clean surfaces are brought together.

Progress and Plans: To date, the experimental and theoretical aspects of surface energy have been subjected to a thorough literature survey, and the survey continues at a modified pace. A card file lists a total of 291 reference articles cross-indexed

by author and subject. Of course, 125 articles have been collected and cataloged, and are in a metal file cabinet housed in the Solid State Physics Laboratory, 114 Siegel Hall. Subject matter is listed under the following file headings:

Theoretical Calculations

Experimental Determinations

Surface Measurements

Surface Preparation

Environment Effects

Temperature Effects

Plastic Flow at Crack Tip

Initiation and Propagation of Crack: Dislocation Models

Ultra-High Vacuum Technology

Solid-Liquid Interfaces

Liquid Metal Embrittlement

Photomechanical Effect

Books - general

The research file has been organized in a manner to help solve four exceedingly difficult experimental sub-problems of the primary surface energy problem:

I. Production of ultra-high vacuum, of the order 10^{-10} to 10^{-11} torr in a chamber capable of containing the microbalance and sample handling and measuring equipment;

II. Measurement of the short-range attractive forces:

III. Control and measurement of the inter-surface separation;

IV. Production and measurement of the atomically-clean sample surfaces.

Progress has been most rapid in solving the first sub-problem. After receiving

bids and advice from Ultek, Varian and Veeco, an ultra-high vacuum system has been ordered from Ultek. The TNB-X-75 Ultek system offers the greatest flexibility of the three systems, and appears to be the most satisfactory for the experiment. It consists of two sorption pumps for roughing to 10^{-2} torr in about 3 minutes, a middle stage of titanium sublimation pumping using a copper cryo panel which can be cooled with liquid nitrogen, and final stage of differential ion pumping consisting of three, 25 liter/second units. Additional ion pump units may be purchased and installed, if required, to boost total ion pumping to 200 liter/second. The additional cost to do this would be $135 per unit, less than $700 total. Ultek also offered the best working volume, a stainless steel bell jar, 12 inches in diameter by 12 inches high. It has two eight-inch ports, three six-inch ports and four two-inch ports, and was originally designed for Auger spectroscopy and low-energy electron diffraction work. A special poppet valve enables isolation of the pumping section from the bell jar. In order to be capable of vacuums of the order 10^{-11} torr, a bakeable gold-sealedvalve (Granville-Phillips) will be used to isolate the roughing stage, rather than a standard, viton-seated valve. A combination ion pump control and sublimation power supply is standard with the system. The ion pump control includes a meter which will read system pressures from 10^{-4} down to 10^{-9} torr. In order to read pressures into the 10^{-11} torr range, a Bayard-Alpert type gauge will be ordered installed in the system. The gauge is compatible with a Veeco Ionization Gauge Control (Model RGLL-6) which reads into the 10^{-12} torr range, and which is available from the Metallurgical Engineering Department. The Control and original gauge were found to be in working order at an earlier date, though the gauge cannot be used efficiently with system ordered.

Another feature of the Ultek system is the shielding of the bell jar volume

against gas discharge which occurs during operation in the middle stages of pumping. Such discharge destroyed the coil of a Cahn microbalance used in a sytem by RCA, according to Mr. James T. O'Brien of RCA's Special Products Engineering, Sommerville, New Jersey, (private communication). Another factor considered is the stray magnetic field from the ion pump magnets in the volume of the bell jar space. Ultek claimed the lowest field of the three manufacturers, less than 10^{-3} gauss, which compares with Earth's field, and so will not affect operation of the Cahn microbalance.

The UHV system is to be delivered in late July, and will arrive completely assembled and factory pre-tested to achieve pressure in the range 10^{-11} torr. Since it weighs about 500 pounds, a heavy-duty, portable winch is being outfitted with stainless steel cable and hooks, so the system may be moved into proper mounting position. The winch will also serve to lift the stainless stell bell jar from the system to facilitate mounting experimental equipment within the system, and to service the system on occasion. The system will be mounted on an aluminum base plate measuring 36 x 48 x 3/4 inches, which is on order. Ultimately, the base plate will be suspended on a vibration isolation device. It is expected that both Haber Instrument, Inc. and Lansing Research Corporation will be consulted more closely before September, regarding particular problems of vibration isolation. Lansing manufactures isolation tables which are in effect mounted on cushions of air.

After the UHV system has been mounted on the base plate, it will be tested without opening it to atmosphere, in order to see that it meets specifications. This is expected to occur by the middle of August. Once the system performs satisfactorily, the bell jar will be opened to an atmosphere of dry nitrogen, and a chemically cleaned specimen of KCl will be introduced in order to test its outgassing properties. Such tests will be repeated with metallic specimens as well, and practical information will be obtain about the need for bakeout of different types of specimens.

A means of baking out the entire system at temperatures in their range of 90°C to 400°C is currently being designed, and should be ready to fit to the system during August and September.

Sub-problem II, the measurement of the short-range attractive forces, is solved in principle by the model RH-UHV automatic recording electrobalance made by Cahn Instrument Company. The balance is designed for use in vacuums into the 10^{-10} torr range, and capable of continuous recording of changes in force over at least two orders of magnitude. Measurement of small forces is limited by the sensitivity of the balance to 2 micrograms change of force, while large forces are measured to four significant figures up to a force of 20 grams weight. However, the balance may not satisfy the requirements of the experiment completely, a characteristic of the balance which must be established is how steadily the beam of the balance maintains a constant position, which in turn determines how well a given inter-surface separation can be maintained between the surface-energy specimens. Such knowledge is directly related to solving sub-problem III, the control and measurement of inter-surface separation. It is known that the model G-2 balance is sensitive to change of beam position of 1000 Å, but for the present work a sensitivity down to the order of 10 Å, would be desirable. In a recently discovered article titled "Adaptation of the Cahn Electrobalance Control System to the Automatic Operation of A Quartz Beam Vacuum Microbalance, (Vacuum Microbalance Techniques, vol. 6, Plenum, New York, p.45), W. E. Boggs reported modifying the optics of the balance to be external to the vacuum system. With the knowledge that this is practical, it should be possible to design an external, optical interference system to read and control the balance beam position. It is not clear what the limiting design factors are, and communication with the Cahn Instrument Company is proceeding in order to determine what data exists

for the model RH-UHV so far as beam position steadiness is concerned. This information should be available before the end of June, if it is known, but it may well be that the data will have to be established in this laboratory, along with modification of the optical and control system of the balance. The balance will very probably be ordered before the end of June, and should be available for testing and preparation of preliminary experiments before the end of August. The experiments will measure attractive forces between surfaces in air using techniques similar to those of Derjaguin, (see status report 2, reference 6) and should be carried out during the fall term of 1970. Design of the system to measure the separation of the surfaces (SSS) being tested will begin during July, with the view of coupling the SSS into the electro-optical system of the balance in order to control balance beam position as well as measure it. Construction of the SSS will begin during the fall term.

After the microbalance and UHV systems have been tested and are operable, preliminary experiments will be run to observe how the systems operate in combination. Such experiments will probably precede the construction and successful operation of the SSS, and will simply measure the adhesive force between various types of specimens brought into contact with each other under UHV. Specimens will be both alkali halide and metallic couples, and it is expected that various cleaning techniques will be tried in order to observe the effects on adhesive force. Such experiments will be of some direct empirical interest to LME, since the adhesive force may be measured both in the presence and absence of the liquid metal, or other forms of metallic embrittlement agents, such as the leaded steels.

Two auxiliary problems related to the surface energy measurement are progressing satisfactorily. Crystals of NaCl are now growing from solution, and are believed to be highly pure and perfect in structure. The first crystallites have formed, and by

late July or August they should have grown sufficiently large for our experimental purposes. They will be subjected to tests such as ionic conductivity measurements and thermoluminescence in order to check on purity. Etch techniques will be used to check dislocation density. The crystals will ultimately be used in surface energy measurements to help calibrate the apparatus.

The second problem is to test for the existence of a photomechanical effect in fracture energy measurements of KCl. The photomechanical effect consists of the reversible increase in yield strength when the crystals are illuminated with green light at temperatures below the boiling point of liquid nitrogen. It is expected that measured fracture surface energy will follow the reversible changes in yield strength. The fracture energy apparatus is that used in previous work. To achieve the low and carefully-controlled temperatures, a cryostat has now been constructed and tested. A mercury manostat is used to control the vapor pressure of the liquid nitrogen by regulating the pressure produced in the system by a vacuum pump. The precise control of pressure guarantees control of temperature to within $0.1^{\circ}C$. This is important, since the results of Nadeau (J. Appl. Phys., 35, 669 March 1964) shows a sharp dependence of yield strength on temperature in temperature ranges to be studied. A thermocouple will be mounted in the cryostat to check on the constancy of temperature in the region of the specimen. Special strain gauges are being mounted on the aluminum strain-gauge ring, and are being bonded with a special glue claimed to be good in the low temperature ranges to be used. It is expected that preliminary experiments will begin by the end of July and significant results should be obtained during August. The work should be completed during the fall term.

7. Crystallographic Aspects of Liquid Metal Embrittlement

Chief Investigator: D. L. Albright
Graduate Students: K. H. Buchner
J. A. Wetter (starting June, 1970)

Purpose: The measurement of fracture energies at grain boundaries in bicrystal grown with a range of controlled orientation relationships. The aim is to study the effect of crystallographic factors upon the fracture energies.

Progress and Plans: Resistance heating was used to grow single crystals of aluminum (99.993% purity) by thermal gradient controlled solidification. Portions of these crystals were then removed and oriented for use as seeds in the growth of bicrystals approximately 8 in. long. Initially, some bicrystals were also grown by self-nucleation. In either case it was determined that the bicrystal boundary can be kept relatively straight and in the middle of the specimen by placing a wire (1 mm dia., high melting point alloy) along the centerline of the bottom of the graphite crucible. Typical bicrystals grown in each manner are shown in Figure 48.

Back-reflection Laue photographs are being taken in order to establish the orientation relationships which exist across the two halves of each bicrystal. Table I summarizes the orientation results to date. Even though all samples are now being produced by seeding, the self-nucleated samples have been included to help make several points. First, Table I shows that bicrystals have been grown with both common and uncommon growth directions in the two halves. Second, for either of these above situations, it can be seen that it is possible to produce samples with varying degrees of lattice rotation between the halves. Third, the ability to keep the boundary straight and centered seems to manifest itself in the occurrence of a wide variety of interface "match-ups". All three of these points represent substantial progress toward the goals outlined in the original THEMIS proposal.

TABLE I

Summary of Bicrystal Orientations

Sample	Left Crystal*			Right Crystal*			Remarks
	Growth Direction	Vertical Direction (⊥ G.D.)	Interface Plane †	Growth Direction	Vertical Direction (⊥ G.D.)	Interface Plane †	
I	~⟨311⟩	⟨210⟩	{311}	~⟨311⟩	⟨210⟩	{311}	Seed crystals fully melted; twinned relation
B	⟨110⟩	⟨110⟩	{100}	⟨110⟩	⟨211⟩	{321}	Seed crystals fully melted
C	⟨110⟩	⟨100⟩	{221}	⟨110⟩	⟨221⟩	{100}	Successfully seeded
D	⟨100⟩	⟨100⟩	{511}	⟨110⟩	⟨211⟩	{210}	Successfully seeded
II	⟨100⟩	⟨110⟩	{110}	⟨211⟩	⟨111⟩	{110}	Self-nucleated
III	⟨110⟩	⟨110⟩	{310}	⟨100⟩	⟨110⟩	{320}	Self-nucleated
IV	⟨110⟩	⟨211⟩	{110}	~⟨310⟩	⟨311⟩	{110}	Self-nucleated
A	⟨110⟩	⟨100⟩	{331}	~⟨211⟩	⟨210⟩	{511}	Successfully seeded

* Based upon viewing bicrystal in the growth direction.
† Approximate value reported in order to avoid sectioning sample until after mechanical testing.

Current effort is being directed toward producing a complete set of long bicrystals with precisely controlled orientation relationships. Simultaneously, double cantilever samples for mechanical testing are being machined from the controlled bicrystals already on hand. This testing will be done in a liquid mercury environment. The test permits a measurement of fracture energy, which will in turn be correlated with the crystallographic parameters.

Delivery of the double-crystal diffractometer has been delayed from April to July, 1970. When this equipment arrives, determination of the crystallographic substructure at the bicrystal boundaries will commence.

8. Effect of Cold Work on Lead Embrittlement of Alloy Steels

Chief Investigator: N. N. Breyer
Associate Investigator: J. W. Dally
Graduate Student: K. L. Johnson

Purpose: To separate out the individual effects of cold working and of strength level on the embrittlement behavior of 4145 leaded steel.

Introduction: Investigators studying the effects of cold working on the LME of solid metals have reported results which are seemingly contradictory. Although these authors have recognized the difficulty in analyzing and interpreting their results no attempts have been made to clearly separate the effects of deformation mode (e.g. rolling, tensile prestrain, die drawing, etc.) as well as the attendent changes in the base material strength level with increasing amounts of cold deformation.

A review of the field of LME by Rostoker, et. al.[20] includes the effect of cold work (room temperature) on the embrittlement of 3003 Al alloy in the presence of Hg + 3% Zn amalgams. The authors conclude that increasing amounts of cold work decrease that alloys susceptibility to LME. The deformation mode in this study,

although not reported, was in all probability cold rolling since the authors report percent elongation at fracture, typical of a thin, sheet type specimen. The degree or susceptibility to embrittlement in these studies is usually defined as the difference in elongation between the dry and wetted specimens for the same degree of cold work.

Subsequent work by Rostoker and Nichols[21,22] on age hardened Al alloys deformed by pre-stretching shows that cold work first produces an increase in susceptibility followed by a progressive recovery with additional cold deformation. The effect of tensile prestrain on the tensile properties of α-brass in the presence of Hg has been detailed by[23]; it was shown that the susceptibility to embrittlement increases with increasing amounts of cold pre-strain. Reference[24] reports the effect of cold rolling 70:30 α brass tested in the presence of Hg - 2% Na amalgams. These authors show that beyond 25% cold reductions the susceptibility to embrittlement progressively diminishes until virtually no embrittlement is observed for materials processed to 95% cold reductions.

It is obvious that the previous studies have not produced consistent results. Furthermore, in most of the prior investigations, the LME characteristics were studied at only one temperature. The present study was initiated to further examine the role that cold working plays in the LME phenomena. The material selected for this investigation was an AISI 4145 alloy steel, available as "split-heat" stock. The material's susceptibility to embrittlement by lead had been extensively characterized.[9] Half of this material was internally leaded and the other half was lead-free. Table I presents the chemical composition of the two portions of this "split-heat".

Table I

CHEMICAL COMPOSITION OF 4145 "SPLIT-HEAT" MATERIAL

Material	C	Mn	P	S	Si	Cr	Mo	Pb
4145-0	0.45	0.80	0.012	0.020	0.22	0.95	0.16	
4145-22	0.47	0.80	0.013	0.025	0.22	0.96	0.17	0.22

This material was selected to demonstrate the sensitivity to lead embrittlement as function of strength level[25,26,27] and the extensive data available for this material permits precise base line comparisons[25,26,28] . Also, this material can be readily processed by various combinations of thermo-mechanical treatments to a singular strength level (200 ksi nominal in this study) thus obviating the complicating effects of changing strength levels with changes in amounts of deformation.

An additional purpose of this study will be to relate the effects of different deformation modes to the embrittlement characteristics and fracture mechanisms of solid metals in the presence of an embrittling agent. In order to gain a better understanding of the role which cold working plays in the LME phenomena a correlation between the cold-working effects and the fractographic features of these specimens will also be attempted.

Experimental Results: In an effort to clarify the exact nature of the thermo-mechanical treatments employed in this study, Table II lists the combination of heat treatments and deformation required to obtain the 200 ksi nominal room temperature tensile properties for this 4145 alloy steel material. The elevated temperature tensile (ETT) properties of the leaded-steel resulting from thermal processing alone prior to subsequent deformation by cold-drawing are given in Figs. 49-51. An examination of these figures reveals that the degree of embrittlement (as measured by % R.A. and true stress at fracture) decreases as the strength level of the steel is lowered.

Table II

ROOM TEMPERATURE TENSILE PROPERTIES OF INTERNALLY-LEADED 4145 STEEL AS ACHIEVED BY HEAT TREATMENT AND THE HEAT TREATMENT DEFORMATION PROCESSING

Thermal Processing	Room Temperature Tensile Properties Achieved by Thermal Processing Only		Deformation by Die Drawing at Room Temperature	Room Temperature Tensile Properties Achieved by Thermal Processing and Die Drawing	
1525°F Aus. Oil Quench plus 900°F Temp.	Y.S.	186.3 ksi	0%	Y.S.	186.3 ksi
	T.S.	194.8 ksi		T.S.	194.8 ksi
	T.F.S	283.5 ksi		T.F.S.	283.5 ksi
	% R.A.	50.0 %		% R.A.	50.0%
1525°F Aus. Oil Quench plus 970°F Temp.	Y.S.	173.9 ksi	10%	Y.S.	201.3 ksi
	T.S.	184.9 ksi		T.S.	209.1 ksi
	T.F.S.	274.7 ksi		T.F.S.	283.2 ksi
	% R.A.	50.7 %		% R.A.	45.3 %
1525°F Aus. Oil Quench plus 1010°F Temp.	Y.S.	168.5 ksi	20%	Y.S.	198.5 ksi
	T.S.	179.9 ksi		T.S.	206.3 ksi
	T.F.S.	270.2 ksi		T.F.S.	281.4 ksi
	% R.A.	50.8%		% R.A.	48.2%
1525°F Aus. Oil Quench plus 1060°F Temp.	Y.S.	156.0 ksi	30%	Y.S.	174.7 ksi
	T.S.	163.6 ksi		T.S.	195.6 ksi
	T.F.S.	251.5 ksi		T.F.S.	274.6 ksi
	% R.A.	55.5%		% R.A.	47.5%

Y.S. Yield Strength 0.19 offset
T.S. Tensile Strength
T.F.S. True Fracture Stress (uncorrected)
% R.A. Percent Reduction in Area @ Fracture

A slight decrease in brittle-ductile (i.e., high temperature recovery) transition temperature is also noted.

The trend was shown to exist for another leaded 4145 heat by Mostovoy and Breyer.[25,26,27] The base line data as a function of heat treated strength (Figs. 49-51) are presented for later comparison for the changes attending cold deformation.

The effect of cold-drawing on the (ETT) properties of this leaded-steel thermally processed followed by 0, 10, 20 and 30% reductions are shown in Figs. 52, 53, 54 and 55 respectively. The specimens used in the determination of these curves were all processed to the same nominal room temperature tensile strength of 200 ksi.

Examination of these figures reveals that at a nominal 200 ksi strength level, a progressive reduction in susceptibility to embrittlement results as the amount of cold-deformation increases. Furthermore, as the percent reduction by die-drawing is increased(lower initial heat-treated strength)the brittle-ductile transition temperature is also progressively lowered.

In order to compare the effects of cold-working on the ductility properties of the leaded steel, the ductility properties both before and after cold drawing are presented inFigs. 56, 57, and 58. The % R.A. at fracture of the 200 ksi specimens processed by the thermo-mechanical treatments and the % R.A. values of the material heat treated to the strength level required prior to cold-drawing (i.e., a lower strength level) are shown.

From Fig. 56 it can be seen that the 10% reduction by die drawing only slightly increased the steel's susceptibility to embrittlement. This increase occurs from room temperature to 550°F, at which point the two curves coincide. Note, however, that a 10% reduction by cold drawing has lowered the brittle-ductile transition temperature below that of the heat treated value prior to the deformation.

Twenty percent cold deformation of the heat treated leaded steel (Fig. 57) again shows a very slight increase in embrittlement susceptibility from room temperature to about 350°F . However, between 350°and 650°F the ductility properties for the cold drawing specimens are higher (i.e., a decrease in LM susceptibility) than for the heat treated specimens prior to deformation. The 20% cold-drawn material also exhibits a lower brittle-ductile transition temperature than the same material prior to deformation.

Fig. 58 illustrates the marked improvement in ductility properties associated with 30% cold deformation by die drawing. Although there is a moderate increase in susceptibility to embrittlement from room temperature to 450°F a substantial increase in ductility is shown in the critical embrittlement trough region. As in the previous cases, the cold drawing has lowered the brittle-ductile transition temperature below that of the leaded steel, heat treated to the prior - to - deformation strength level.

From these results it is quite apparent that in spite of the fact that cold drawing promotes the steel to a higher strength level, a decrease in embrittlement susceptibility occurs in the embrittlement trough temperature range. It was shown earlier (Figs. 49-51) that as the heat treated strength level is lowered the severity of embrittlement is also lowered(as is the brittle-to-ductile transition temperature). Figs. 56-58 illustrate that deformation by cold-drawing lowers the brittle-to-ductile transition temperatures still further, even though the cold drawing process raises the strength level.

The susceptibility to embrittlement as related to the amount of cold work by die drawing can be more properly compared summarizing the ductility properties of the specimens processed by 0, 10, 20 and 30% reductions in which case all specimens have achieved the same ultimate strength level. Fig. 59 contrasts the ductility properties of the specimens thermo-mechanically processed to 200 ksi with the

ductility values for specimens heat treated directly to the 200 ksi level (i.e., no deformation). It is apparent that if one desires to obtain a given strength level in this material, those processes which involve incremental strengthening by cold-drawing result in improved ductility properties in the embrittlement trough region. The susceptibility to embrittlement is decreased with increasing amounts of cold deformation by die drawing. Above 10% cold reductions there is substantial decrease in embrittlement susceptibility. It should be noted that increasing cold deformations also produce larger reductions in the brittle-ductile recovery temperature as compared to the material heat treated directly to the 200 ksi level. Temperature shifts of 45, 50 and 70°F are observed for the 10, 20 and 30% cold drawn material, respectively.

A comparison of the elongation properties of the thermo-mechanically processed leaded steel and the leaded steel heat treated directly to the 200 ksi level is given in Fig. 60. Notice the unusual behavior of the elongation at fracture of the cold drawn material in the temperature range of 400 to 600°F. The effect of increasing cold reductions on shifting the brittle-ductile recovery to lower temperatures is also clearly apparent.

In order to establish base line data of the effect of cold working alone on the ductility properties of this steel, specimens from the non-leaded portion of this "split-heat" were thermo-mechanically processed to 200 ksi(by 20% reduction). The (ETT) properties of this material are shown in Fig. 61. For comparison, the (ETT) properties of the non-leaded portion of the "split-heat", heat treated directly to 200 ksi is also presented (Fig. 62). It can be seen that the 20% reduction has only slightly affected the nature of the yield and ultimate tensile strength curves. In general, however, a decrease in both % R. A. and true stress of fracture is observed

for the cold drawn material. A comparison of the ductility properties at the 200 ksi level of these two materials is given in Fig. 63. The general lowering of ductility due to cold deformation is apparent in this figure. It is felt that the initial increase in susceptibility to embrittlement of the cold worked specimens from the leaded portion of the heat compared to the internally leaded specimens directly heat treated to 200 ksi is merely a reflection of this partial exhaustion of ductility.

Since the mode of deformation was thought to play a significant role in the effect of cold work on the LME phenomena, a series of internally leaded 4145 steel bars were heat treated to a nominal tensile strength of 200 ksi and pre-stretched to their ultimate tensile strength. Specimens were then machined from these bars and Fig. 64 reports the ETT properties of these specimens. Fig. 65 compares the ductility properties of the pre-stretched specimens to those of the 200 ksi direct, heat treated samples. One can see from these two figures that pre-stretching produces a significant increase in susceptibility to embrittlement from room temperature to 725°F, i.e., over the entire embrittlement range. It is further seen that this form of cold working causes no change in the brittle-ductile transition temperature.

In view of the significance of the role of deformation mode, additional studies of the effect of pre-stretching as well as pre-compressing have been initiated. These tests are now underway.

At the present time a systematic study of these cold-worked fracture surface appearance is also being conducted. It is thought that such a study will be beneficial to the understanding and interpretation of the above results.

9. Fracture Toughness of Engineering Metals in Liquid Metal Embrittlement

Chief Investigator: J. W. Dally

Purpose: To measure the change in fracture toughness parameters, such as K_{IC}, induced by various embrittling liquids on AISI - 4145 steel.

Progress and Plans: The program has not been started as yet since a graduate student is not available to work in this area; work will be initiated as soon as a graduate student becomes available.

It is proposed that two series of experiments be conducted with 4145 steel as the structural metal. In the first series, the fracture toughness expressed as K_{ILME} would be measured as a function of temperature under both wetted and non-wetted conditions. The embrittling agents would be applied externally at the pre-existing crack tip. Since initiation of the fracture has occurred it may be possible to obtain data pertaining to crack propagation rates which will give some insight on the transportation mechanism in LME.

The second series of tests would be on 4145 steel containing embrittling agents alloyed with the steel. With these internal and locally available embrittling sources, fracture toughness and crack propagation rates may be significantly different than those measured with external application of the embrittling agent.

10. Effect of Combined Stresses on LME

Chief investigator: L. J. Broutman
Associate Investigator: J. W. Dally
Graduate Students: G. K. Mahajan (Summer 1969, only)
T. F. Fugiel (Summer 1970)

Purpose: To obtain quantitative information on the effects of combined stresses in altering LME severity.

Progress and Plans: The research is in the apparatus-developing stage. A torsion frame, designed for 2000 in.-lb., producing maximum shear stresses of 80,000 psi on a 1/2" diameter specimen, has been built to be attached to an Instron testing machine already at hand. Control equipment has also been provided. A special adapter for self aligning specimens, has also been constructed, using molten Woods metal to float the upper specimen grip for aligning followed by solidification of the Wood's metal for testing.

Two additional torsion frames utilizing the same principles have been constructed specifically for static fatigue experiments. These frames have been calibrated and the torque is applied by adding weights to a loading pan. Initial experiments have been conducted using 2024 T4 aluminum specimens wetted with mercury. The mercury was placed on the specimen surface using a heat shrinkable plastic tubing. The lower portion of the tubing was shrunk onto the specimen and the mercury was then placed in the unshrunk portion which formed a cup. A typical torsion brittle fracture was obtained and also initial experiments in static fatigue proved successful producing failure times of up to two hours at loads slightly reduced from the failure load obtained at constant loading rate.

During the forthcoming year, the testing program will be concerned with investigating a commercially available aluminum alloy, 2024T4, and liquid mercury as the embrittlement agent. Torsion tests on round bars will be performed which give a ratio of 1:1 tension to compression stress at 45° to the bar axis. Also, the use of circular flat plates, simply supported around the circumference, and loaded at the center, will be investigated as this produces equal biaxial stresses at the center of the plate. It is possible that the application of a compressive stress in one direction may act to retard the embrittlement process and thus raise the embrittlement strength in the

orthogonal direction. This would be not only of practical significance but would aid in the understanding of the crack initiation process.

Two types of measurements will be made for all the above experimental methods. The embrittlement strength will be measured by suitably wetting surface before it is loaded. Thus, the embrittlement strength can be determined for the various stress states and a failure envelope can be created. Delayed failure or static fatigue embrittlement can be measured for several stress ratios by applying stresses less than those required for short time fracture.

It is expected that in the second contract year the static fatigue curve for mercury-wetted aluminum in torsion will be completed and compared to the static fatigue curve obtained in tension or bending. In addition, at least two other combined stress states obtained by either pressurization of a closed end tube or central loading of a flat circular plate will be investigated. Cyclic fatigue in torsion can also be compared to cyclic fatigue in tension with the aluminum-mercury system. This will also allow us to determine whether there is a difference between static and cyclic loading of a material subjected to embrittlement.

II. Statistical Mechanics of Fracture and LME

Chief Investigator: R. D. Larsen
Postdoctoral Investigator: C. G. Miller
Research Associate: I. Bumstein

Purpose: To develop the statistical mechanics associated with the concept that fracture, embrittlement, and related materials phenomena can be treated as many-body, cooperative phenomena, i.e., geome - catastrophies arising from unstable lattice configurations.

Progress: Our group has made substantial progress this past year in attempting to model

features operable in fracture and embrittlement from the viewpoint of statistical mechanics. We outlined in our second status report some qualitative features of a first-order geometric fracture/embrittlement model. The details of this model are the subject matter of a forthcoming technical report. We have also completed another technical report in which we have carried out some exact calculations relevant to our geometric model. These exact calculations of the molecular pair distribution functions for the two-dimensional cell model and for the correlated-cell model are, unfortunately, of such a degree of difficulty that they cannot be extended beyond the order to which they have been taken. The analytical techniques that were used therein are virtually the same, however, that we (C. G. Miller) have applied to another calculation of considerable importance to our program.

We have been especially interested in the characterization and quantification of the meaning of crystalline (lattice) stability inasmuch as we have suggested that unstable lattice configurations imply fracture. It is possible to ascertain a relative thermodynamic stability from a knowledge of the relative free energies of various lattice arrays. Dr. Miller of our group has virtually completed a very tedious and lengthly analytical calculation of the configurational partition functions of a family of 2-dimensional lattices which are generated by translation of the hexagonal lattice. As the hexagonal lattice gives rise to the densest packing of 2-spheres the family generated corresponds to a continuous sequence of ordered lattice configurations and packings that are successively less dense. The cell-cluster formalism which we have employed in this work is exact in the (high density) limit of close packing but was not intended to be applied to other than the limiting configurations. Nevertheless, we have been able to clearly define the exact configurational regions of Euclidian space to which a system of 2-spheres is accessible. The content of the exact regions cannot be readily calculated but we may construct and define limiting polytopes which

are lower bounds to the exact regions. While the calculations are able to be done exactly for a given subfigure (polytope) construction the content of these polytopes is but an approximation to the exact configurational free volume. The replacement of hypercylindrical surfaces by their tangent hyperplanes is exact only in the $V \to V_0$ limit. Moreover, the calculations are able to be done only for small N so it is not clear what the convergence properties of the individual Q_ℓ contributions are. Nevertheless, on the basis of those lower bounds, subject to the approximations involved, we will be able to calculate the relative free energies of the family of lattice close packings mentioned above. This entire calculation and its relationship to plastic deformation and crystalline stability will be the subject matter of another technical report.

A further aspect of the work being carried out in group is that being done by Dr. Burnstein. She is in the process of translating an extensive computer program which will enable us to implement the integration of a certain class of rigid disk configuration space integrals on a digital computer. The unique character of this work is that the integrations are able to be done exactly and analytically. It is simply not possible to do "pencil-and-paper" integrations of this variety beyond second order. However, the algorithm will allow such calculations to be taken to any order, subject only to memory size and running time requirements. The integrals are of the form

$$I = \int_{L_N}^{U_N} dx_N \int_{L_{N-1}}^{U_{N-1}} dx_{N-1} \cdots \int_{L_1}^{U_1} dx_1 \prod_{k=1}^{M} A(P_k)$$

where,

$$A(X) = \begin{cases} 1 & X \geq 0 \\ 0 & X < 0 \end{cases} ,$$

and, P_k is a polynomial in N variables:

$$P_k = a_0(k) - \sum_{i=1}^{N} a_i(k) x_i$$

The integral corresponds to an N-dimensional polytope enclosed by (N-1)-dimensional hyperplanes defined by the arguments of the step function $\Lambda(R)$. The configurational partition function, Q_N, is able to be reduced to an evaluation of such integrals. The programs are being written in ALGOL for the IIT Univac 1108.

Plans. In order to simulate additional aspects of fracture and embrittlement in the hard-sphere lattice model we must work with other than the perfect lattices that we have been considering so far. To test the assumption further that a (geometric) lattice instability implies fracture and embrittlement we must have some information as to the relative stabilities of lattices that contain various kinds of imperfections. An especially interesting calculation that we have been considering is the effect of an introduction of inclusions to an otherwise perfect lattice of equi-sized hard particles. We may be able to formulate a "cell theory" for such inclusions from which we should be able to ascertain the lattice free energies. By varying the size of the inclusion continuously from much larger than the size of the host lattice particles to much smaller we may observe the effect of inclusion size on lattice stability. In fact, we have the fascinating situation that in the limit of the size of the inclusion becoming vanishingly small we may also generate lattice vacancies. We are quite interested in the role that vacancies play in destabilizing a lattice either by local collapse with or without the generation of a dislocation or by a "condensation" of neighboring vacancies. During our second year in the program we also intend to attempt a modelling of various grain boundary phenomena. We may consider the features of a hard-particle tunnel model in this context. To simulate an embrittling environment we can construct a grain boundary "tunnel" having a liquid-like density of interacting particles. The analytical details of the statistical mechanics associated with such a model would be reasonably [illegible]

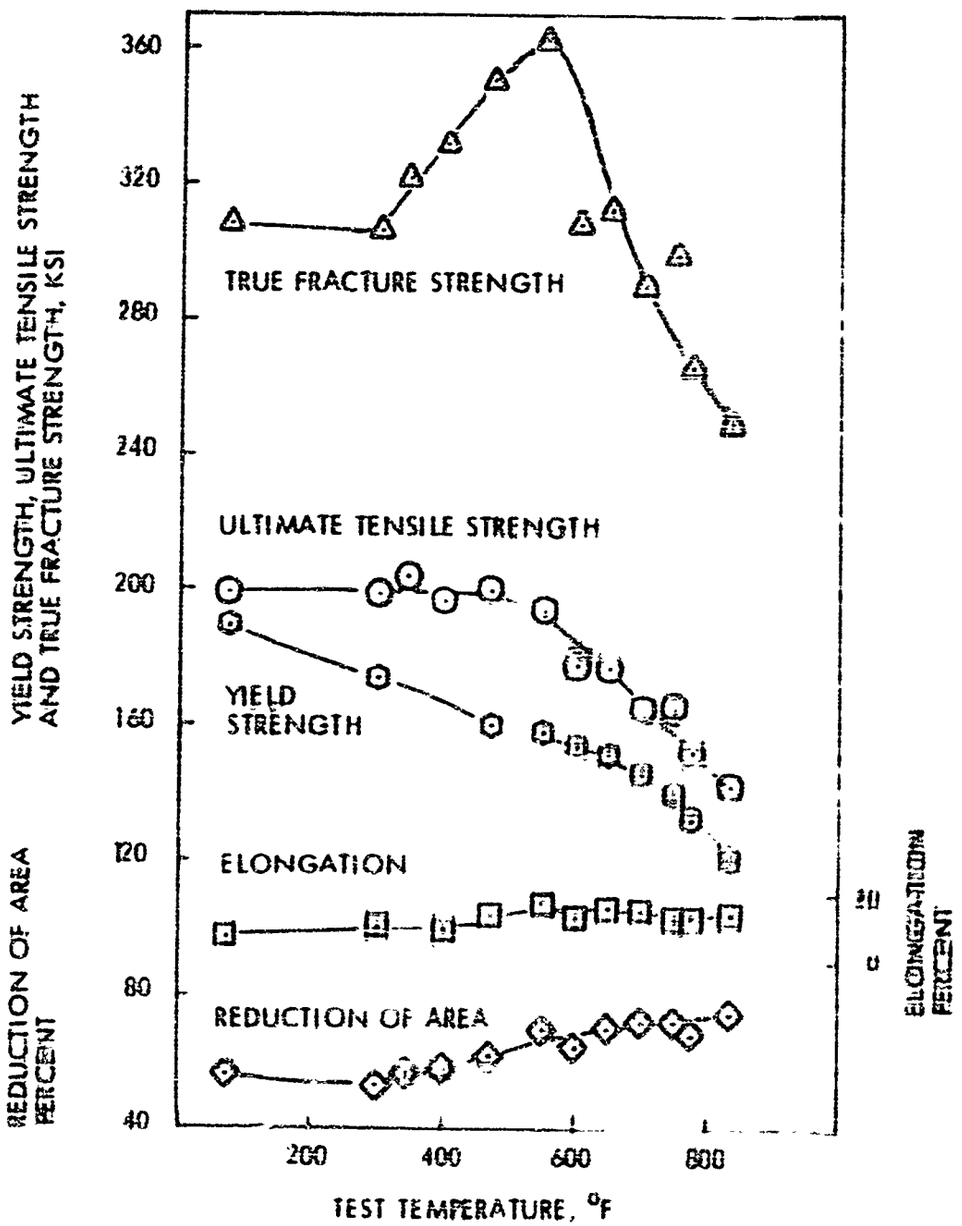

Fig. 1 Elevated Temperature Tensile Properties of 4140 Steel at 200 ksi Nominal Strength Level

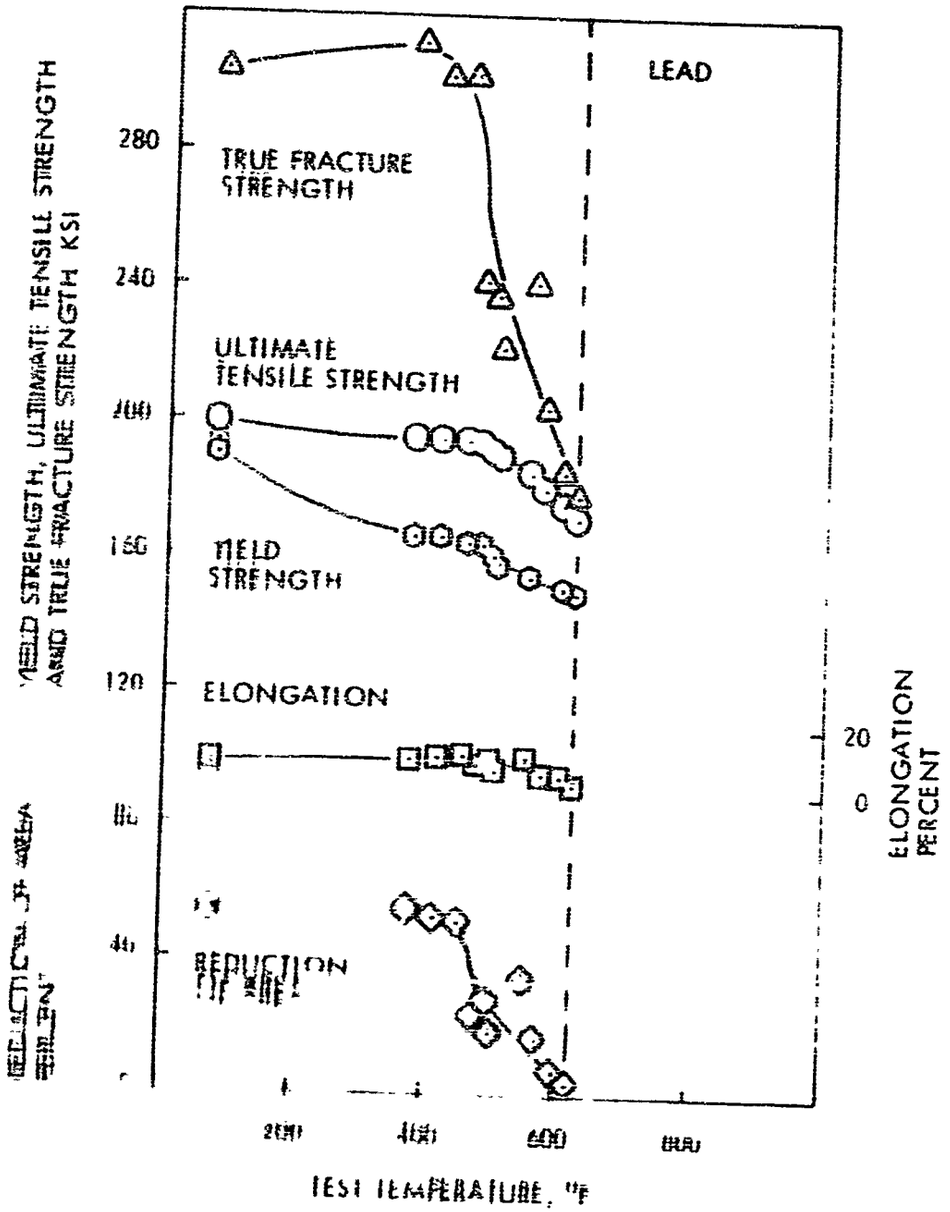

Fig. 2 Elevated Temperature Tensile Properties of 4140 Steel at 180 ksi Nominal Strength Level, and Butt-e Welded [illegible]

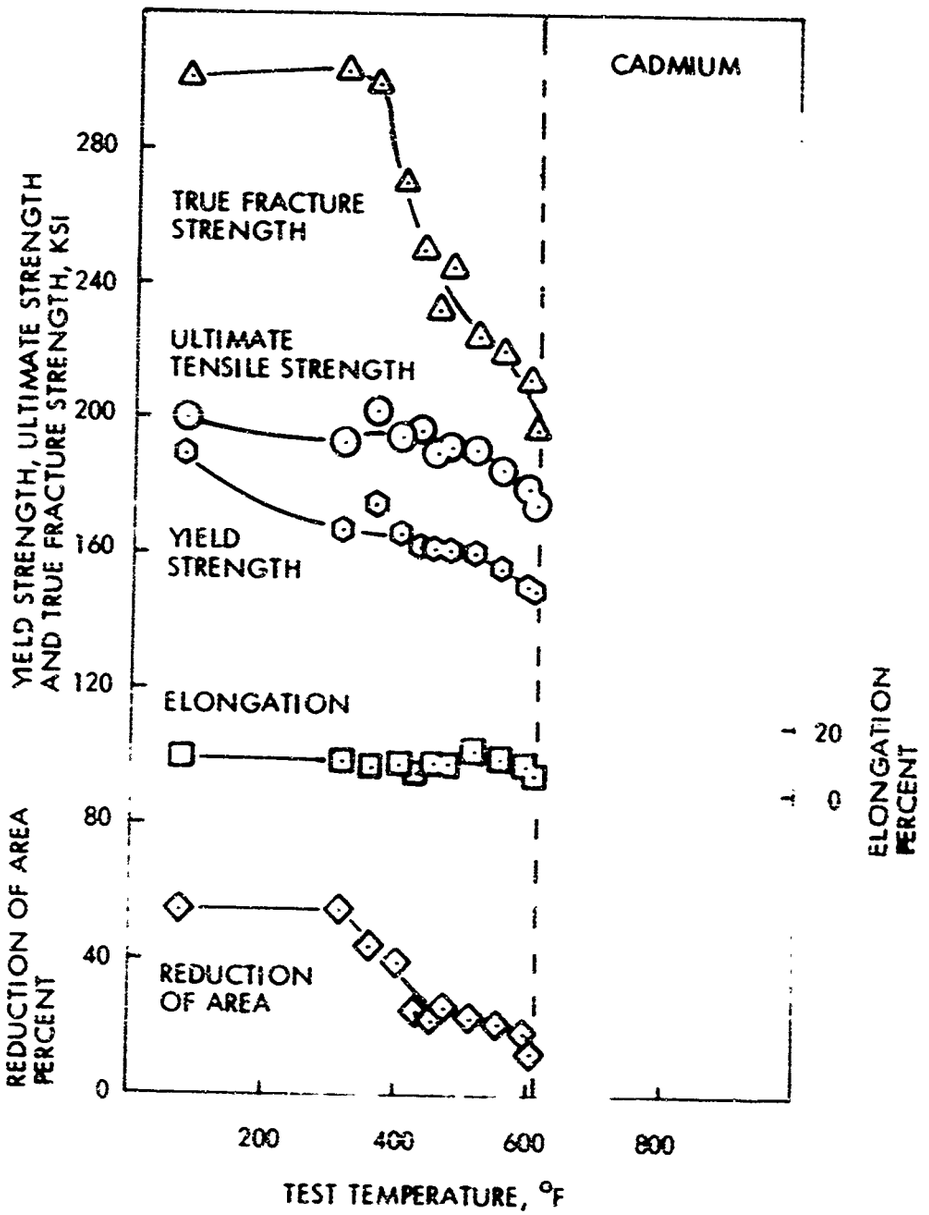

Fig. 3 Elevated Temperature Tensile Properties of 4140 Steel at 200 ksi Nominal Strength Level, and Surface Wetted with Pure Cadmium (99.9999%).

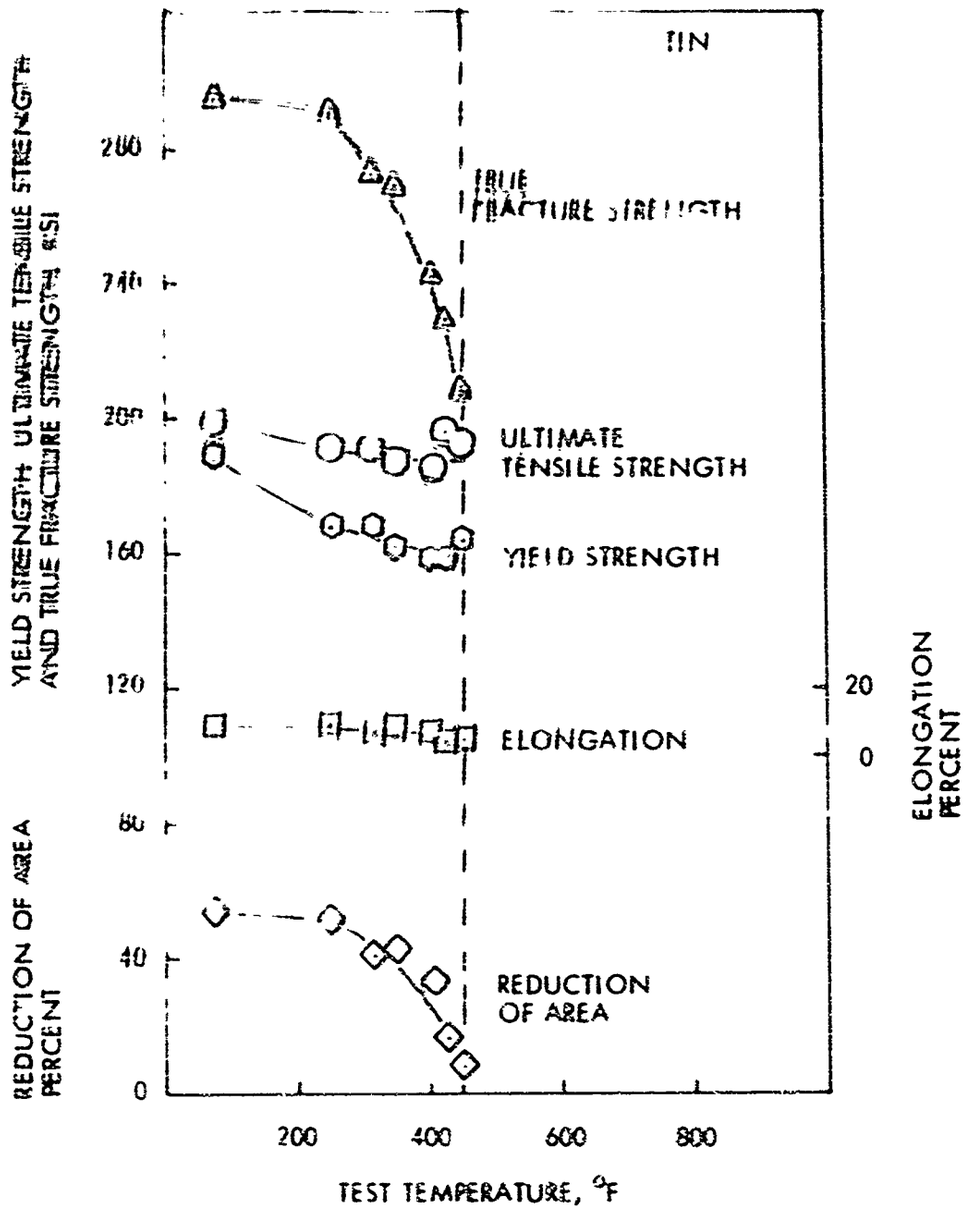

Fig. 4 Elevated Temperature Tensile Properties of 4140 Steel at 200 ksi Nominal Strength Level, and Surface Wetted with Pure Tin (99.999%).

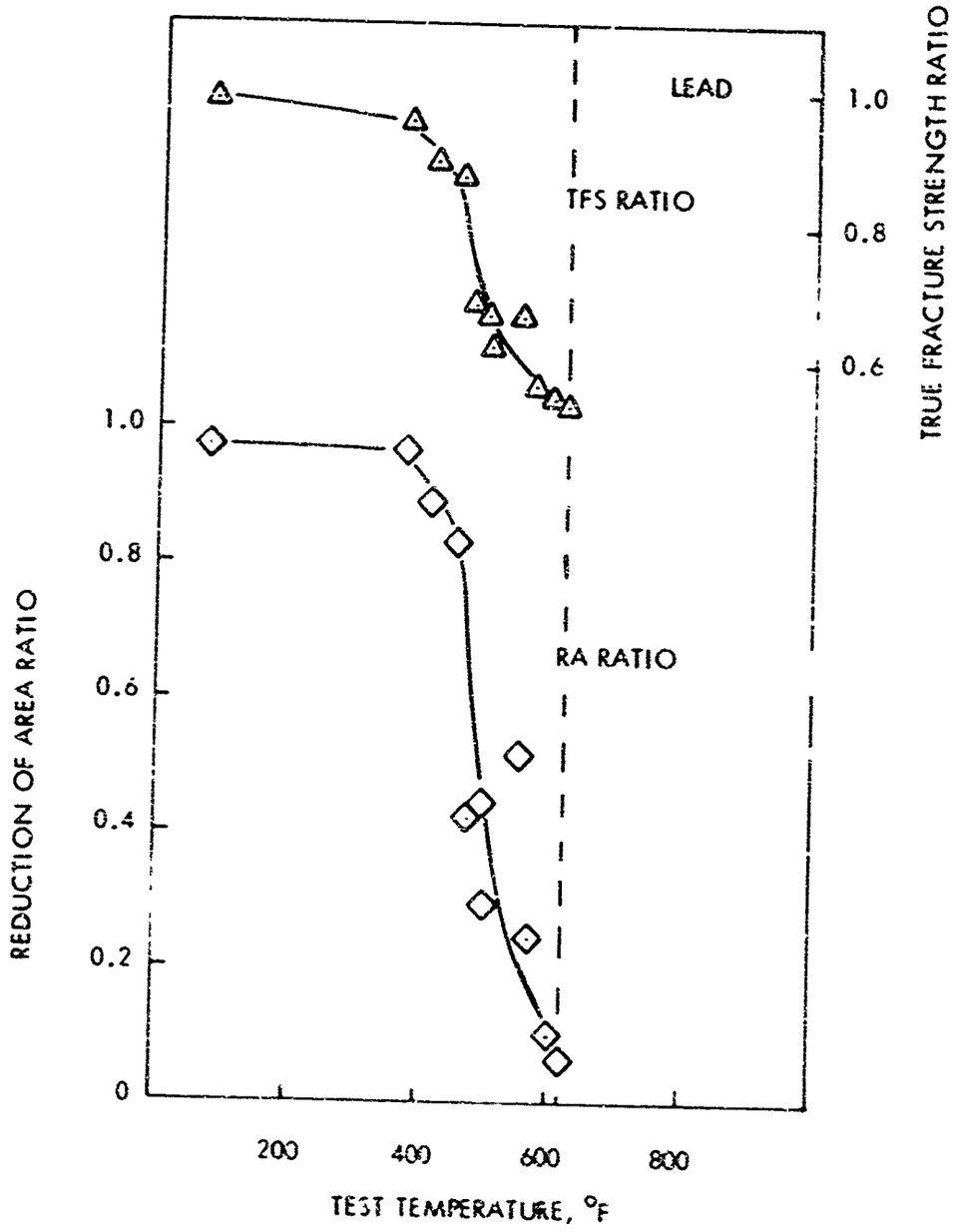

Fig. 5 Normalized True Fracture Strength and Reduction of Area for 4140 Steel Surface Wetted with Pure Lead.

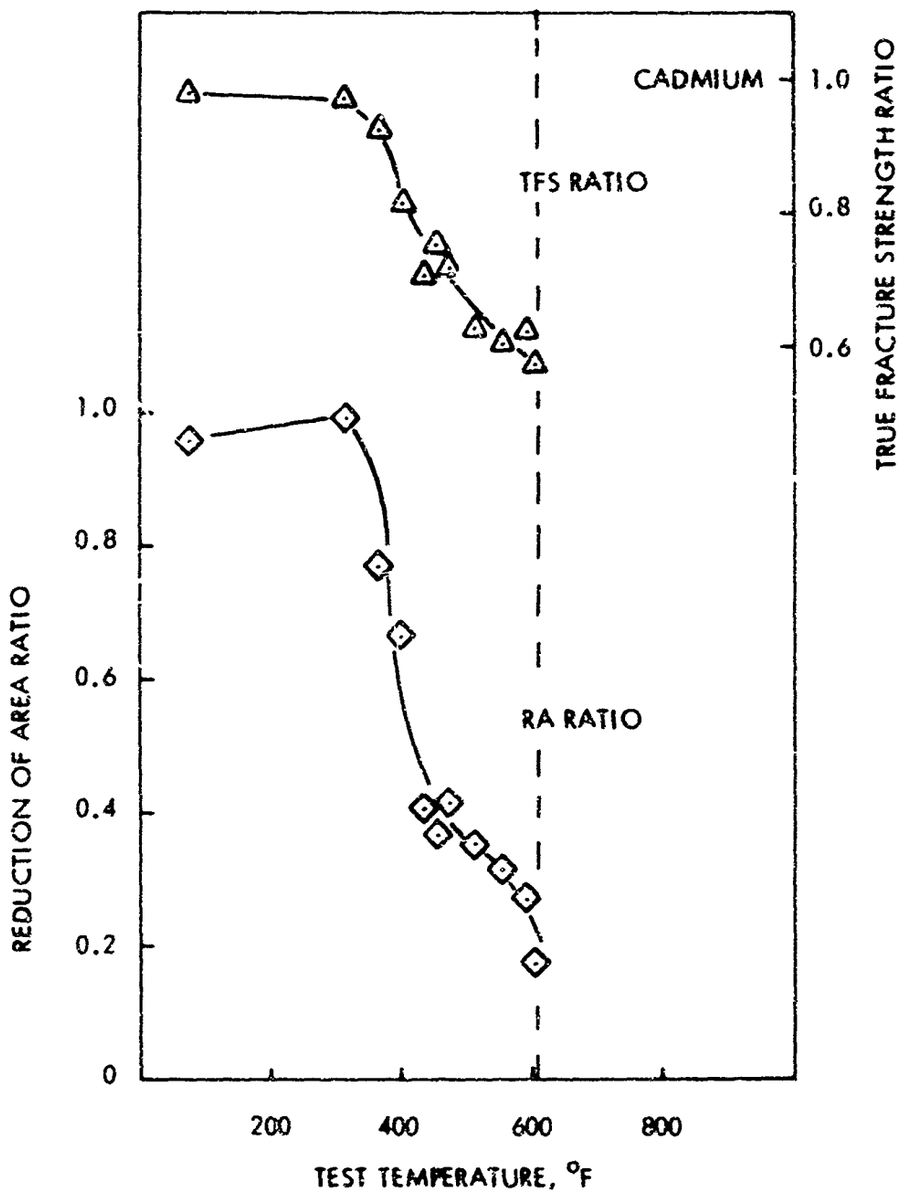

Fig. 6 Normalized True Fracture Strength and Reduction of Area for 4140 Steel Surface Wetted with Pure Cadmium.

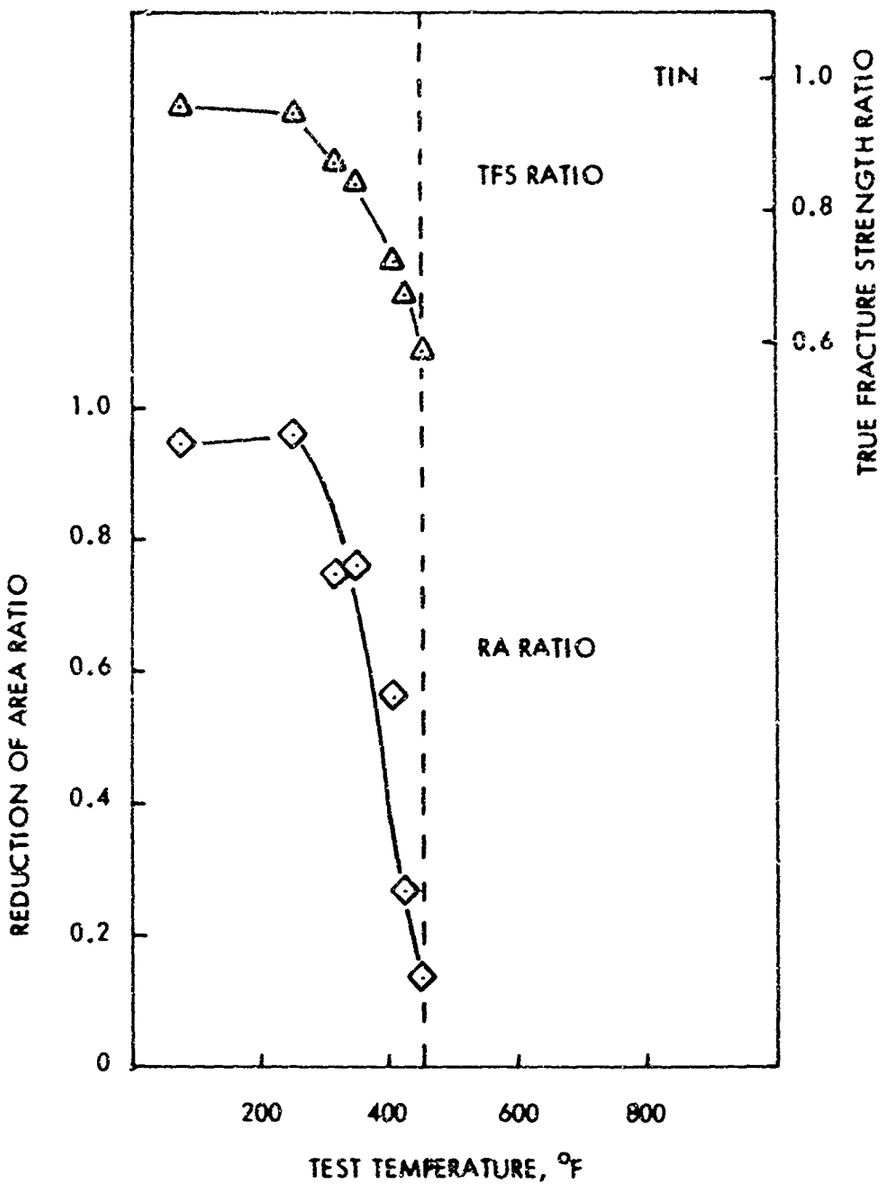

Fig. 7 Normalized True Fracture Strength and Reduction of Area for 4140 Steel Surface Wetted with Pure Tin.

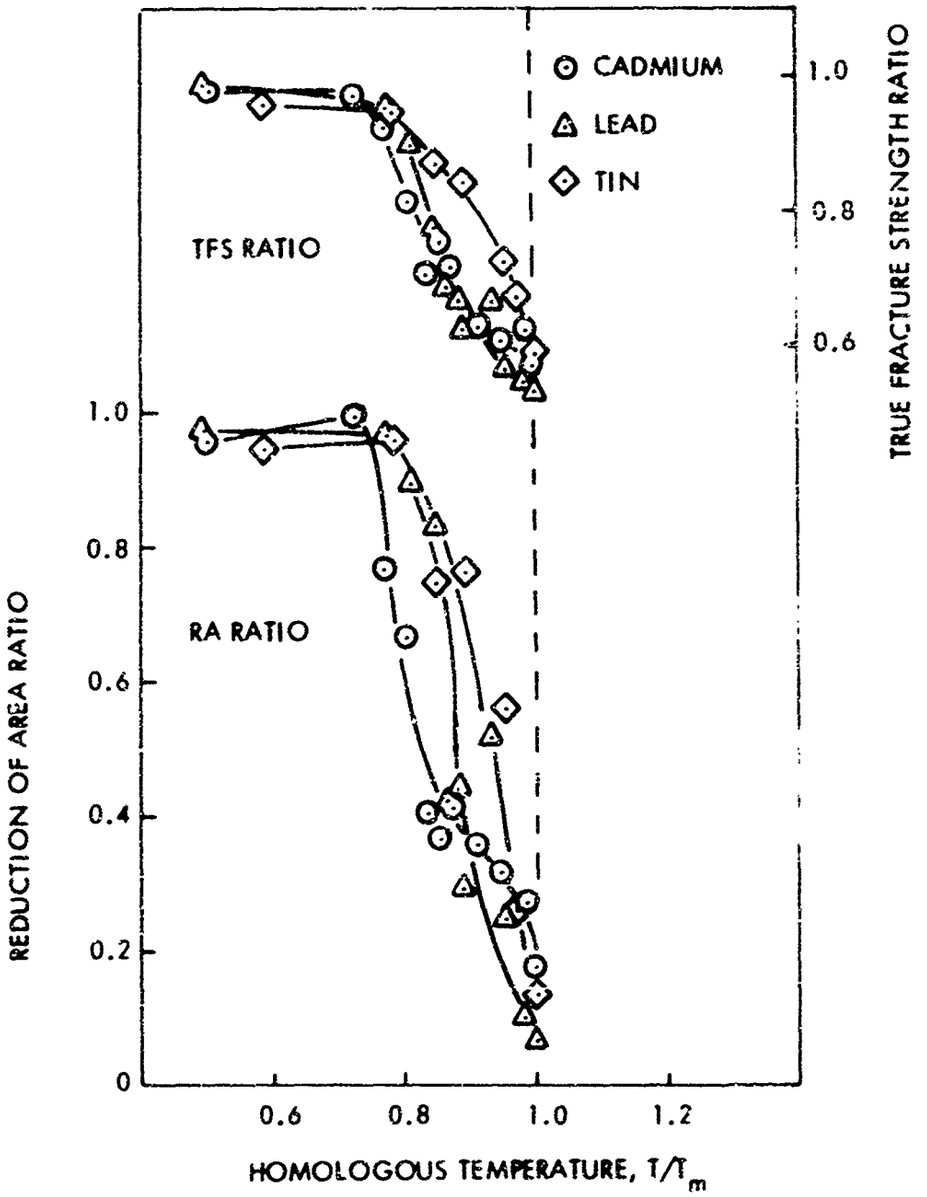

Fig. 8 Comparison of Normalized True Fracture Strength and Reduction of Area as a Function of Homologous Temperature for 4140 Steel Surface Wetted as Indicated.

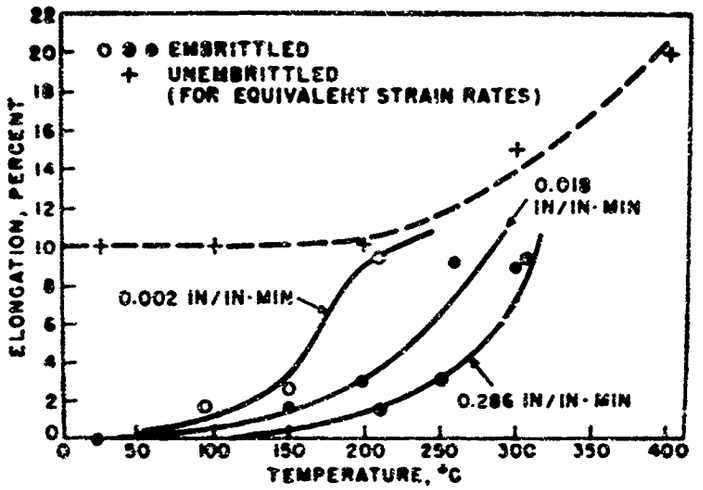

Fig. 9. ELONGATION AS A FUNCTION OF TEMPERATURE AND STRAIN RATE FOR Al 2024 T4 WETTED WITH MERCURY AMALGAM, AFTER ROSTOKER, (REF. 3).

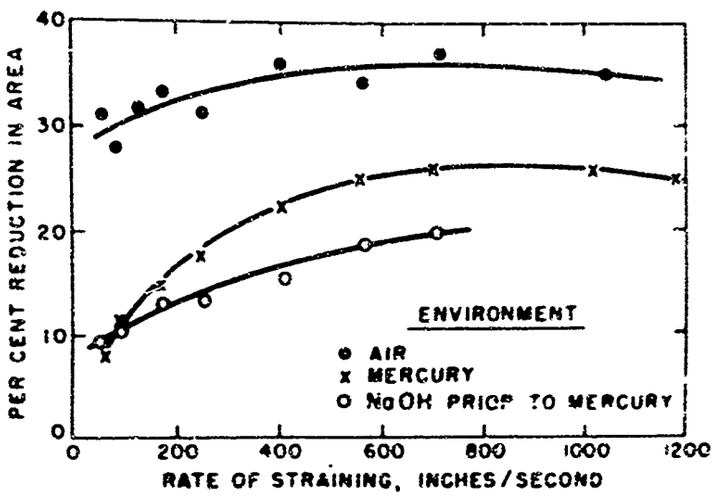

Fig. 10. PER CENT REDUCTION IN AREA AS A FUNCTION OF LOADING RATE FOR Al 2024 T4, AFTER BARCLAY AND THINES, (REF. 4).

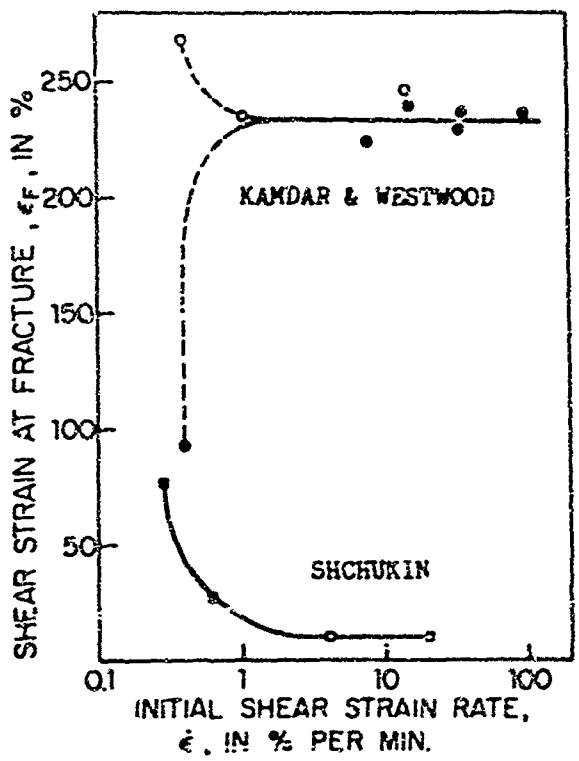

Fig. 11. STRAIN RATE EFFECTS ON FRACTURE STRAIN ASSOCIATED WITH ZINC MONOCRYSTALS COATED WITH LIQUID Ga, FROM KAMDAR AND WESTWOOD, (REF. 5 and 6).

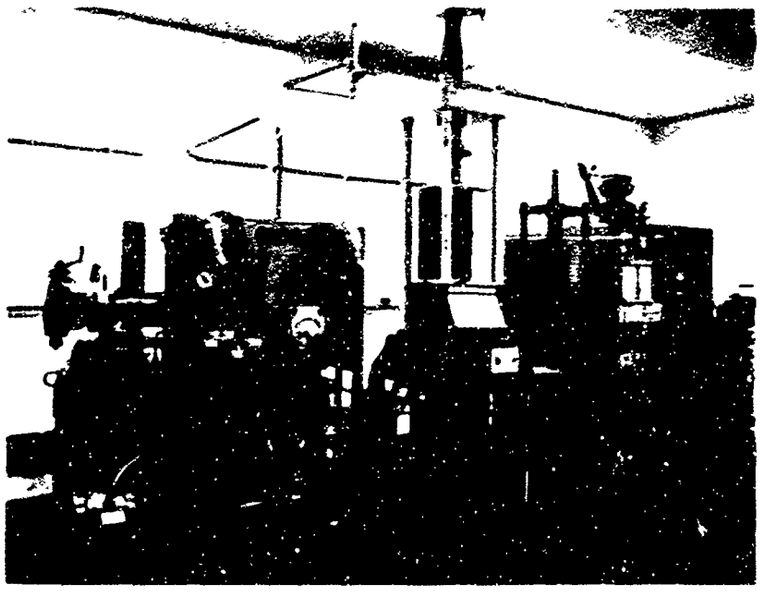

Fig. 12 SERVO-CONTROLLED HYDRAULICALLY ACTUATED LOADING SYSTEM.

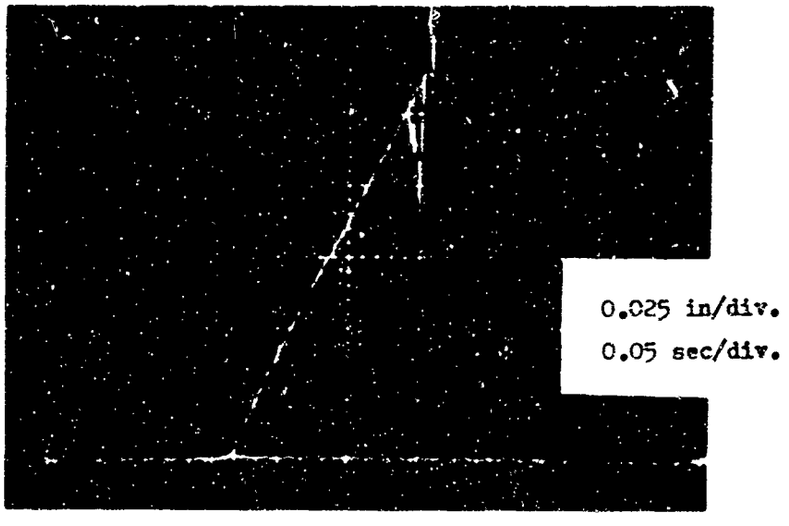

Fig. 13 ACTUATOR DISPLACEMENT AS A FUNCTION OF TIME.

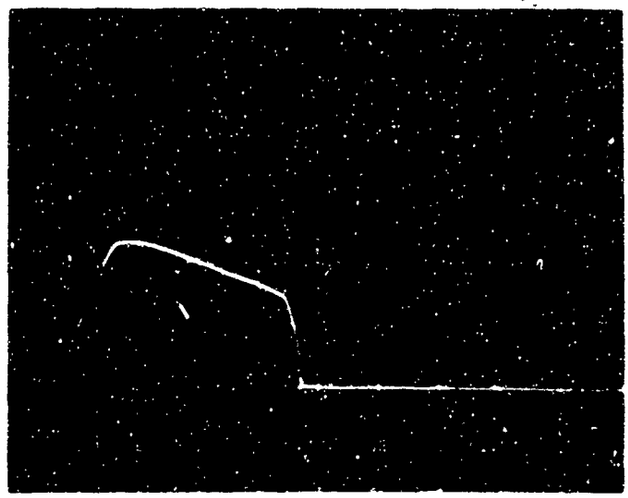

1.6 in/min.
1 sec/div.
1000 lb/div.

TESTED IN AIR
500°F

1.6 in/min.
1 sec/div.
1000 lb/div.

TESTED IN Hg
500°F

Fig. 14 TYPICAL FORCE TIME RECORDS FOR Al 2024 T4.
STRAIN RATE = 0.30 in/in/min.

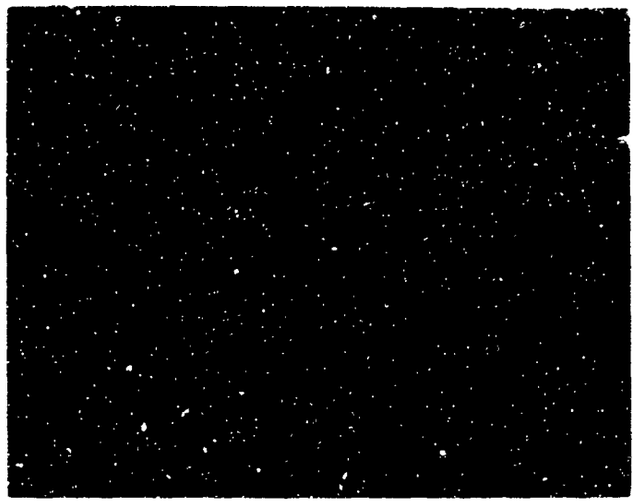

1000 in/in/div
0.5 sec/div

Fig. 15. TRANSVERSE STRAIN AS A FUNCTION OF TIME SHOWING CHANGE IN STRAIN RATE WHEN YIELDING OCCURS.

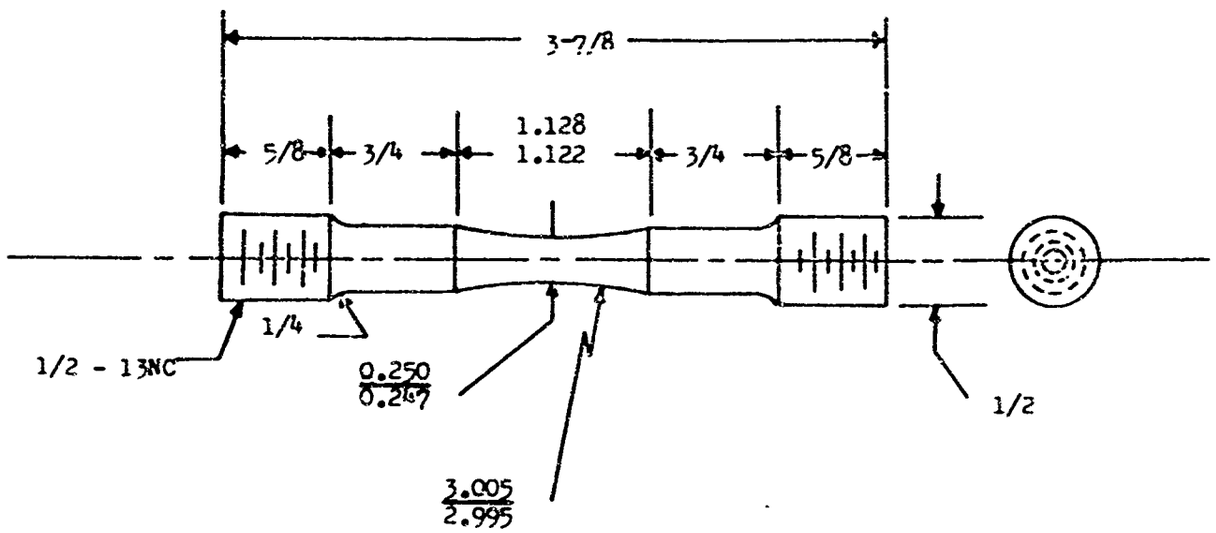

Fig. 16. GEOMETRY OF TENSILE SPECIMEN USED FOR STRAIN RATE TESTING.

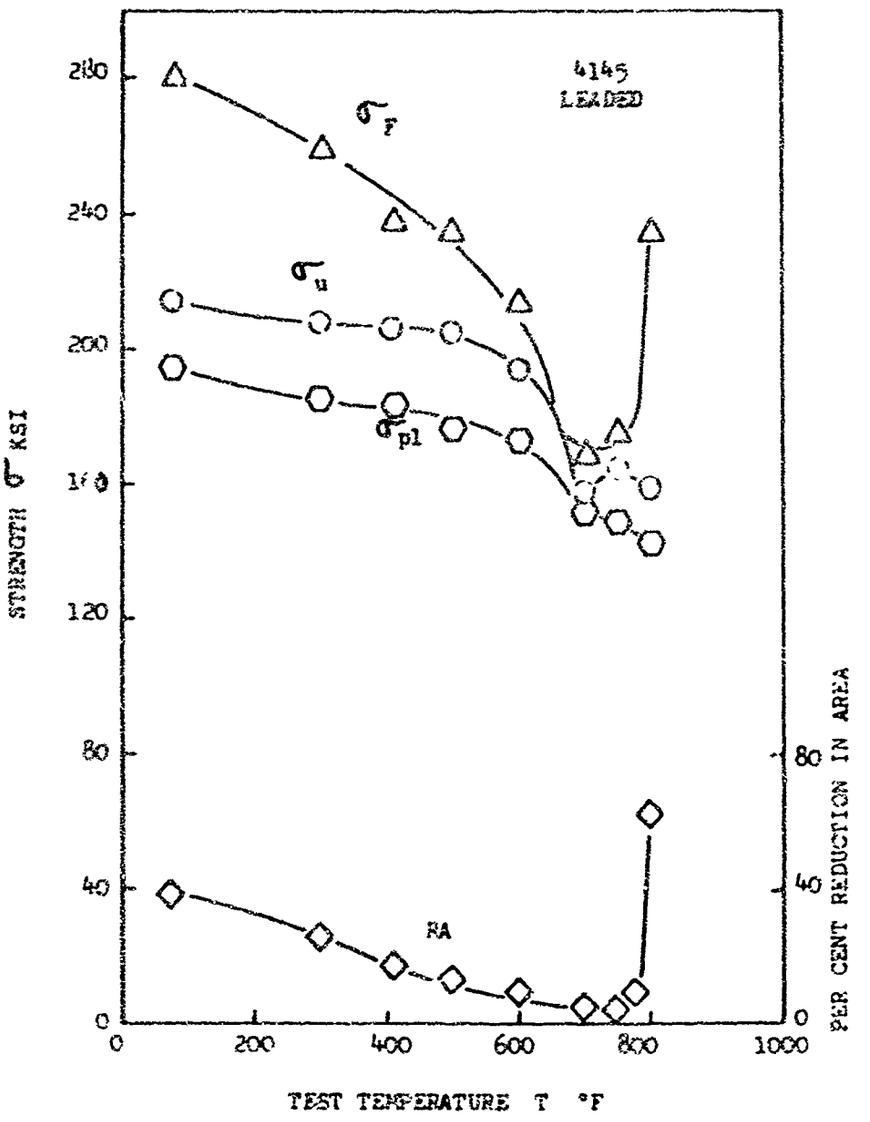

Fig. 17. STRENGTH AND REDUCTION OF AREA AS A FUNCTION OF TEST TEMPERATURE
STRAIN RATE 0.0025 in/in/min.

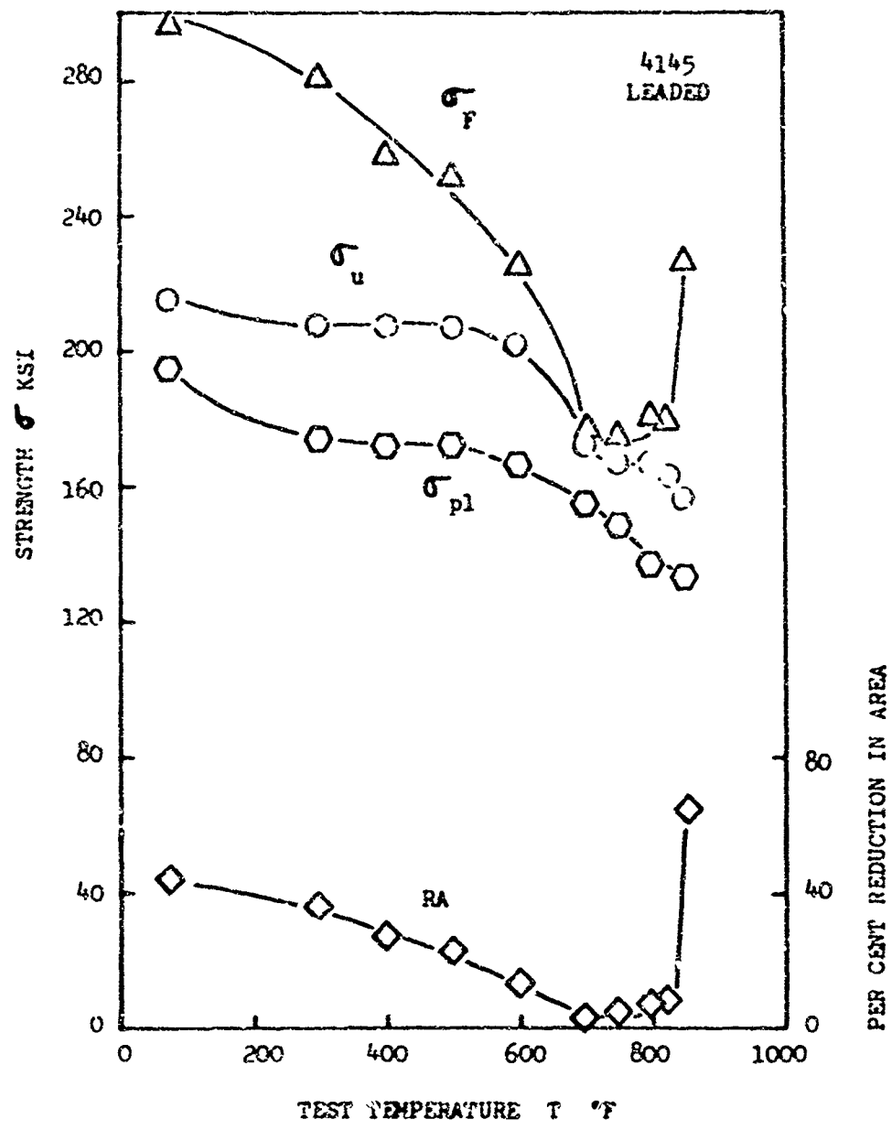

Fig. 18. STRENGTH AND REDUCTION OF AREA AS A FUNCTION OF TEST TEMPERATURE
STRAIN RATE 0.025 in/in/min.

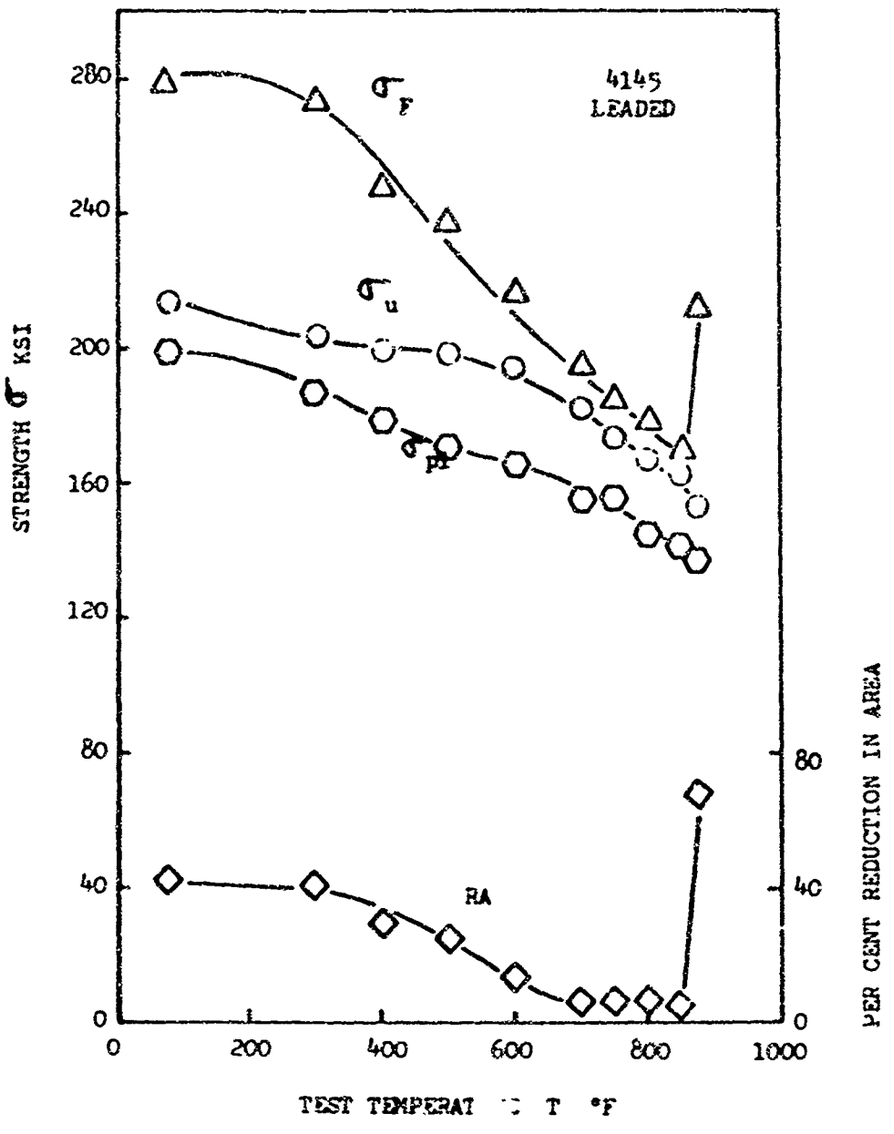

Fig. 19. STRENGTH AND REDUCTION OF AREA AS A FUNCTION OF TEST TEMPERATURE
STRAIN RATE 0.25 in/in/min.

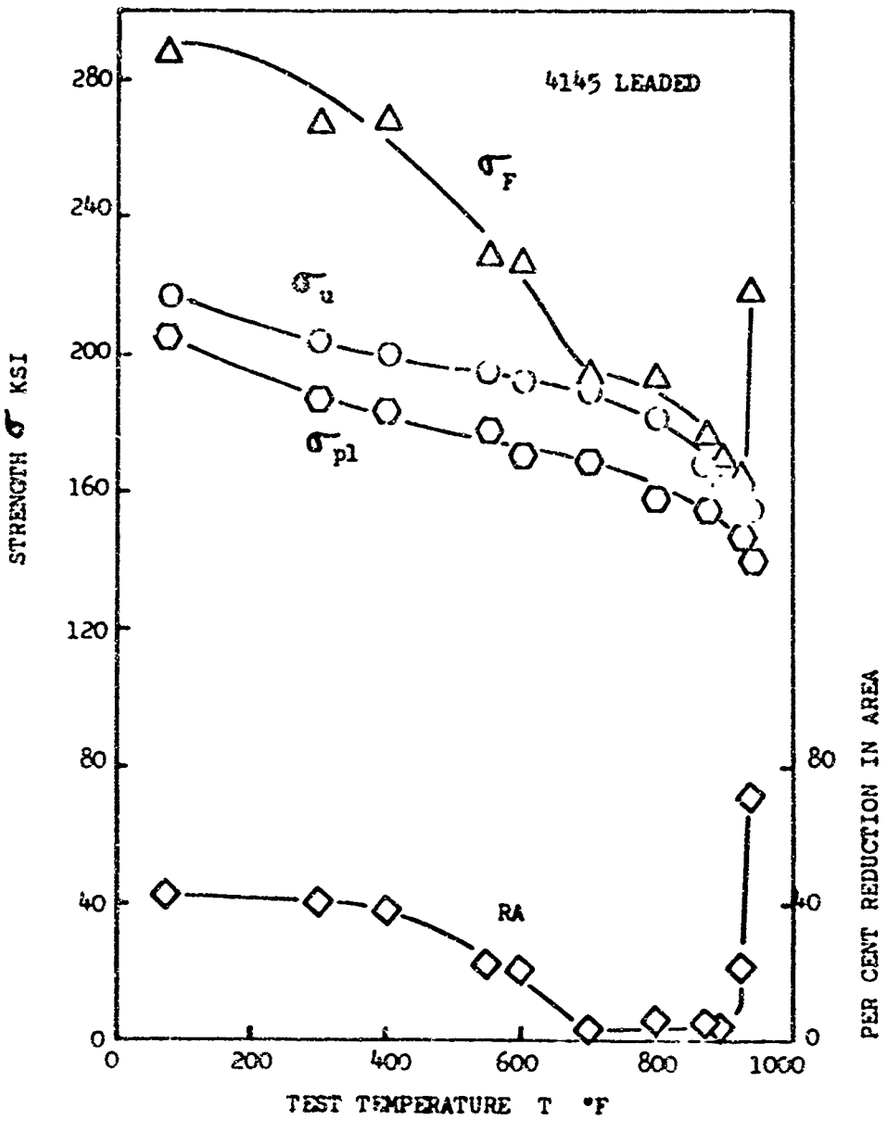

Fig. 20. STRENGTH AND RE ;ON OF AREA AS A FUNCTION OF TEST TEMPERATURE STRAIN RATE 2.46 in/in/min.

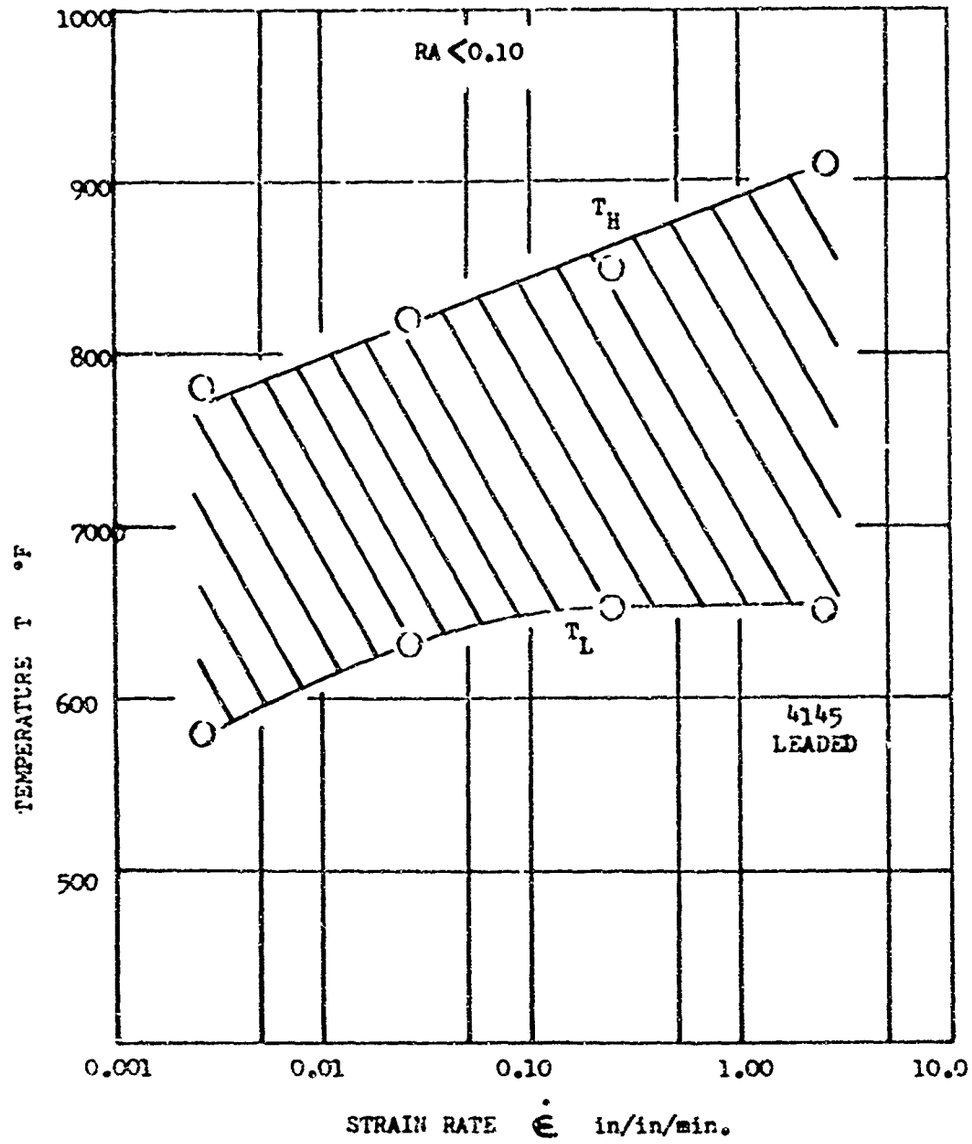

Fig. 21. EMBRITTLEMENT BAND AS A FUNCTION OF STRAIN RATE FOR LEADED 4145 STEEL.

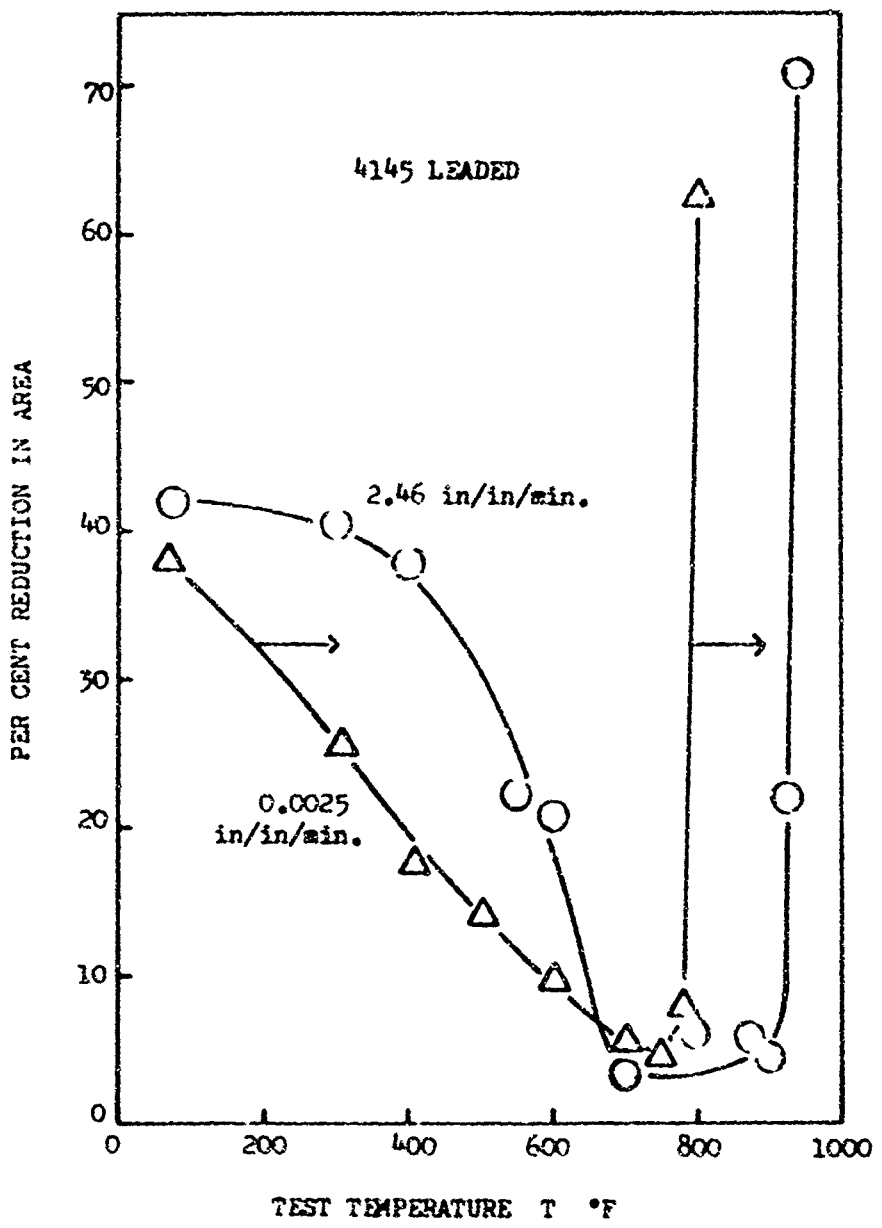

Fig. 22. EFFECTS OF STRAIN RATE ON DUCTILITY-TEMPERATURE PROFILES.

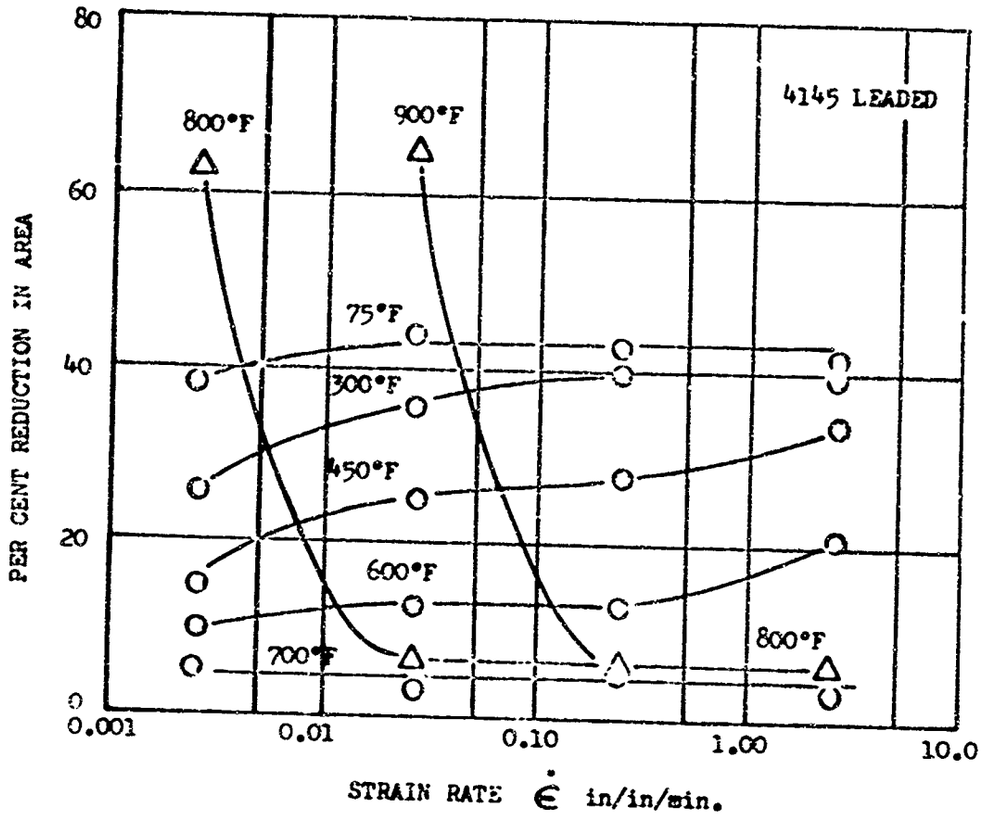

Fig. 23. EFFECT OF STRAIN RATE ON PER CENT REDUCTION IN AREA FOR DIFFERENT TESTING TEMPERATURES.

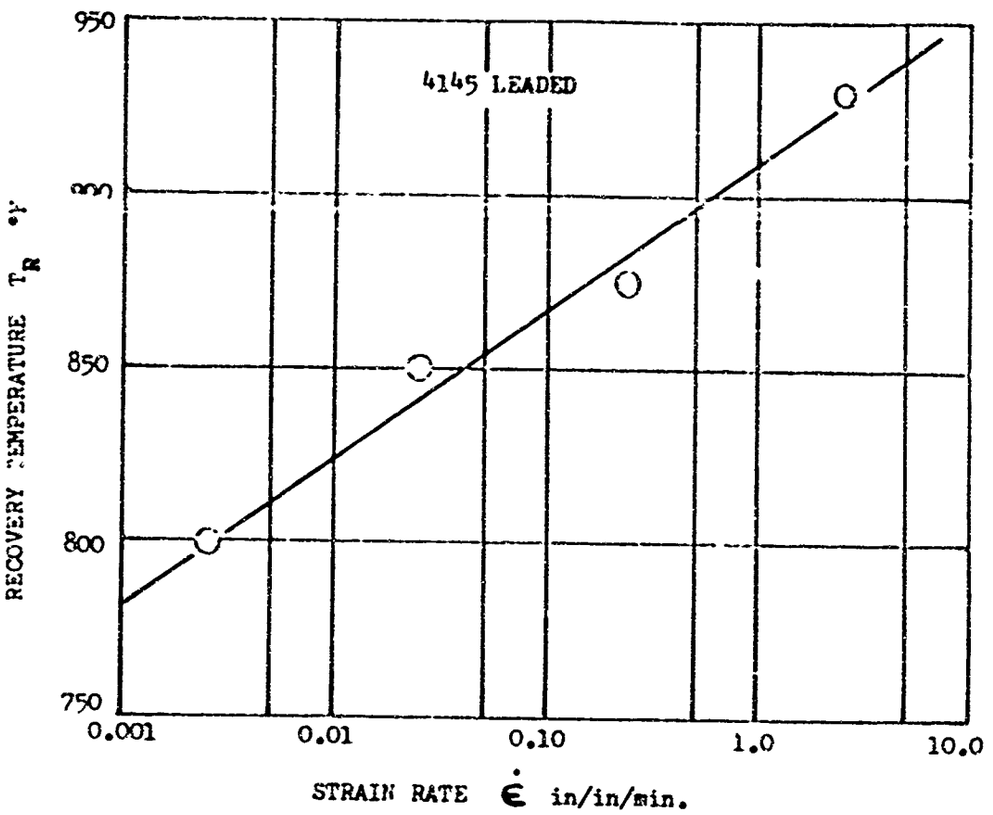

Fig. 24. RECOVERY TEMPERATURE T_R AS A FUNCTION OF STRAIN RATE.

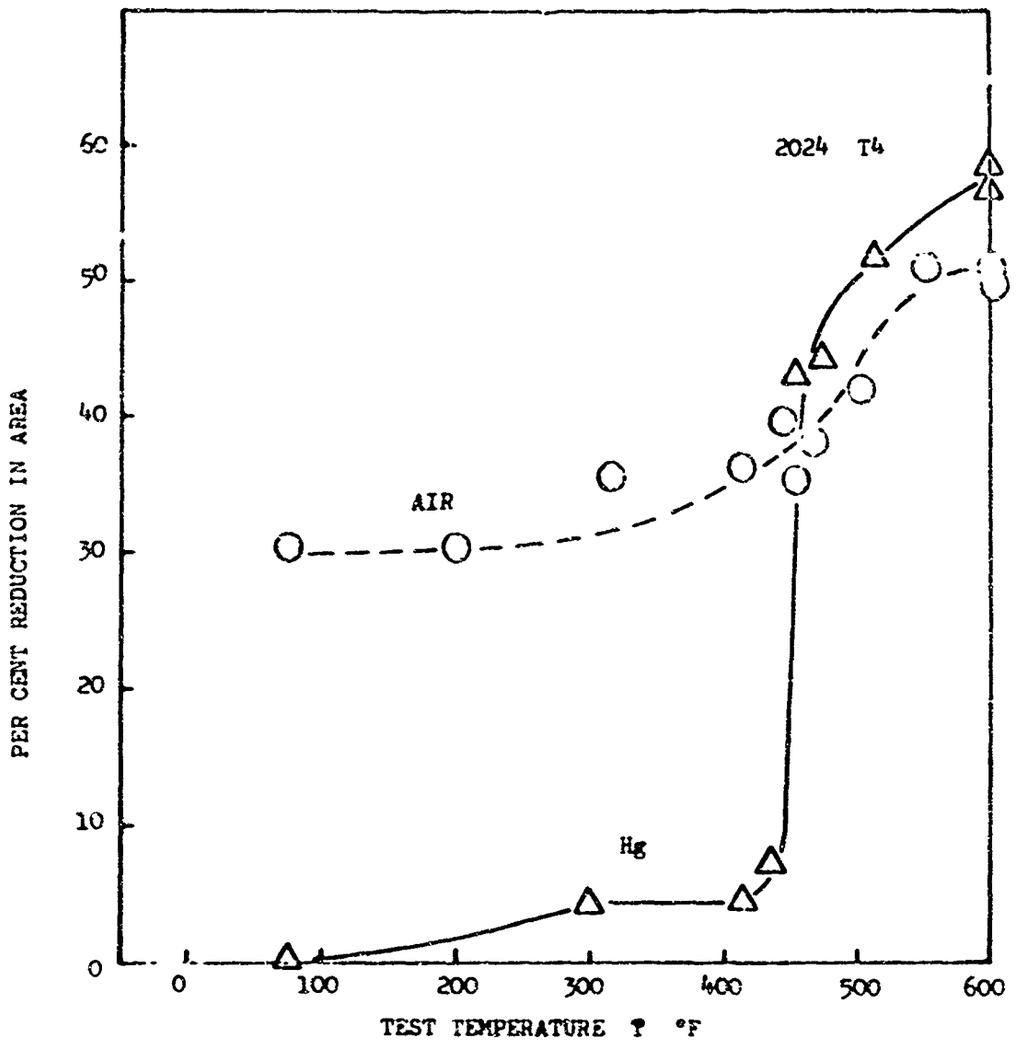

Fig. 25. PER CENT REDUCTION IN AREA AS A FUNCTION OF TEST TEMPERATURE FOR A STRAIN RATE OF 0.003 in/in/min.

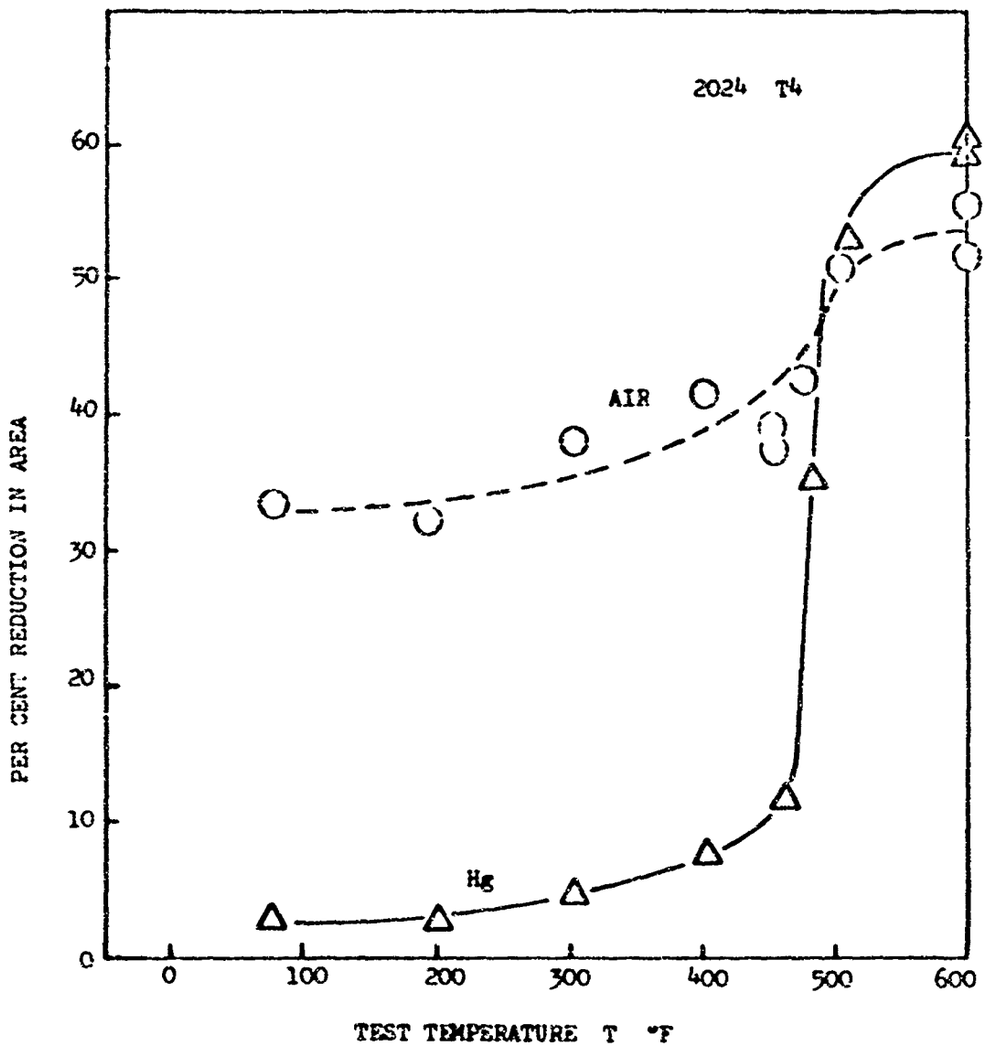

Fig.26. PER CENT REDUCTION IN AREA AS A FUNCTION OF TEST TEMPERATURE FOR A STRAIN RATE OF 0.03 in/in/min.

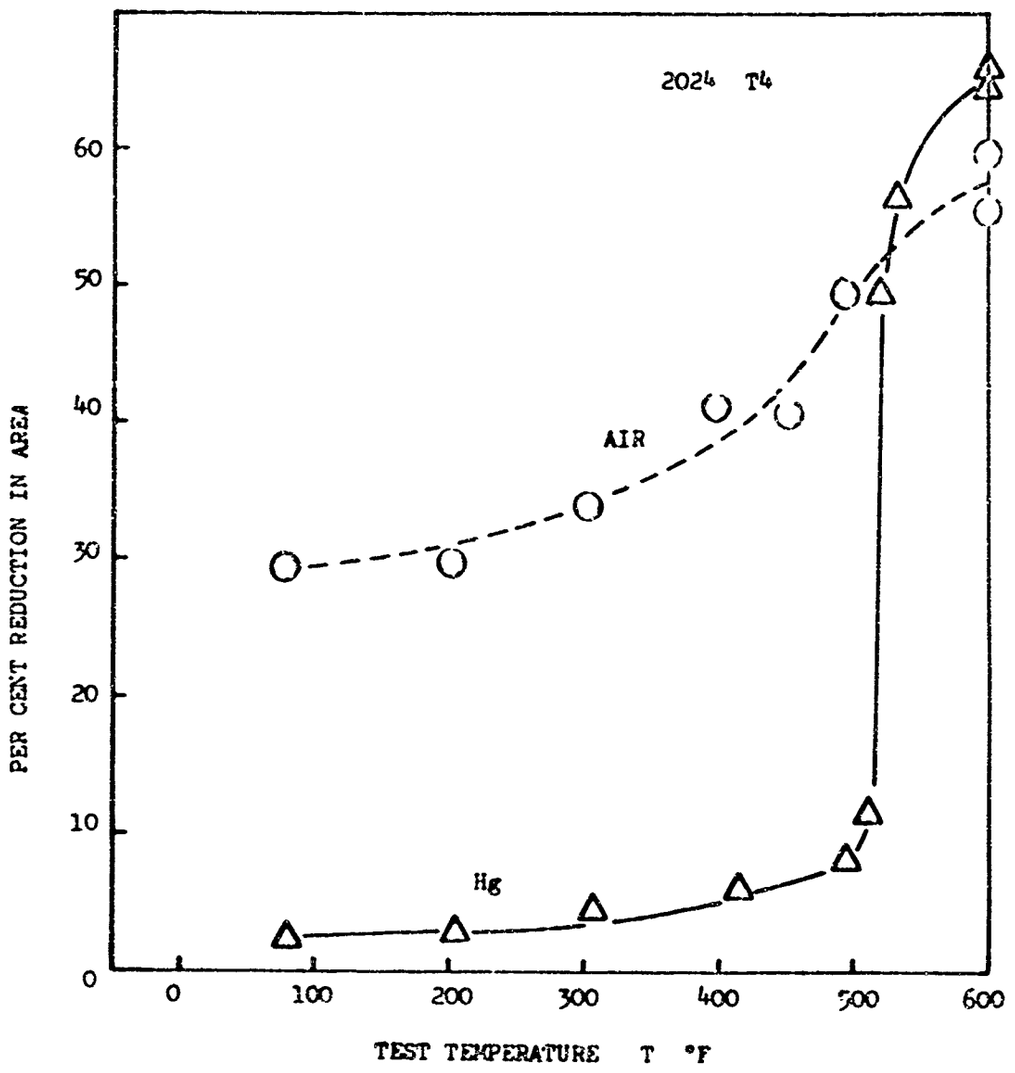

Fig.27. PER CENT REDUCTION IN AREA AS A FUNCTION OF TEST TEMPERATURE FOR A STRAIN RATE OF0.30 in/in/min.

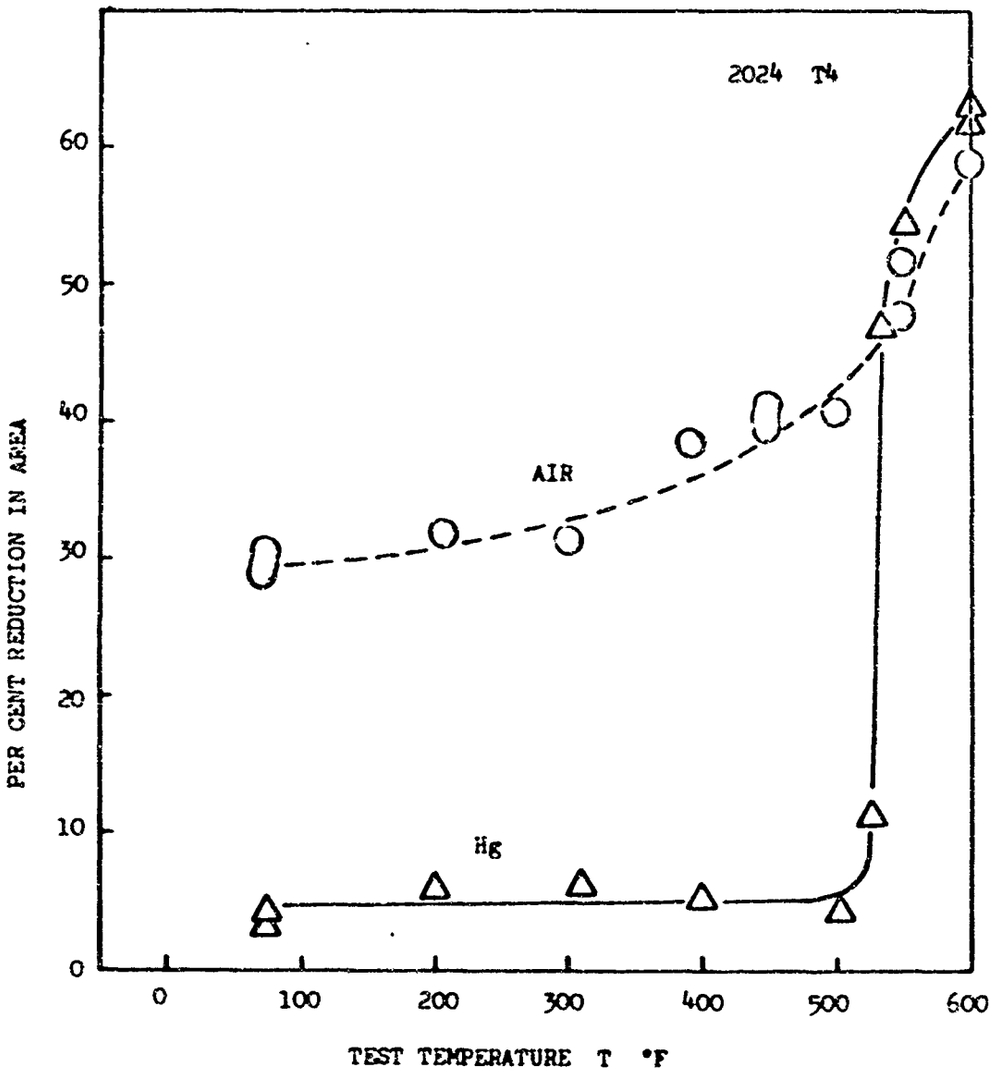

Fig. 28. PER CENT REDUCTION IN AREA AS A FUNCTION OF TEST TEMPERATURE FOR A STRAIN RATE OF 3.02 in/in/min.

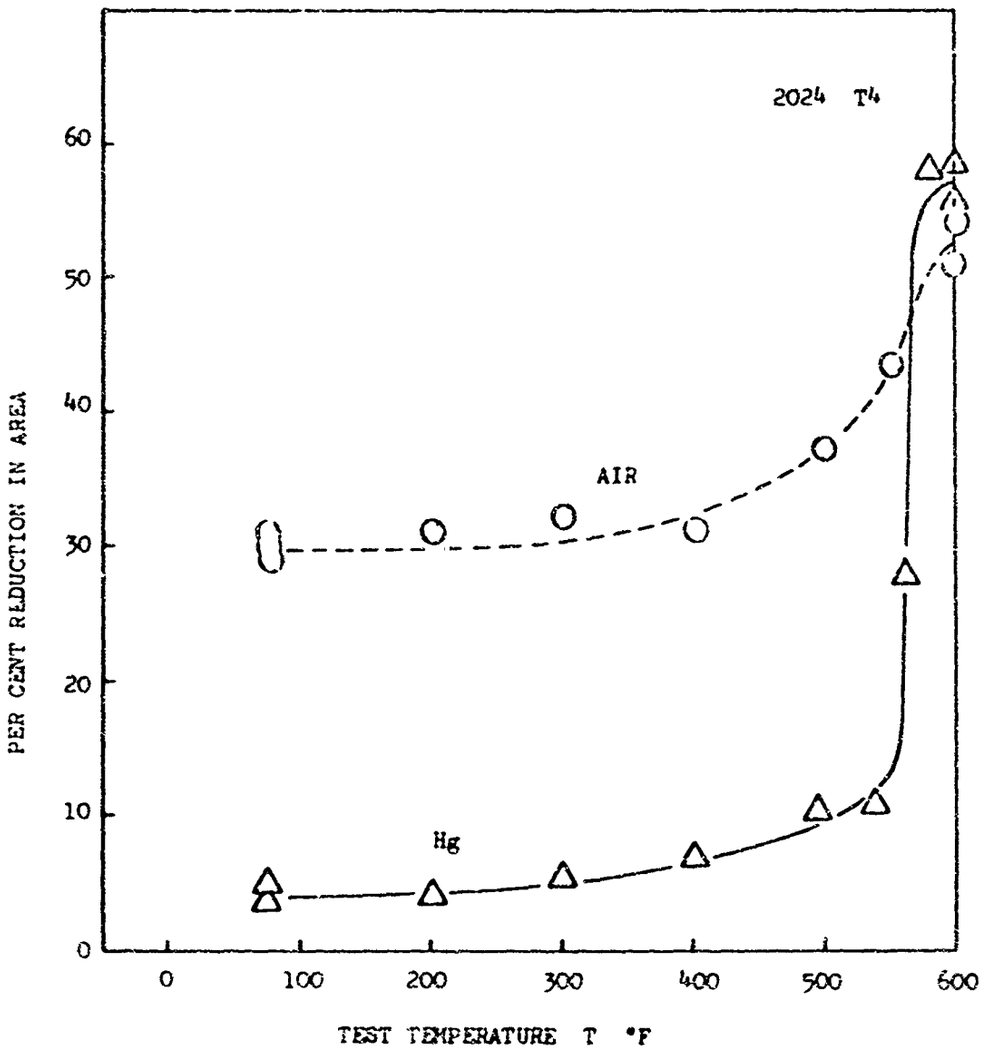

Fig. 29. PER CENT REDUCTION IN AREA AS A FUNCTION OF TEST TEMPERATURE FOR A STRAIN RATE OF 30.2 in/in/min.

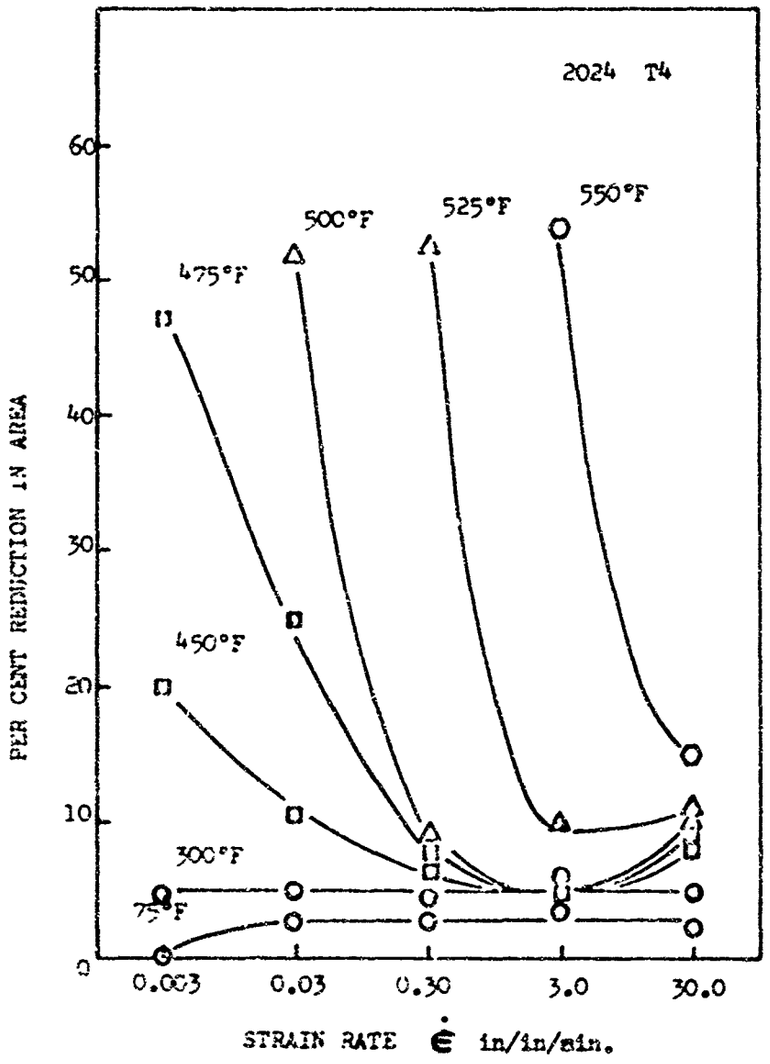

Fig. 30. EFFECT OF STRAIN RATE ON PER CENT REDUCTION IN AREA FOR DIFFERENT TESTING TEMPERATURES.

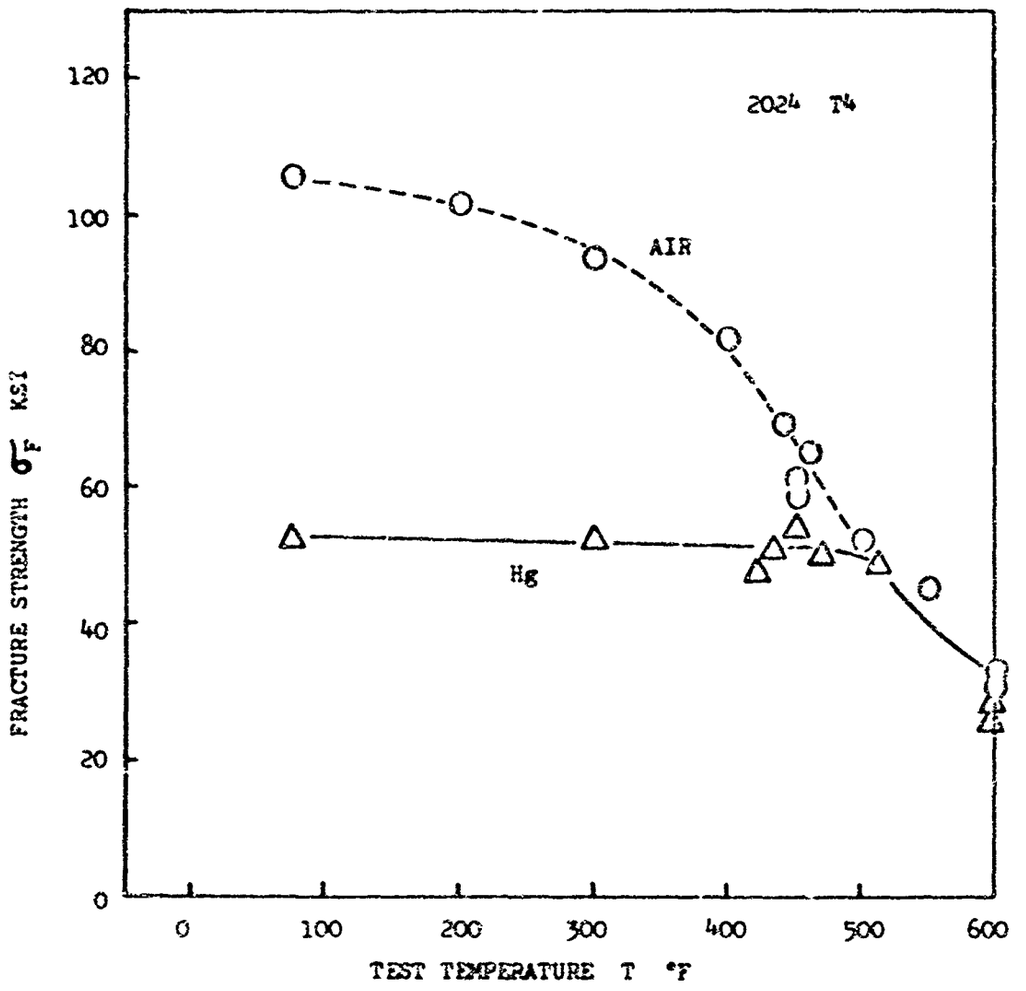

Fig. 31. FRACTURE STRENGTH $\bar{\sigma}_F$ AS A FUNCTION OF TEST TEMPERATURE STRAIN RATE 0.003 in/in/min.

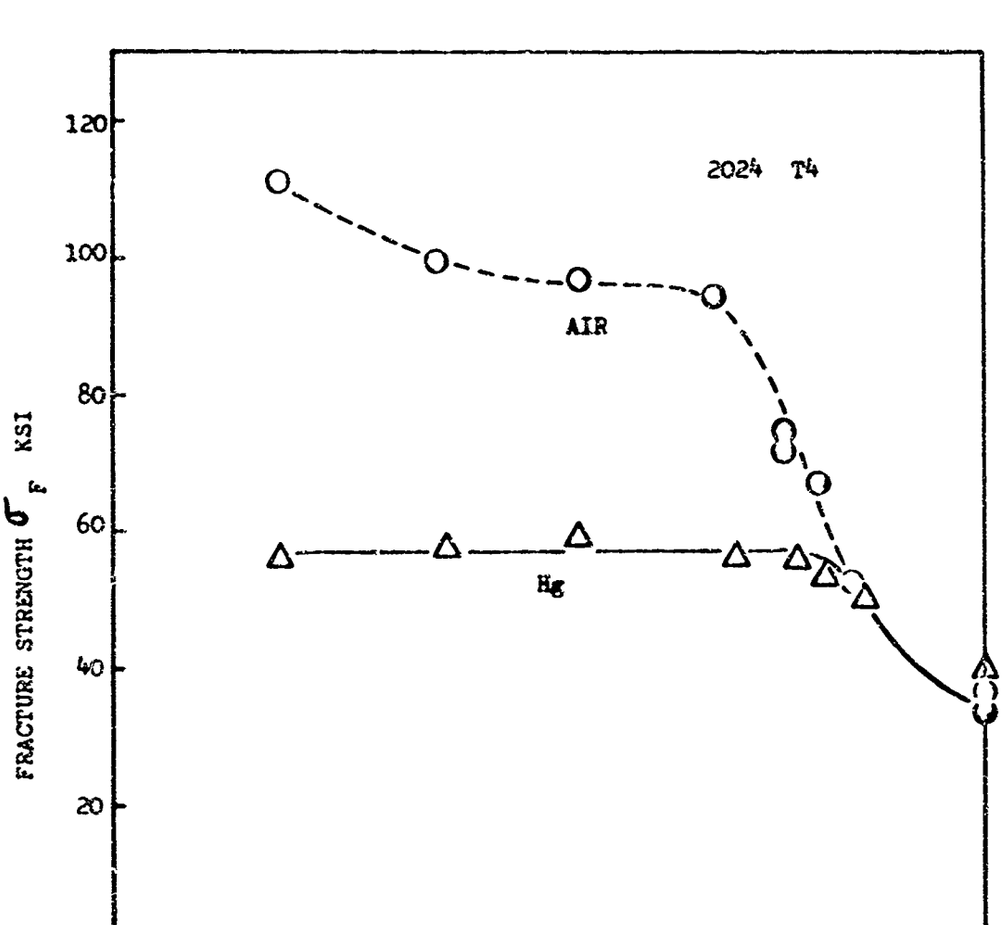

Fig. 32. FRACTURE STRENGTH $\bar{\sigma}_F$ AS A FUNCTION OF TEST TEMPERATURE
STRAIN RATE 0.03 in/in/min.

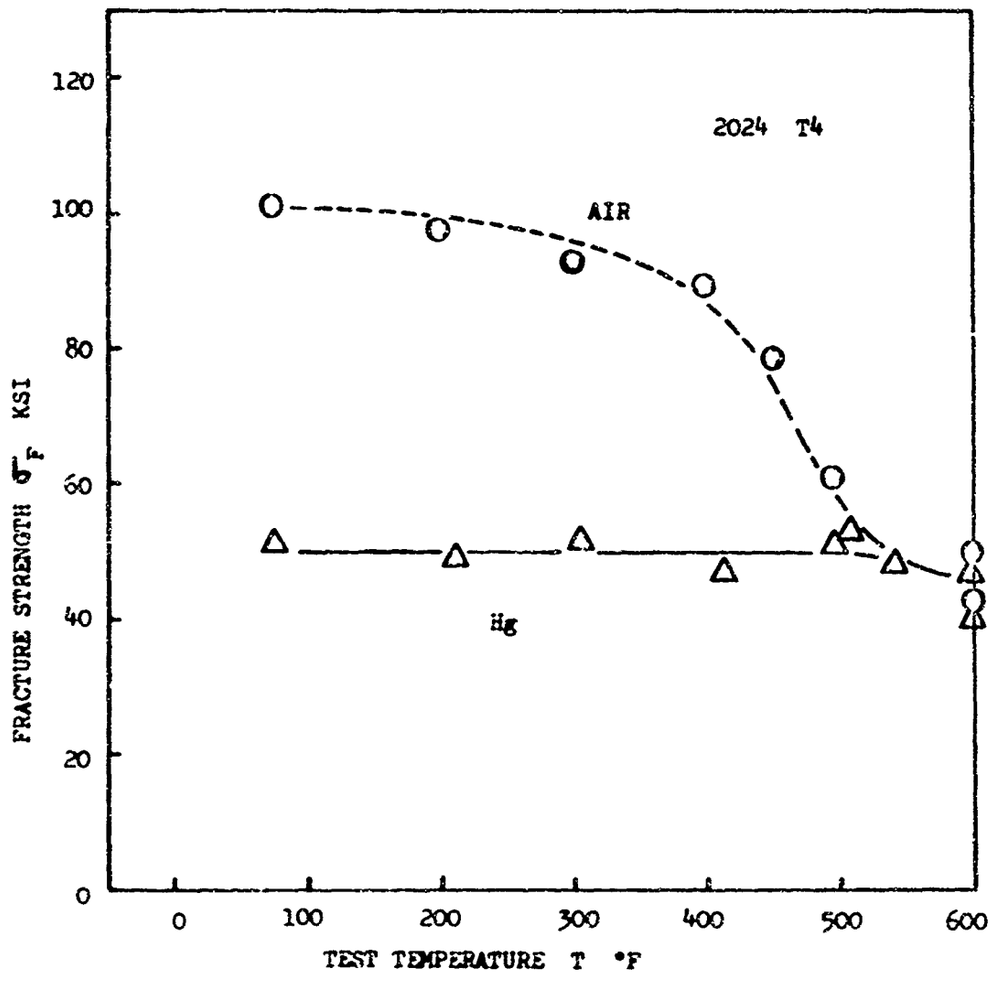

Fig. 33. FRACTURE STRENGTH σ_F AS A FUNCTION OF TEST TEMPERATURE
STRAIN RATE 0.30 in/in/min.

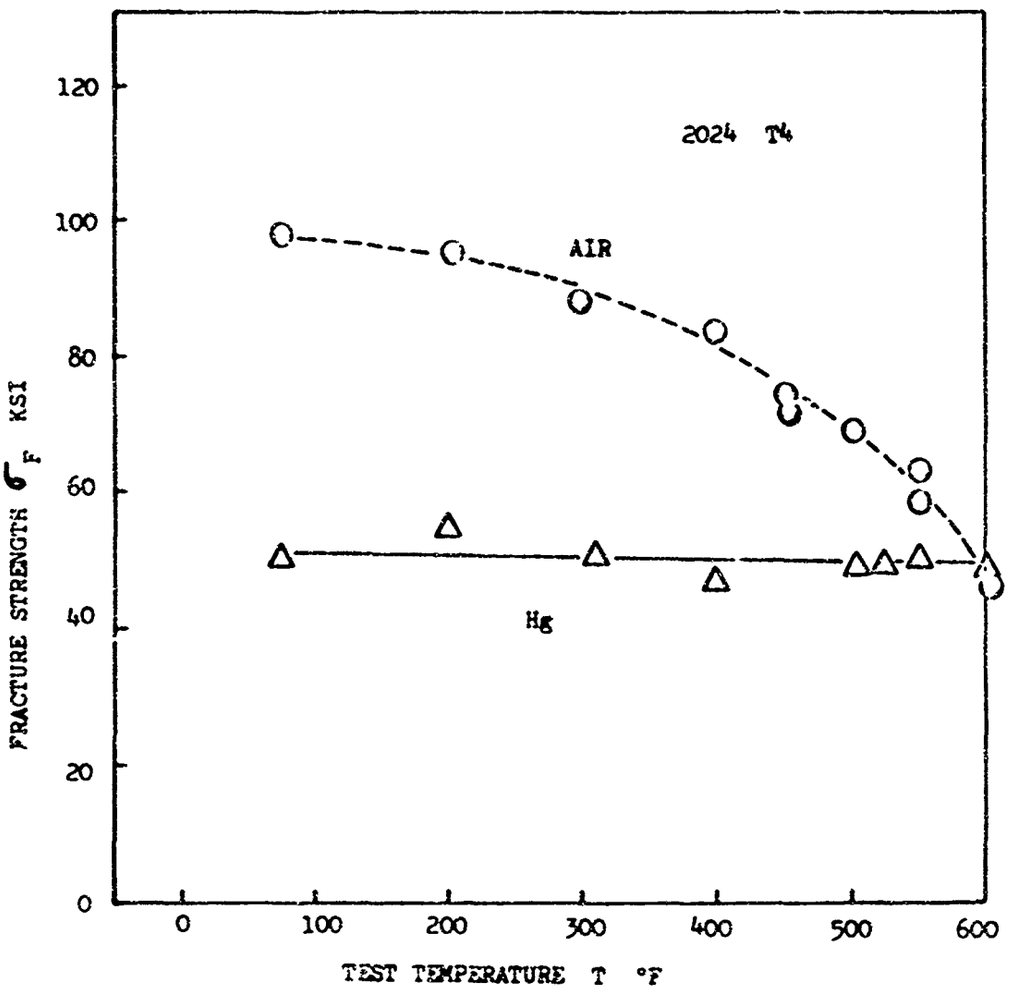

Fig. 34. FRACTURE STRENGTH σ_F AS A FUNCTION OF TEST TEMPERATURE
STRAIN RATE 3.02 in/in/min.

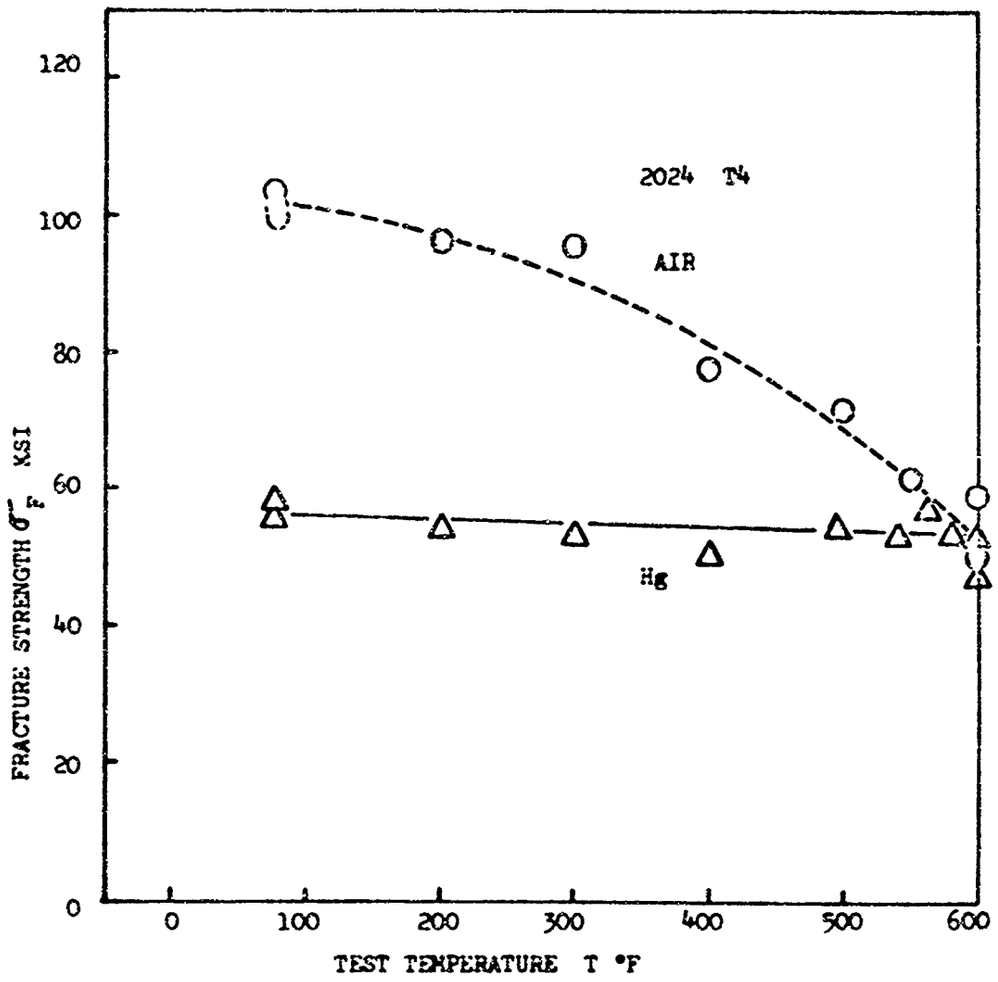

Fig. 35. FRACTURE STRENGTH σ_F AS A FUNCTION OF TEST TEMPERATURE
STRAIN RATE 30.2 in/in/min.

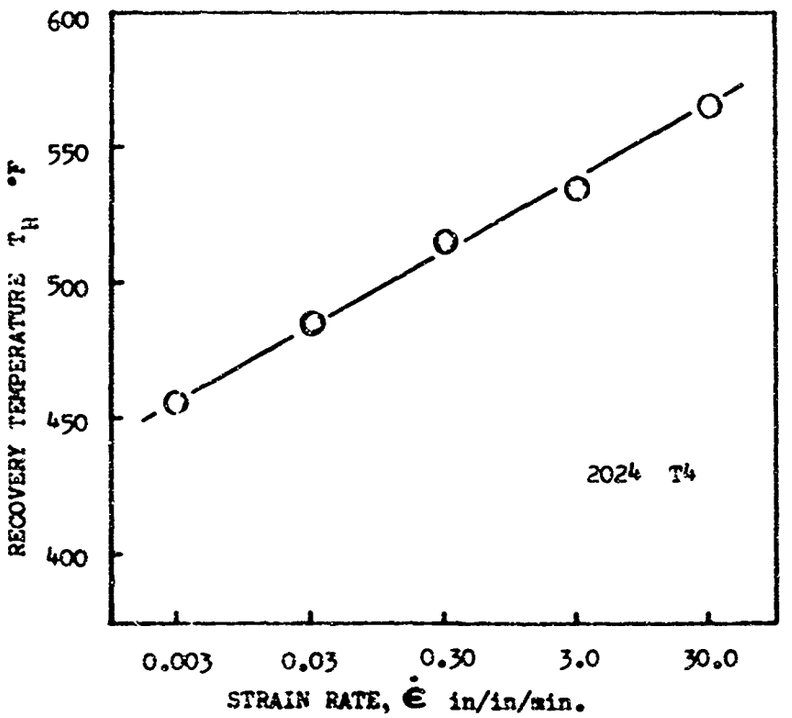

Fig. 36. RECOVERY TEMPERATURE T_R AS A FUNCTION OF STRAIN RATE

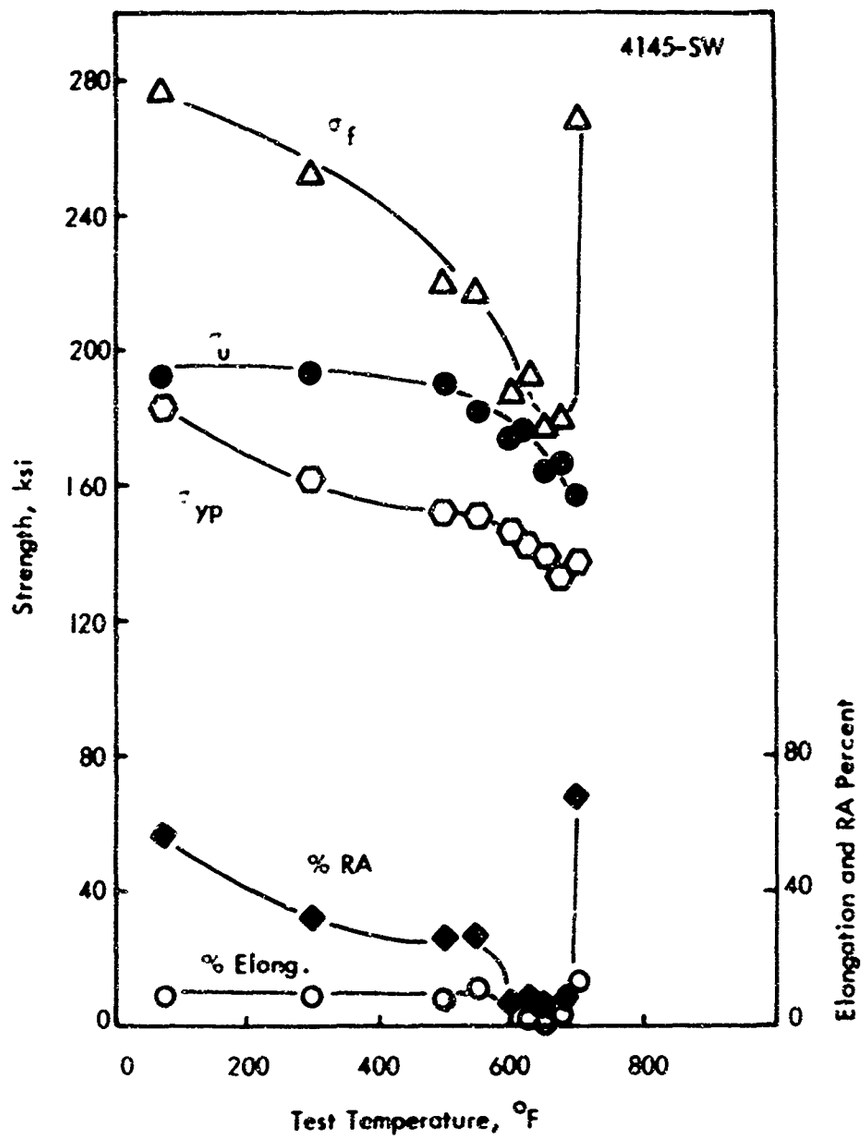

Fig. 37. Elevated Temperature Tensile Properties of 4145 Steel (non-leaded) at 200 ksi Nominal UTS, Surface Wetted with Pure Pb.

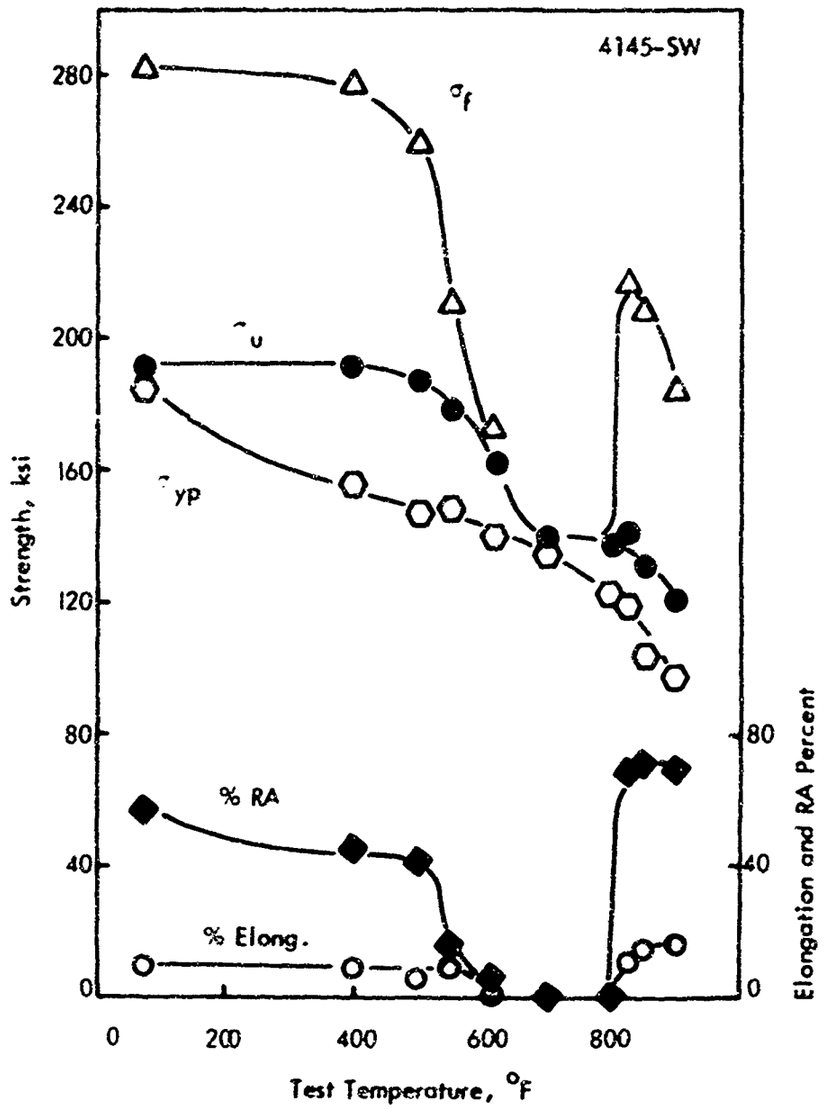

Fig. 38. Elevated Temperature Tensile Properties of 4145 Steel (non-leaded) at 200 ksi Nominal UTS, Surface Wetted with Pb-0.5% Zn Alloy.

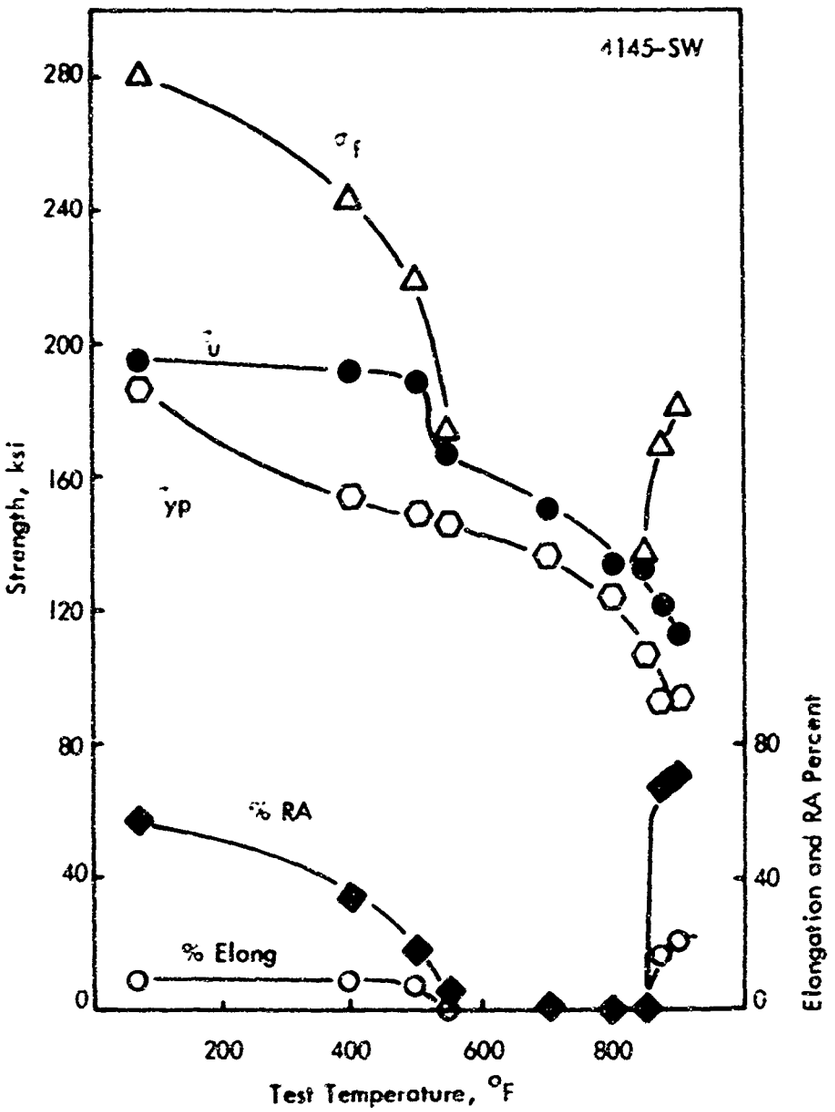

Fig. 34. Elevated Temperature Tensile Properties of 4145 Steel (non-leaded) at 200 ksi Nominal UTS, Surface Wetted with Pb-9% Sn Alloy.

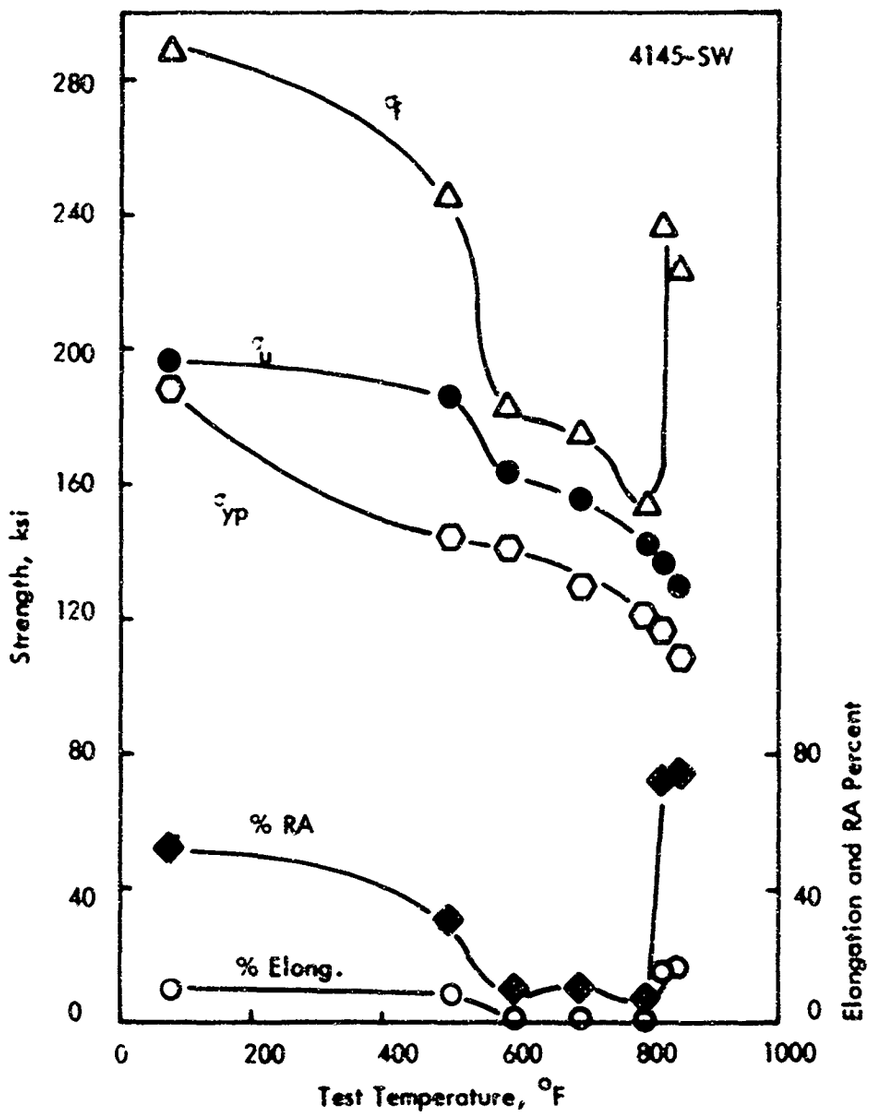

Fig. 40. Elevated Temperature Tensile Properties of 4145 Steel (non-leaded) at 200 ksi Nominal UTS, Surface Wetted With Pb-4% Sn Alloy.

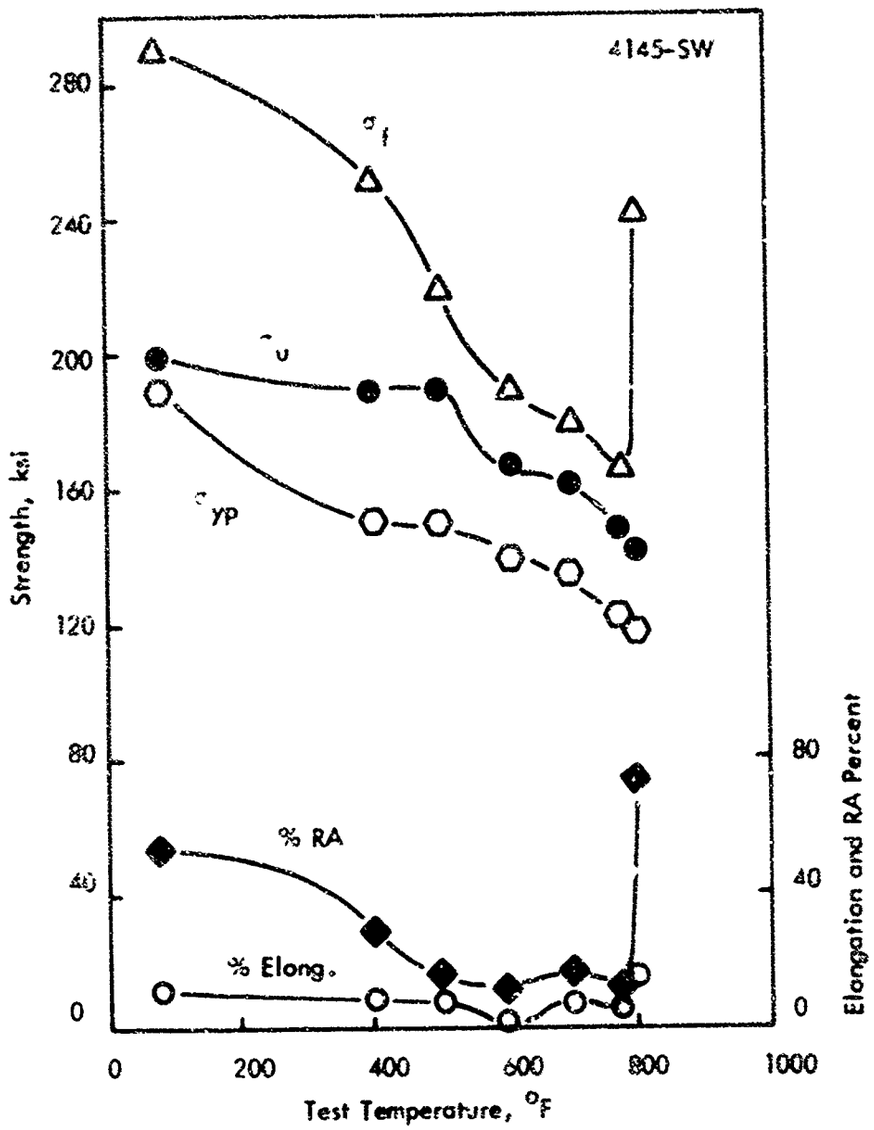

Fig. 41. Elevated Temperature Tensile Properties of 4145 Steel (non-leaded) at 200 ksi Nominal UTS, Surface Wetted with Pb-1% Sn Alloy.

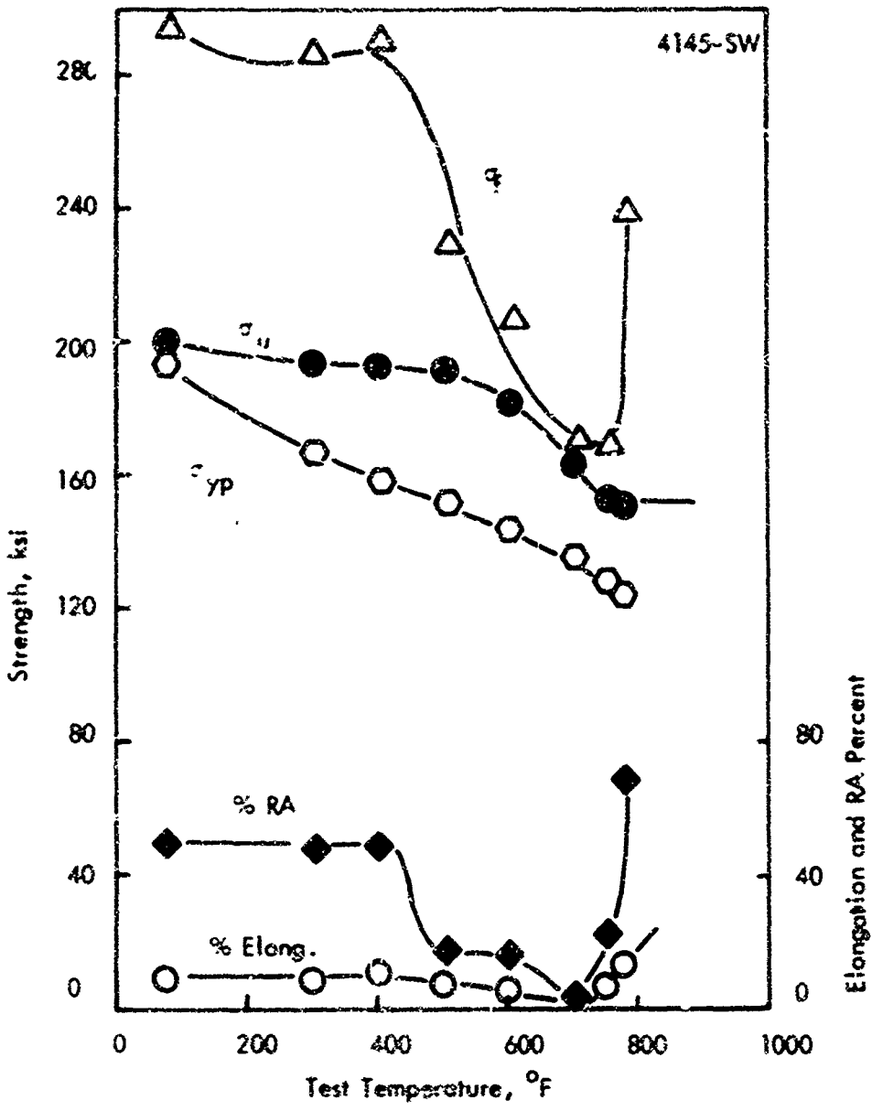

Fig. 42. Elevated Temperature Tensile Properties of 4145 Steel (non-leaded) at 200 ksi Nominal UTS, Surface Wetted with Pb-0.5% Sn Alloy.

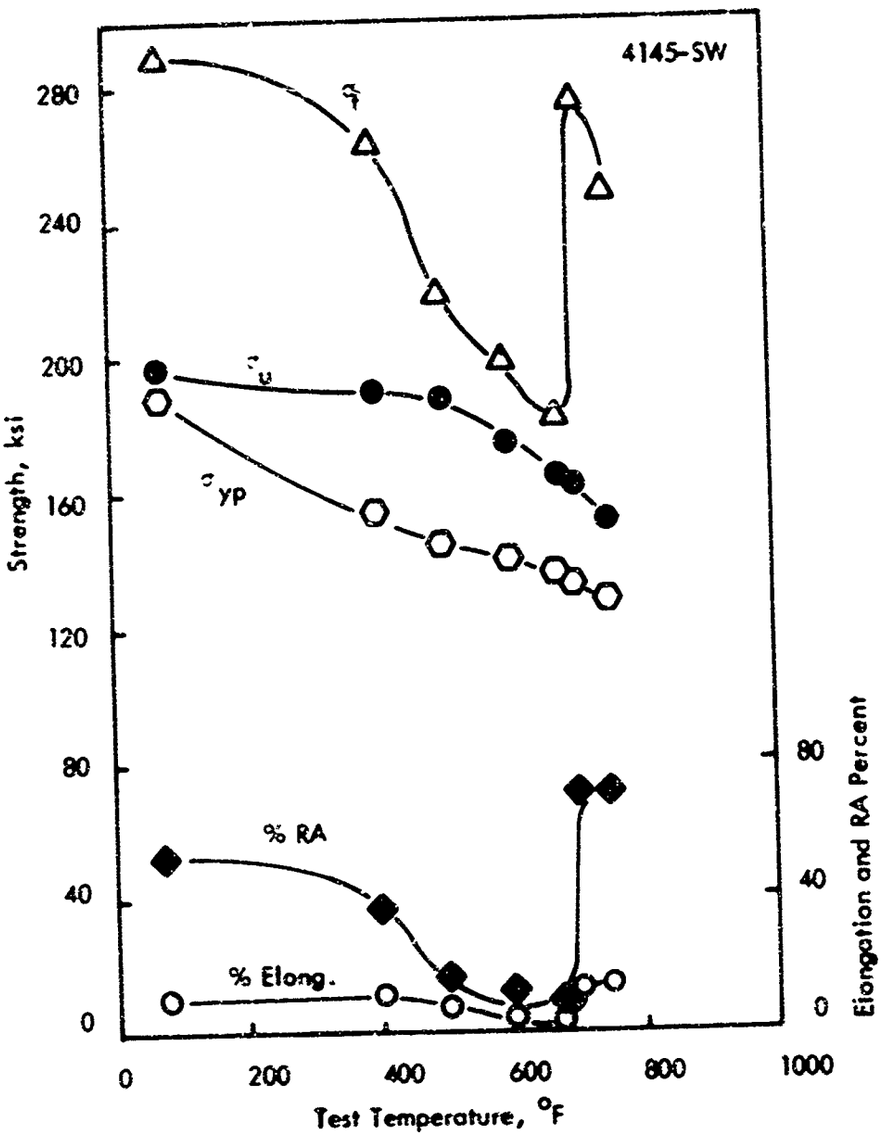

Fig. 43. Elevated Temperature Tensile Properties of 4145 Steel (non-leaded) at 200 ksi Nominal UTS, Surface Wetted with Pb-0.1% Sn Alloy

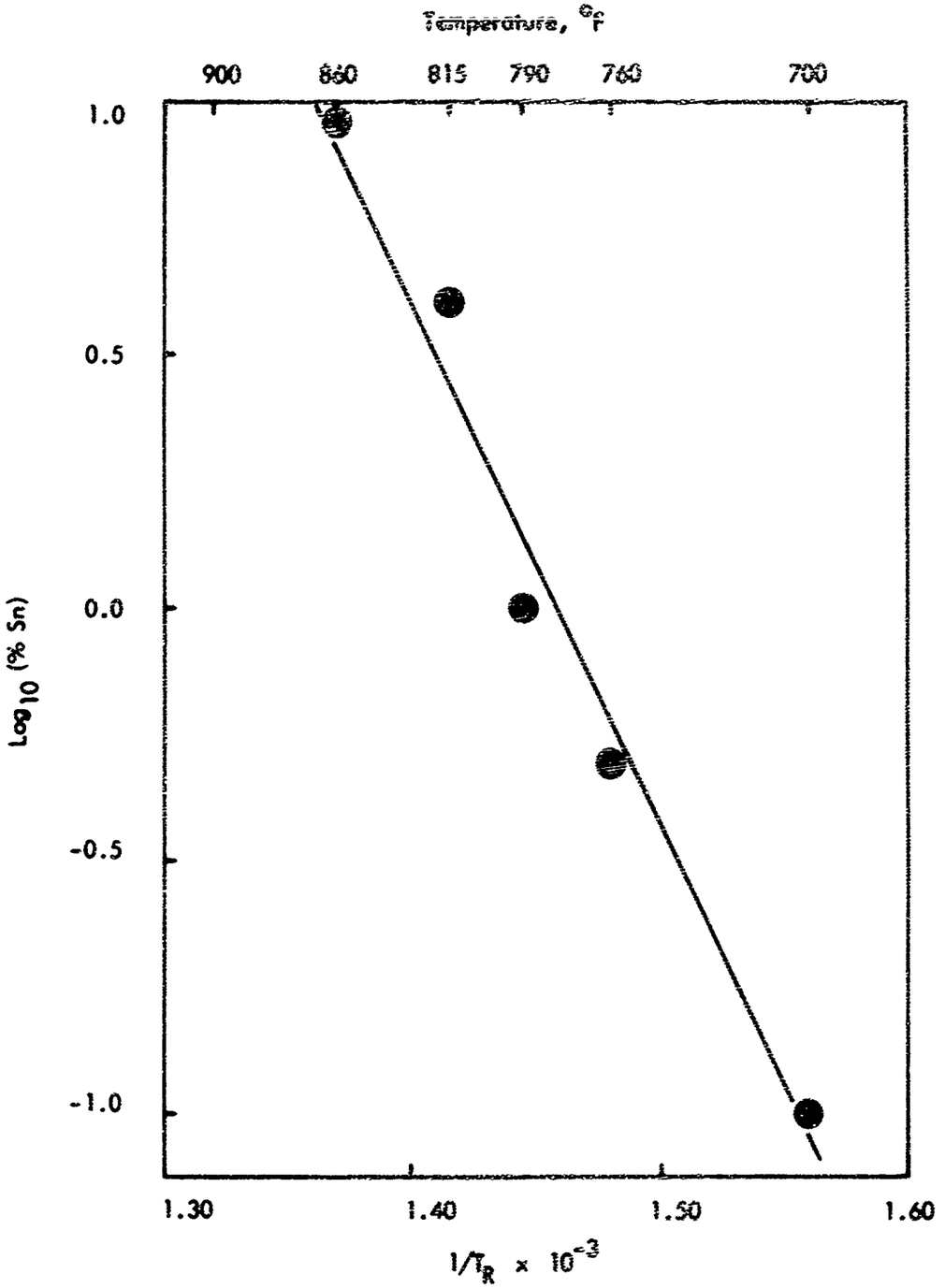

Fig. 44. Relationship Between Absolute Recovery Temperature and Percentage Sn for Pb-Sn Surface Wetted Alloys.

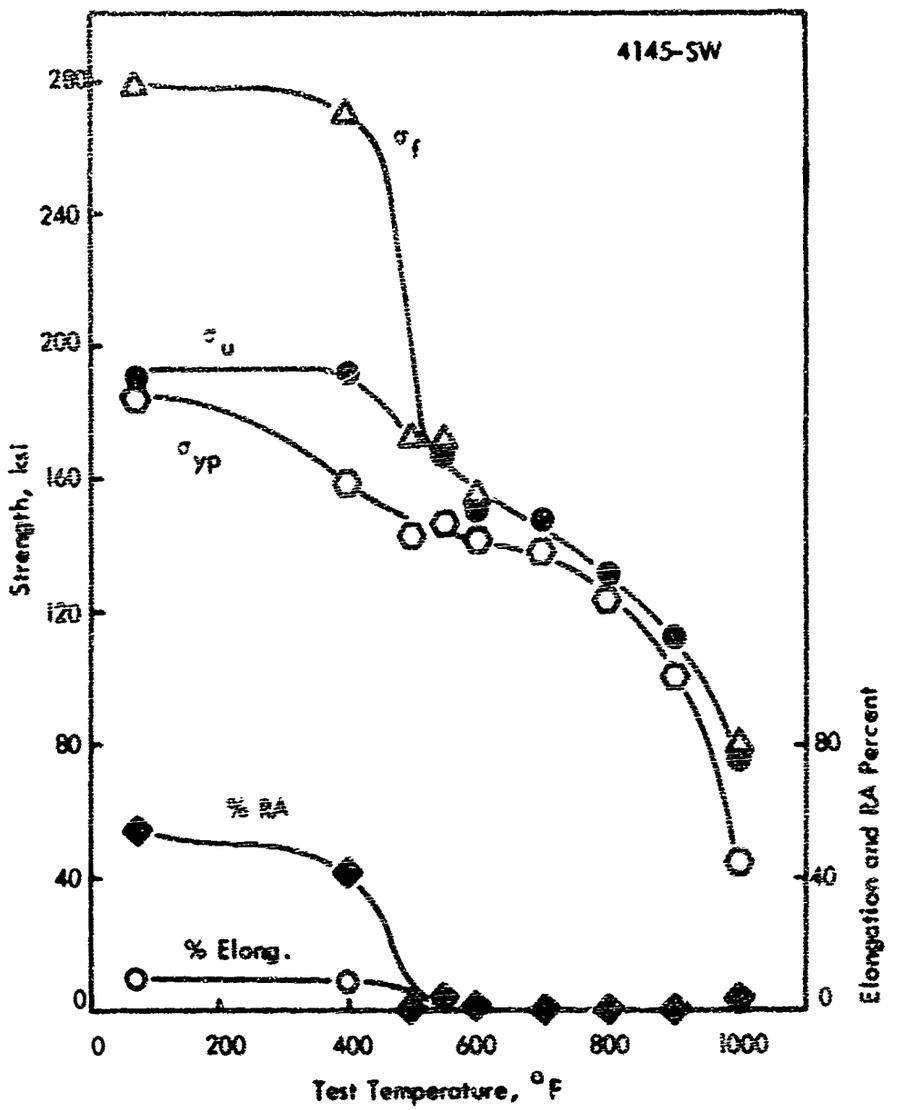

Fig. 45. Elevated Temperature Tensile Properties of 4145 Steel (non-leaded) at 200 ksi Nominal UTS, Surface Wetted with Pb-2% Sb Alloy.

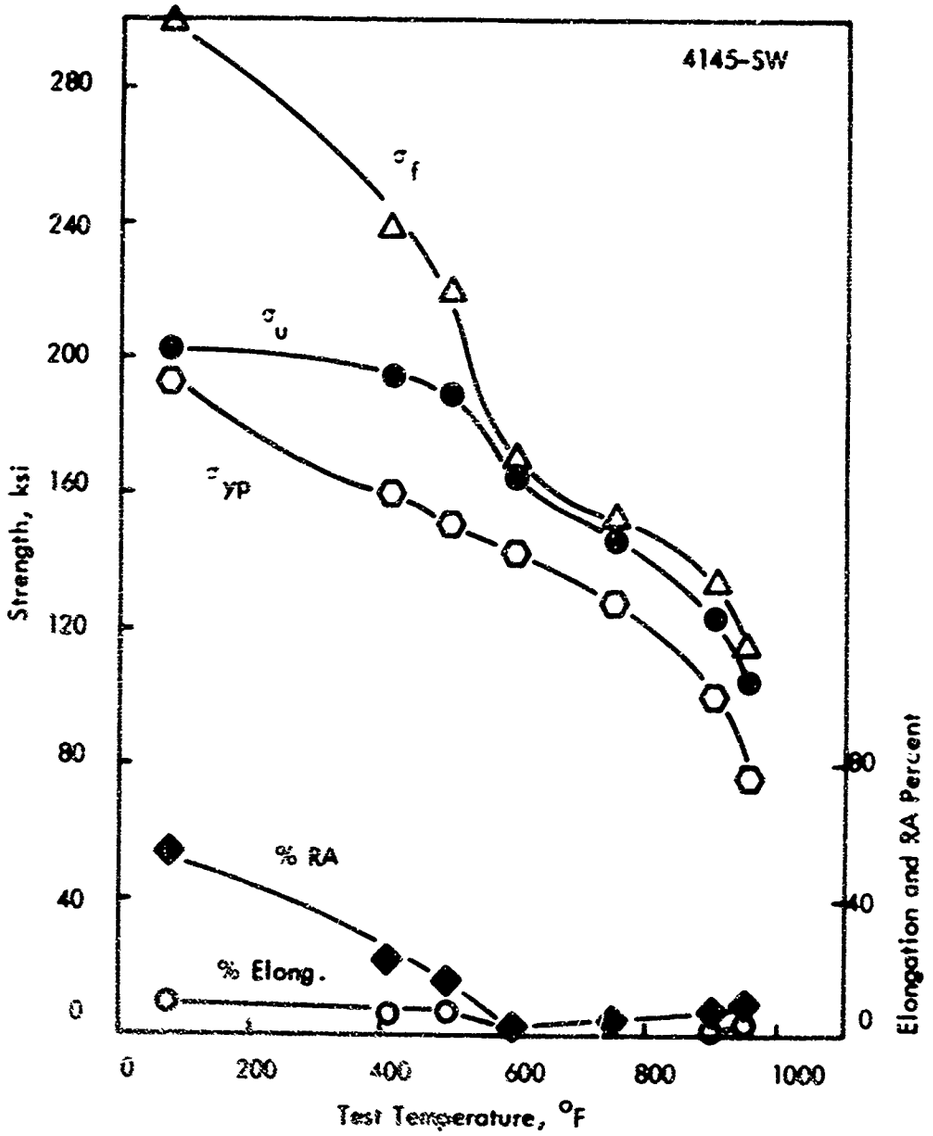

Fig. 46. Elevated Temperature Tensile Properties of 4145 Steel (non-leaded) at 200 ksi Nominal UTS, Surface Wetted with Pb-1% Sb Alloy.

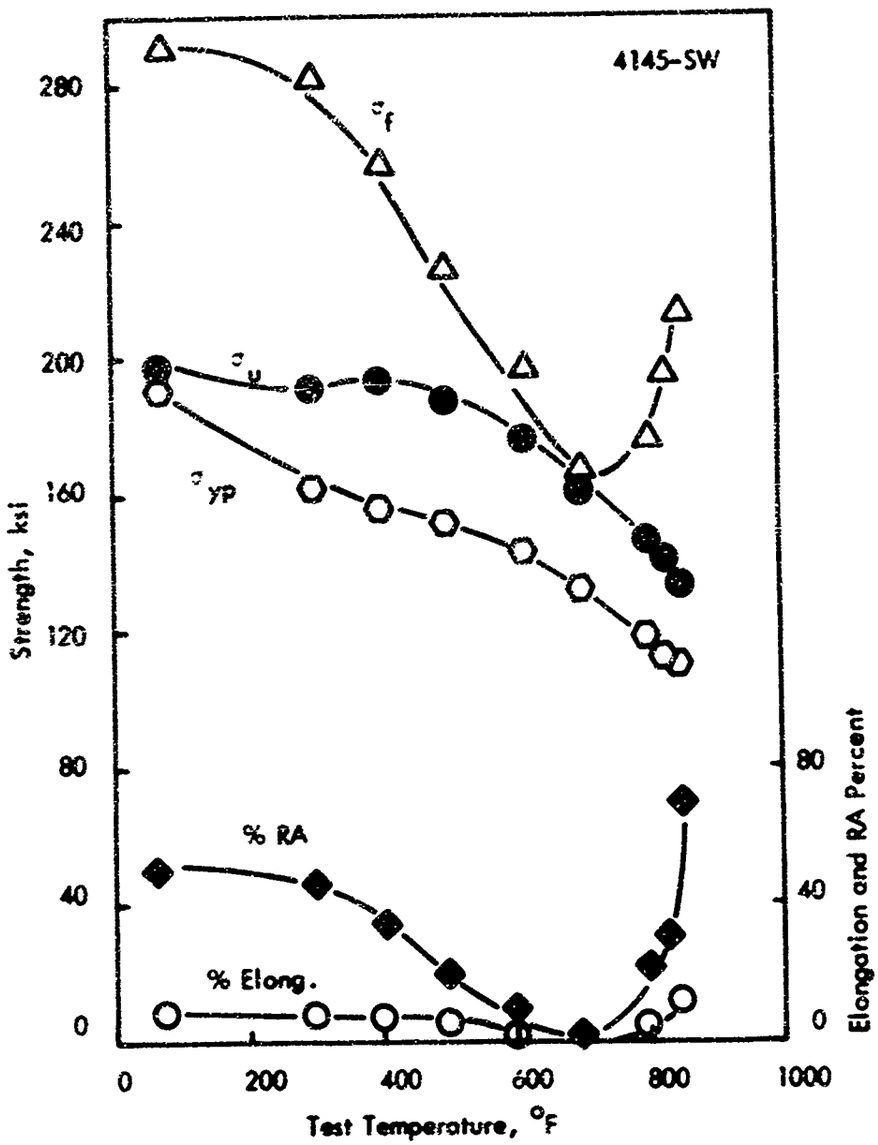

Fig. 47. Elevated Temperature Tensile Properties of 4145 Steel (non-leaded) at 200 ksi Nominal UTS, Surface Wetted with Pb-0.1% Sb Alloy.

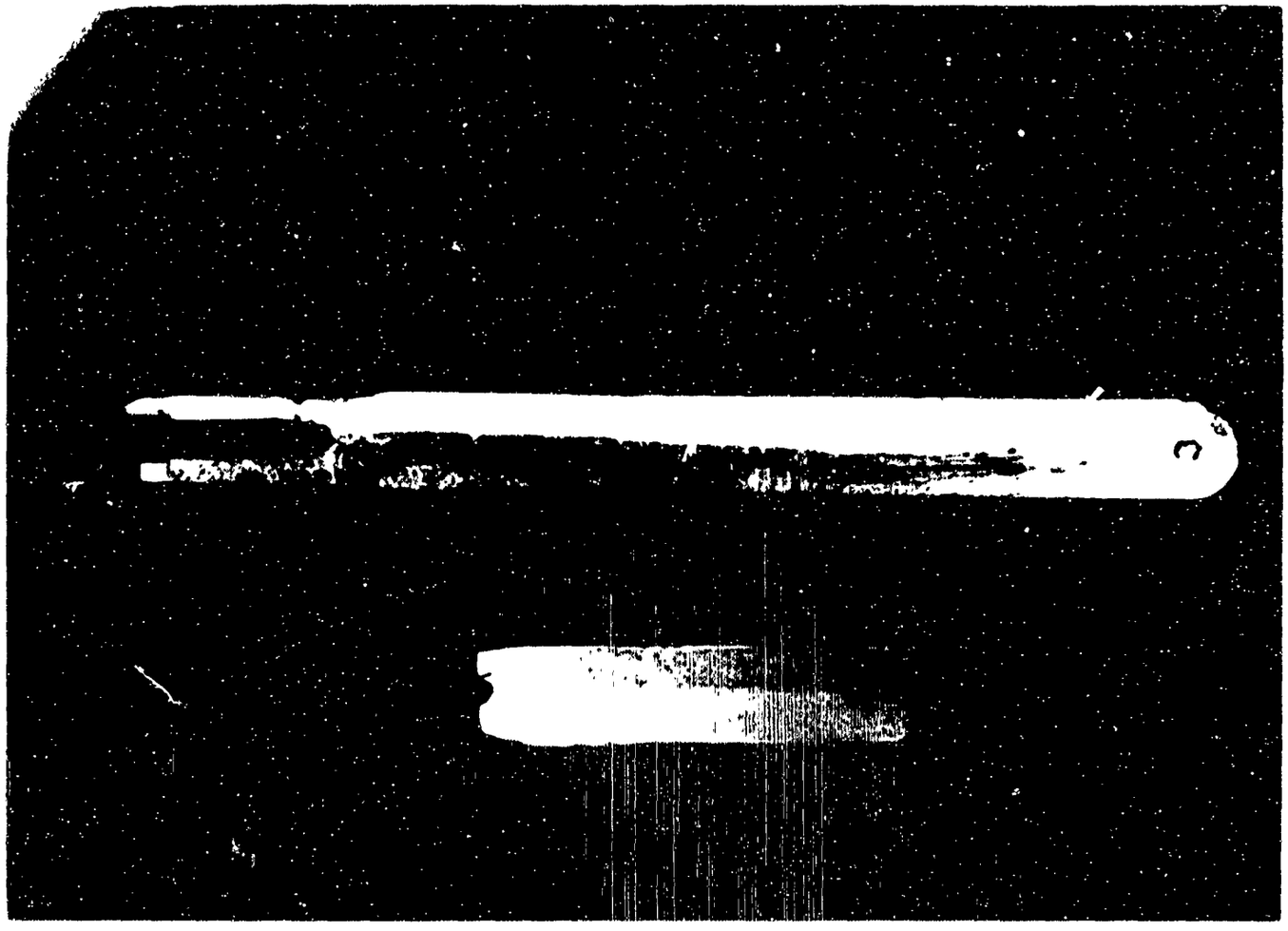

FIGURE 48

Aluminum Bicrystals Grown by Seeding (top) and Self-Nucleation (bottom). Growth Direction from Left to Right. Magnification 0.8 times.

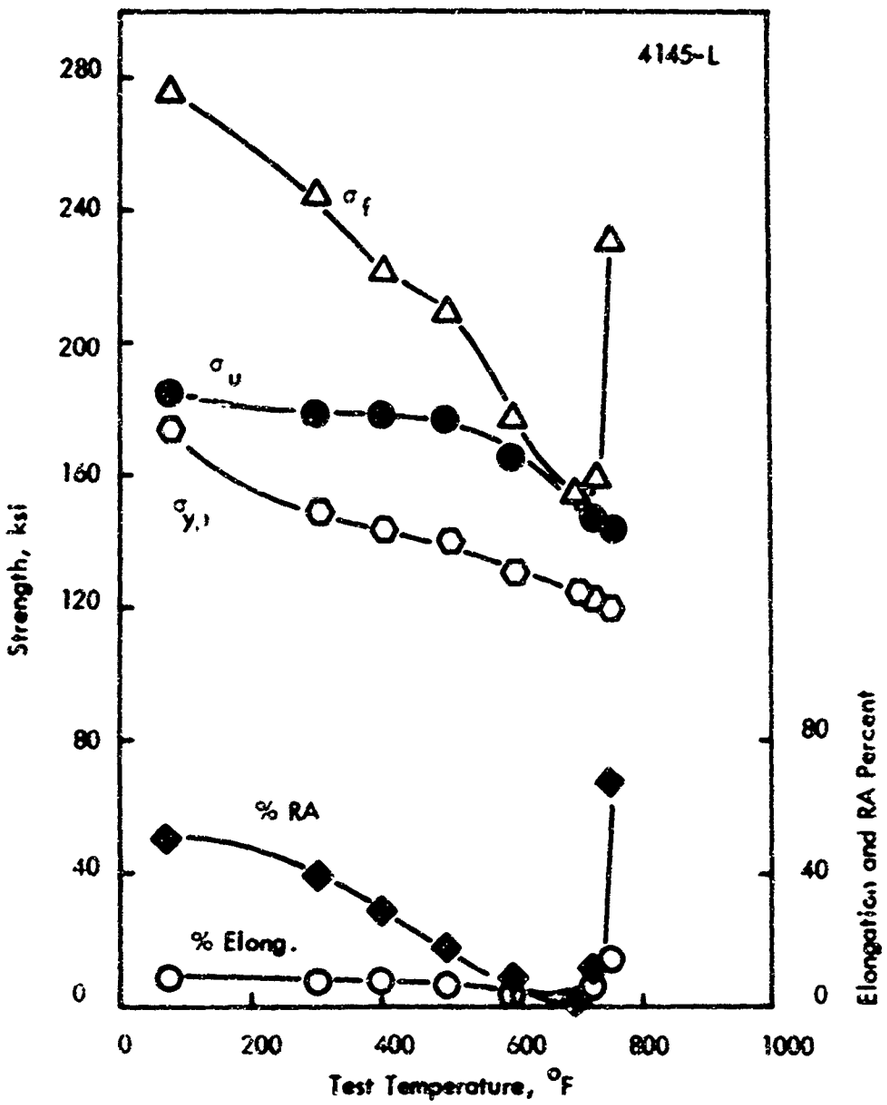

Fig. 49. Elevated Temperature Tensile Properties of Internally Leaded 4145 Steel Heat Treated to the Prior Deformation Strength Level (185 ksi) Used in the 10% Cold Working by Die Drawing Process.

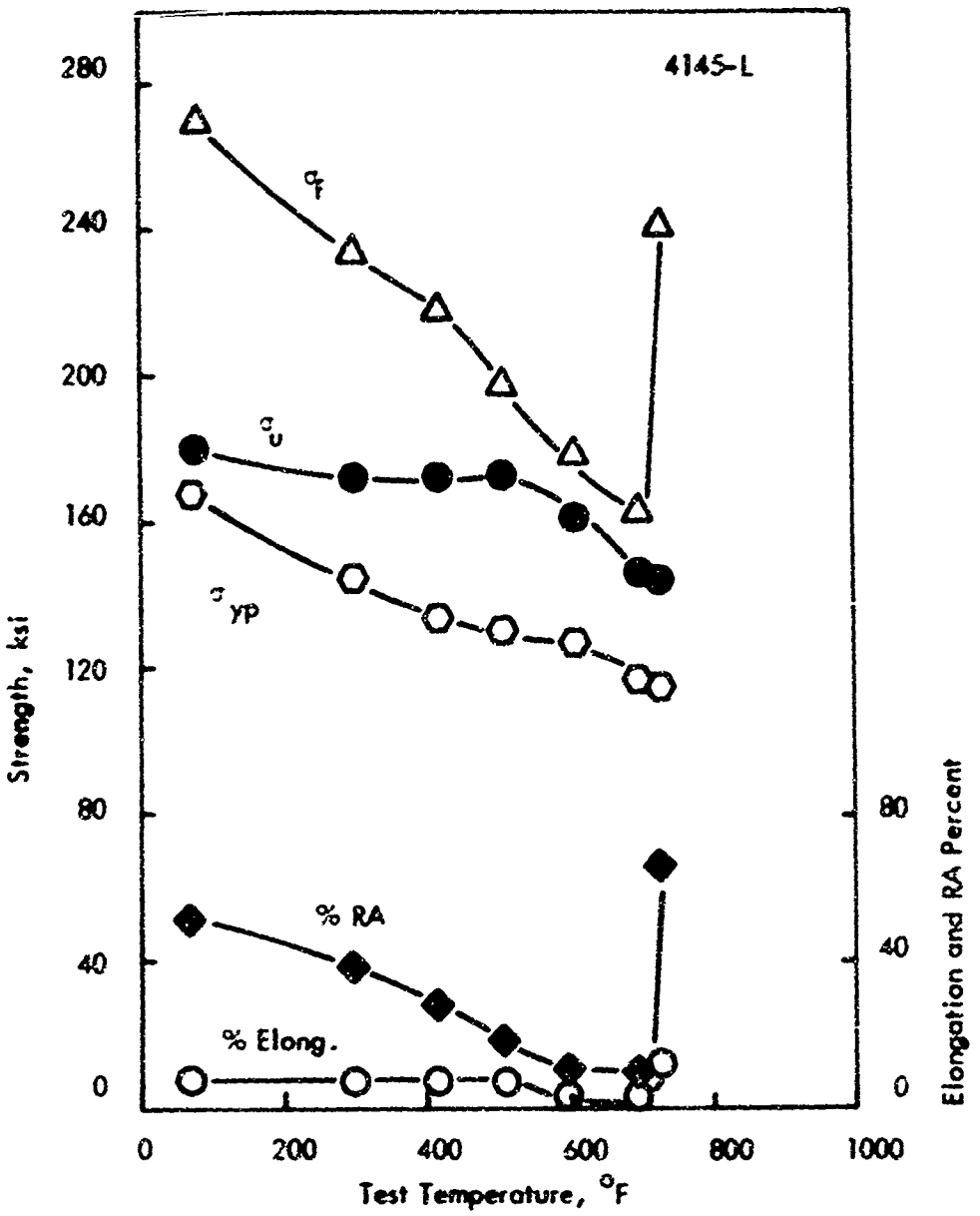

Fig. 50. Elevated Temperature Tensile Properties of Internally Leaded 4145 Steel Heat Treated to the Prior Deformation Strength Level (180 ksi) Used in the 20% Cold Working by Die Drawing Process.

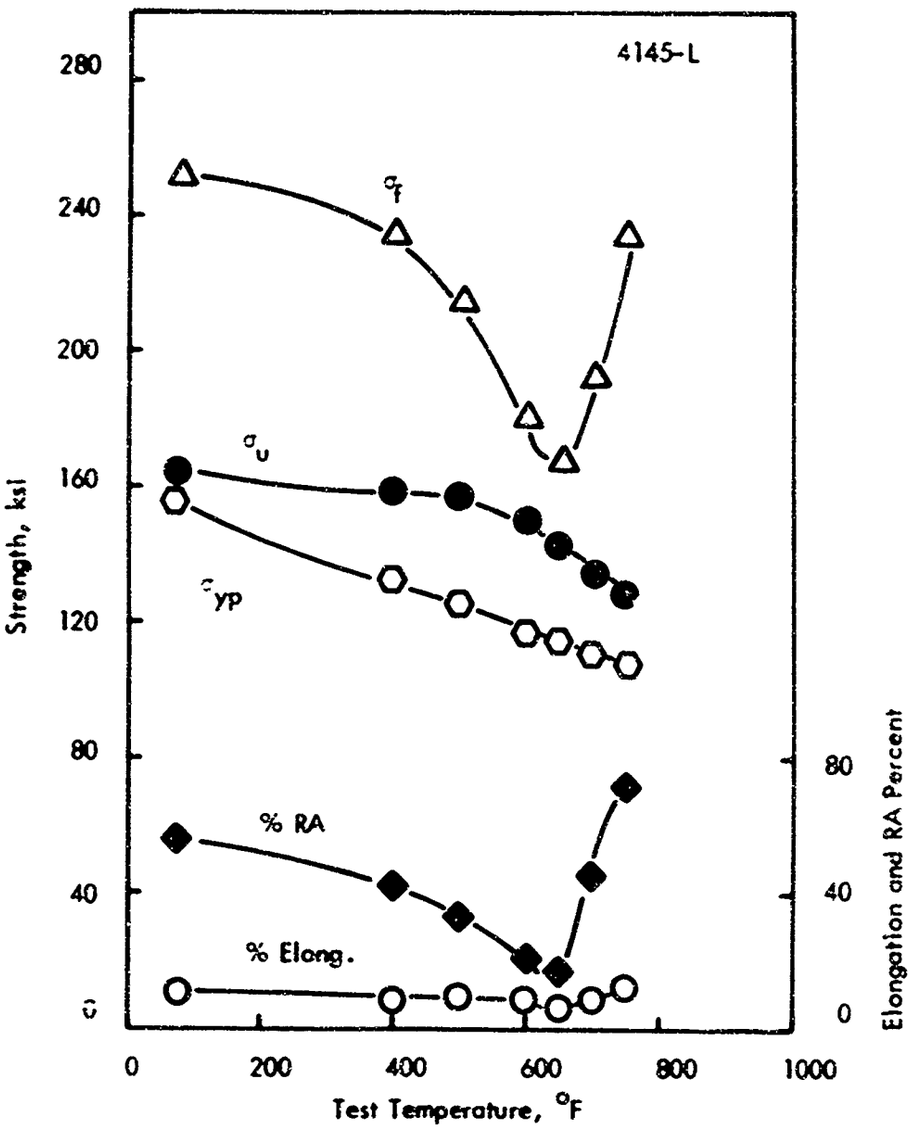

Fig. 51. Elevated Temperature Tensile Properties of Internally Leaded 4145 Steel Heat Treated to the Prior Deformation Strength Level (160 ksi) Used in the 30% Cold Working by Die Drawing Process.

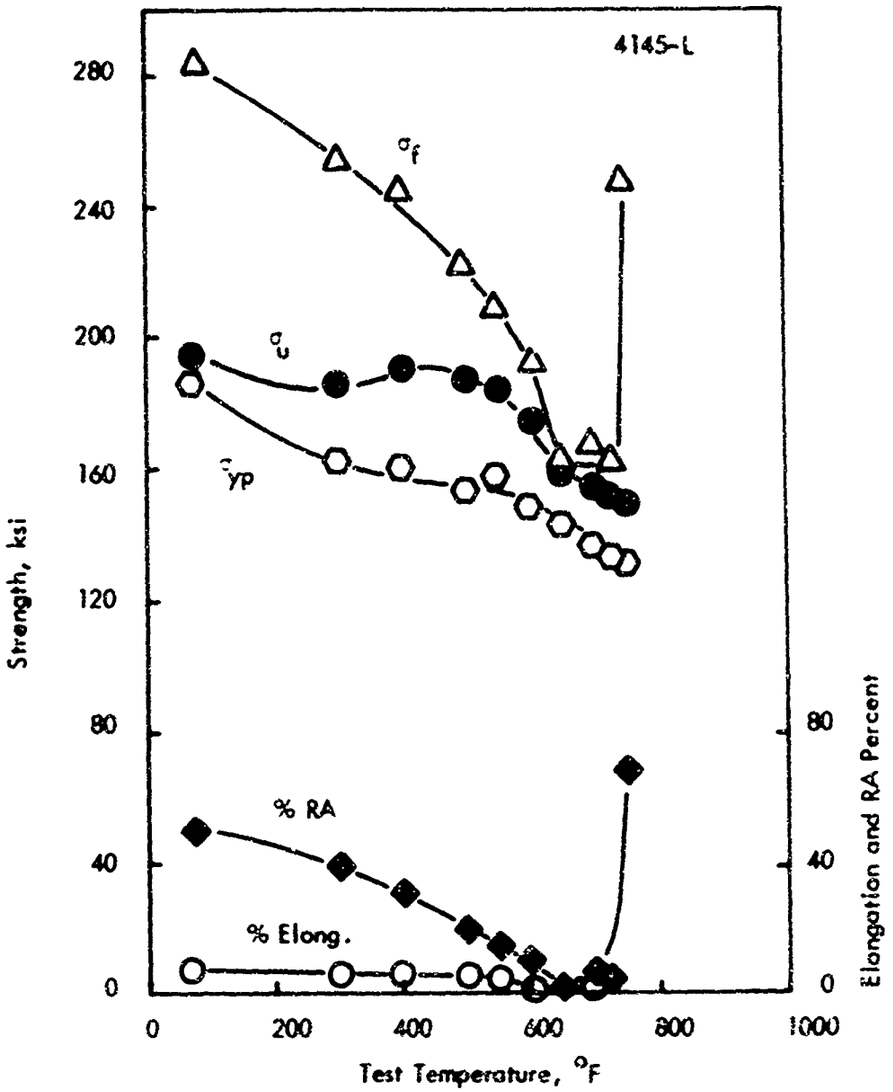

Fig. 52. Elevated Temperature Tensile Properties of Internally Leaded 4145 Steel Heat Treated to 200 ksi Nominal UTS.

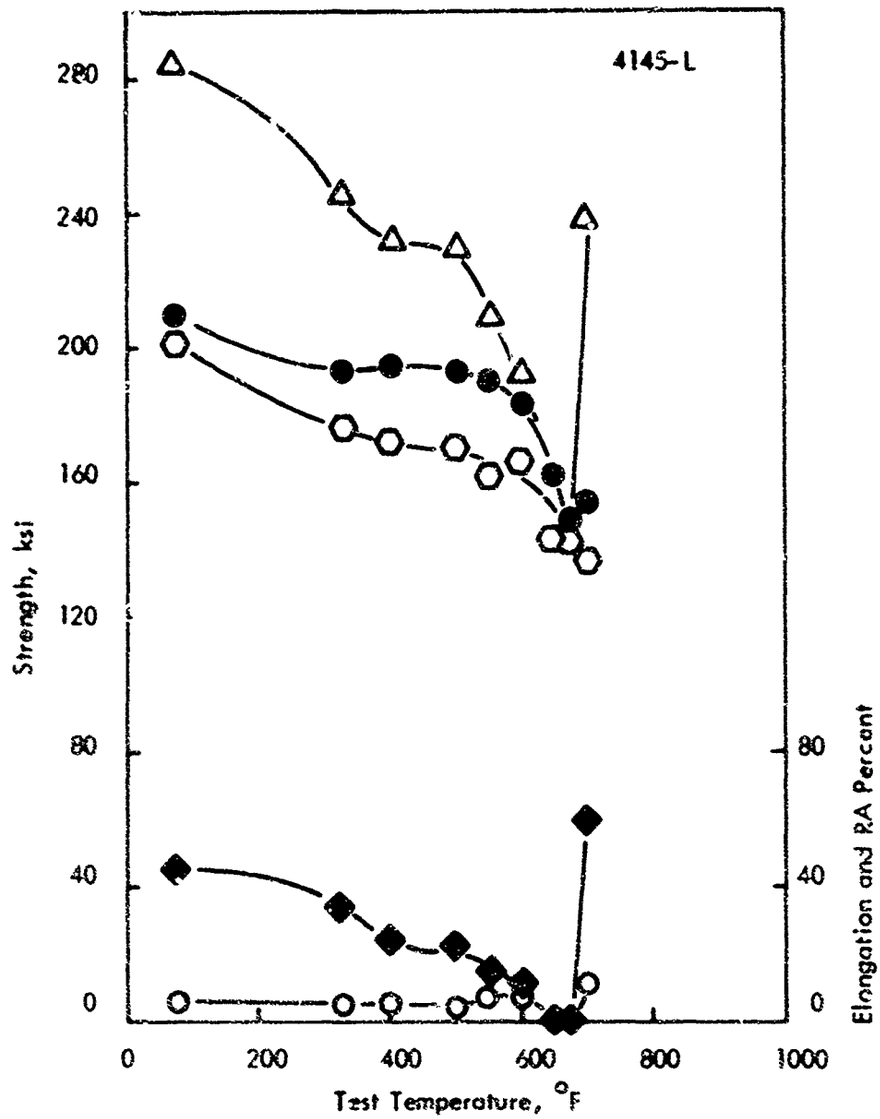

Fig. 53. Elevated Temperature Tensile Properties of Internally Leaded 4145 Steel Heat Treated and Cold Worked 10% by Die Drawing to Achieve 200 ksi Nominal UTS.

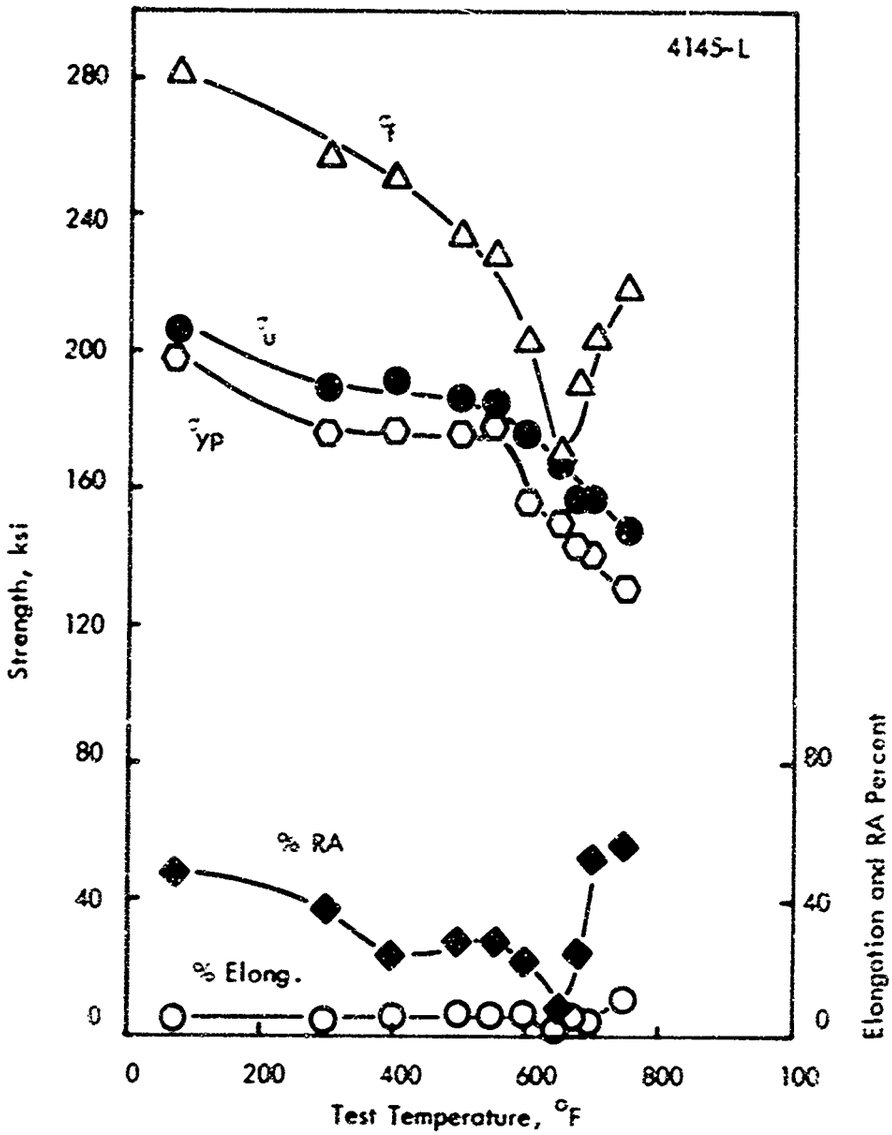

Fig. 54. Elevated Temperature Tensile Properties of Internally Leaded 4145 Steel Heat Treated and Cold Worked 20% by Die Drawing to Achieve 200 ksi Nominal UTS.

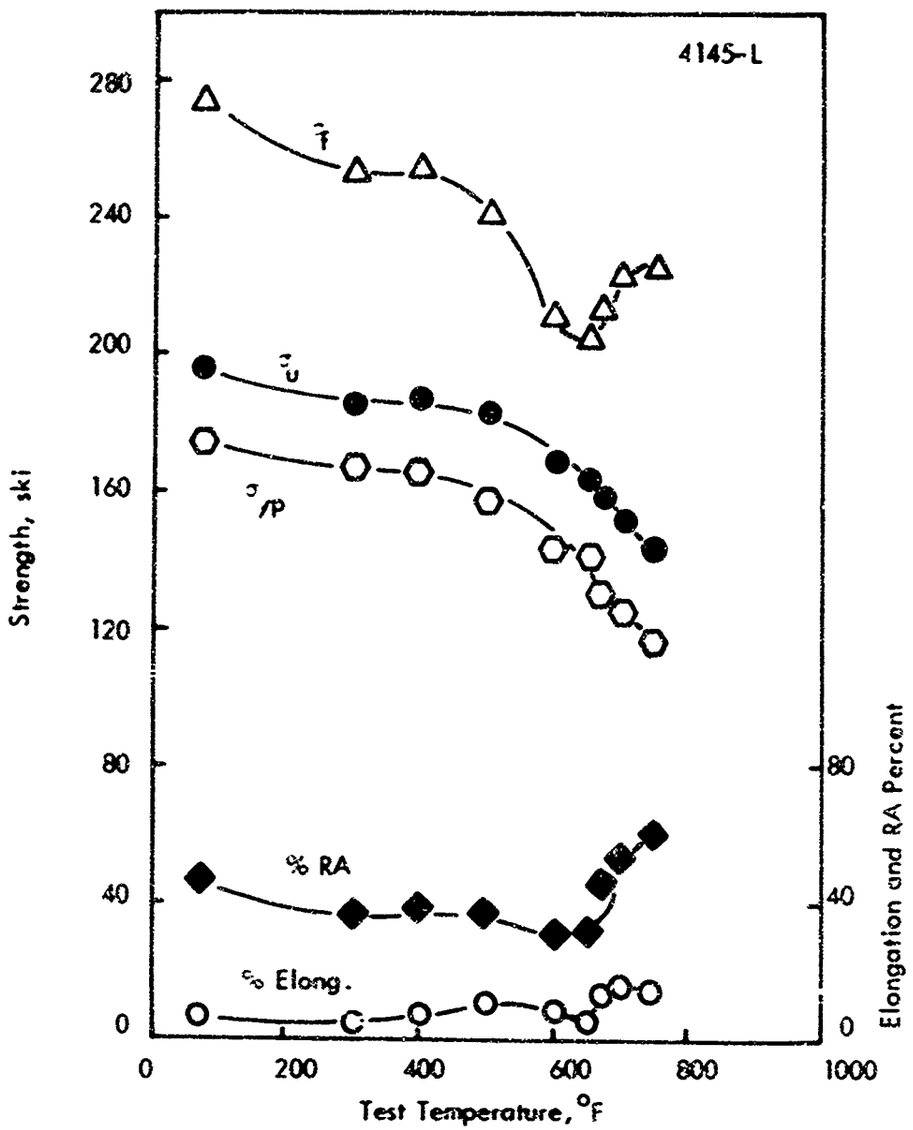

Fig. 55. Elevated Temperature Tensile Properties of Internally Leaded 4145 Steel Heat Treated and Cold Worked 30% by Die Drawing to Achieve 200 ksi Nominal UTS.

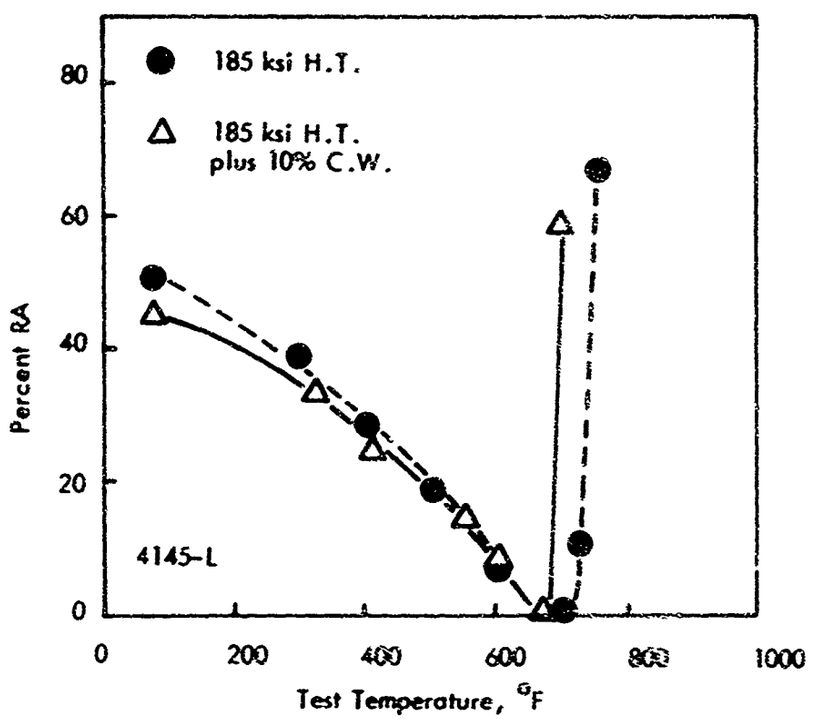

Fig. 56. Ductility Properties of Internally Leaded 4145 Steel Heat Treated and Cold Worked 10% by Die Drawing to Achieve a Final 200 ksi Nominal UTS, Compared with the Ductility Values of the Same Material Heat Treated to the Prior Deformation Strength Level.

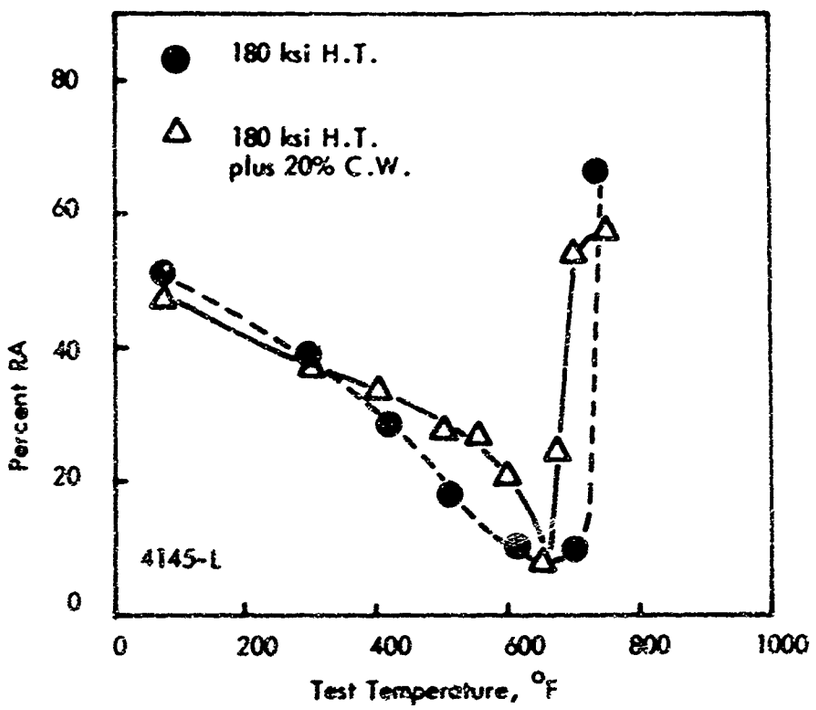

Fig. 57. Ductility Properties of Internally Leaded 4145 Steel Heat Treated and Cold Worked 20% by Die Drawing to Achieve a Final 200 ksi Nominal UTS, Compared with the Ductility Values of the Same Material Heat Treated to the Prior Deformation Strength Level.

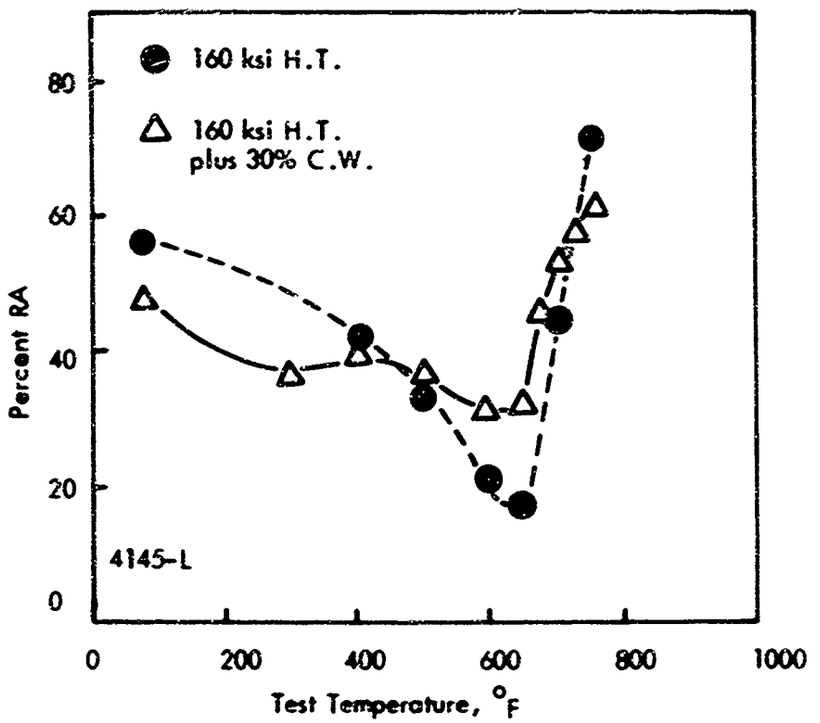

Fig. 58. Ductility Properties of Internally Leaded 4145 Steel Heat Treated and Cold Worked 30% by Die Drawing to Achieve a Final 200 ksi Nominal UTS Compared with the Ductility Values of the Same Material Heat Treated to the Prior Deformation Strength Level.

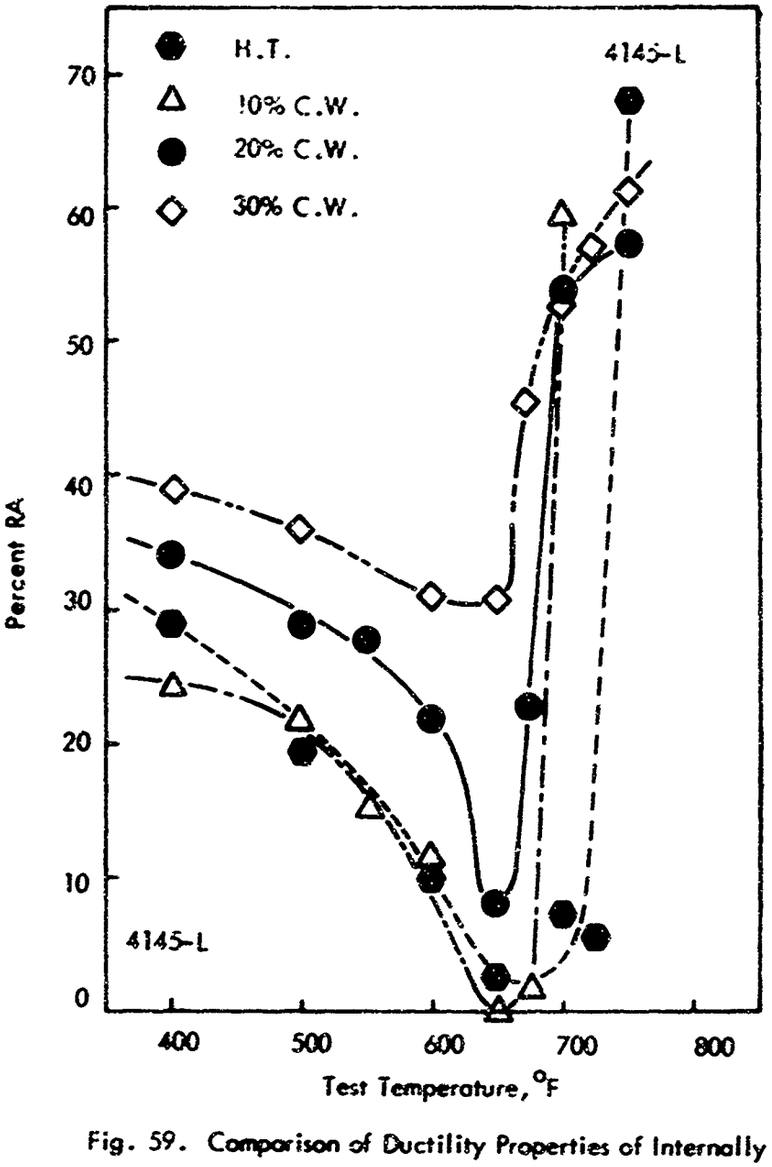

Fig. 59. Comparison of Ductility Properties of Internally Leaded 4145 Steel Processed to 200 ksi Nominal UTS by Heat Treatment Alone and Heat Treatment Plus 10, 20 and 30% Reductions by Die Drawing.

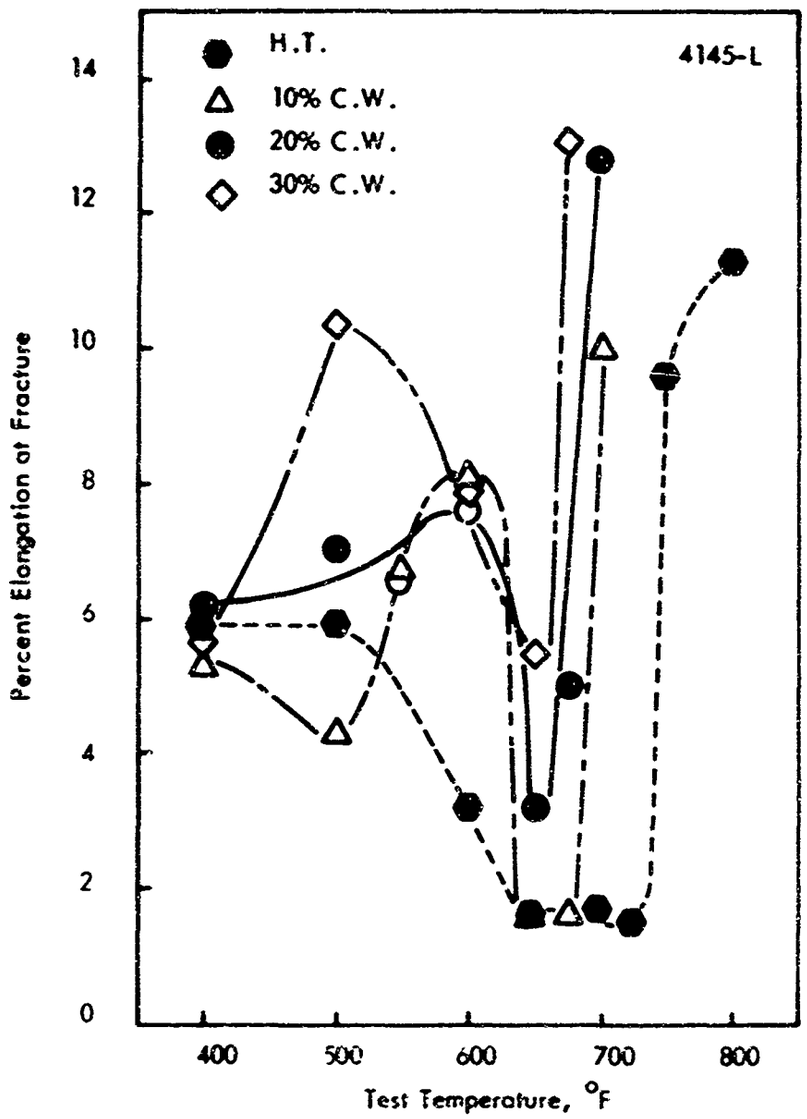

Fig. 50. Comparison of Ductility Properties of Internally Leaded 4145 Steel Processed to 200 ksi Nominal UTS by Heat Treatment Alone and Heat Treatment Plus 10, 20 and 30% Reductions by Die Drawing.

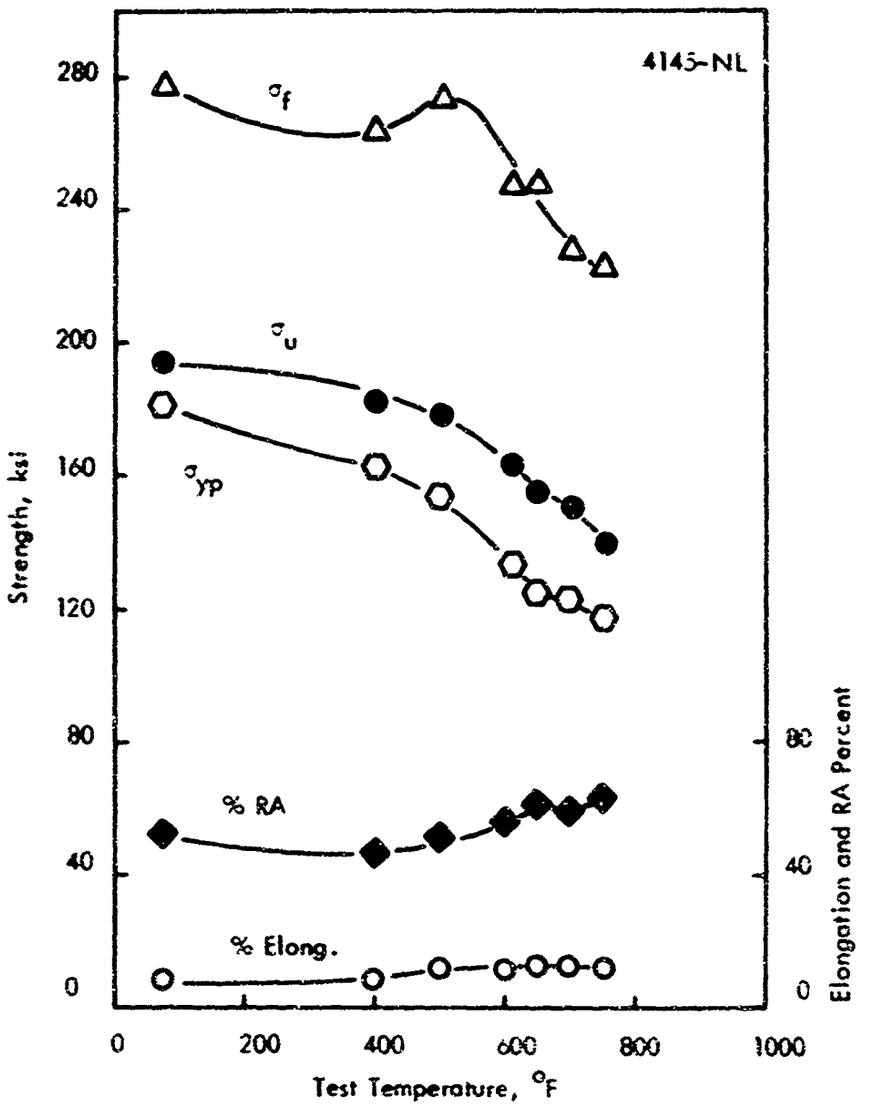

Fig. 61. Elevated Temperature Tensile Properties of Non-Leaded 4145 Steel Heat Treated and Cold Drawn 20% to Achieve 200 ksi Nominal UTS.

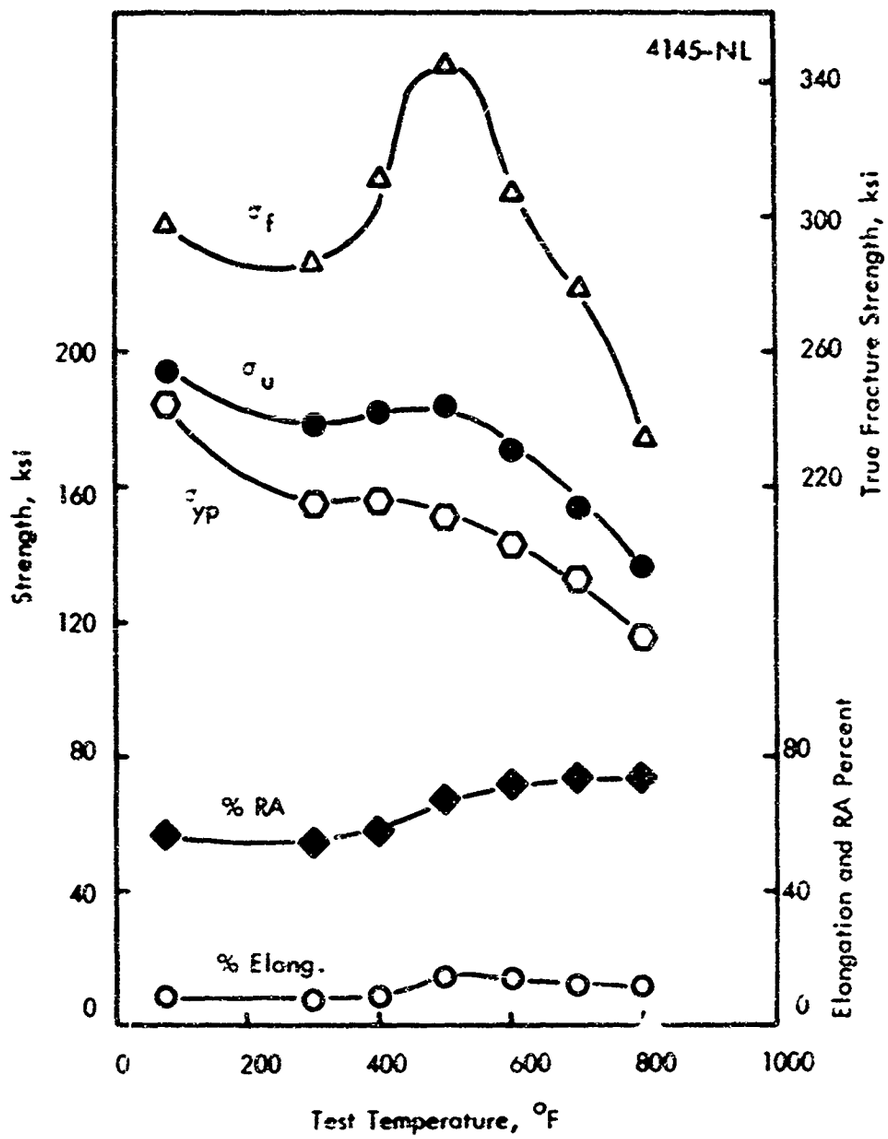

Fig. 2. Elevated Temperature Tensile Properties of Non-Leaded 4145 Steel Heat Treated to 200 ksi Nominal UTS.

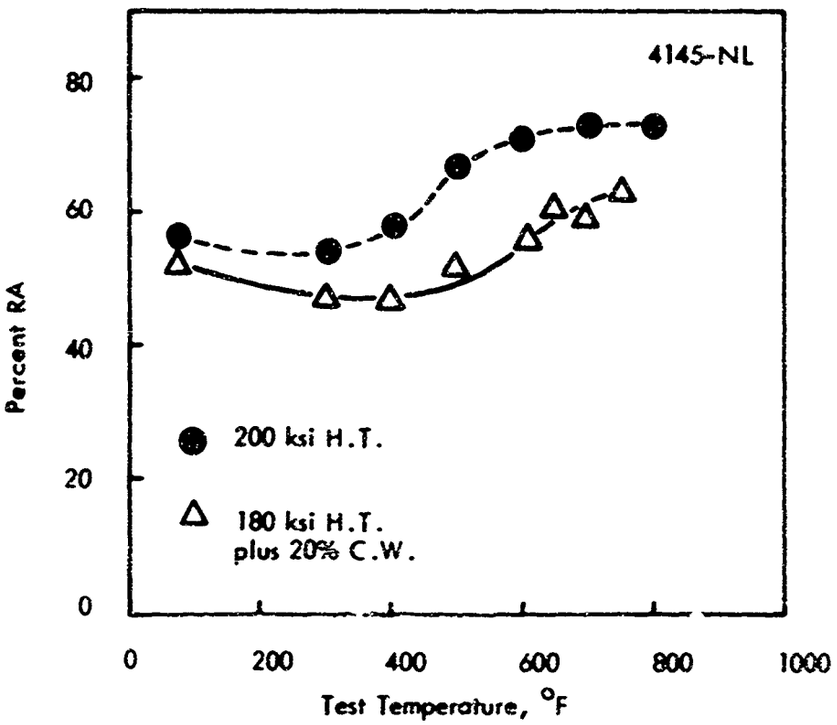

Fig. 63. Comparison of Ductility Properties of Non-Leaded 4145 Steel Processed to 200 ksi Nominal UTS by Heat Treatment Alone and by Heat Treatment Plus 20% Reduction by Die Drawing.

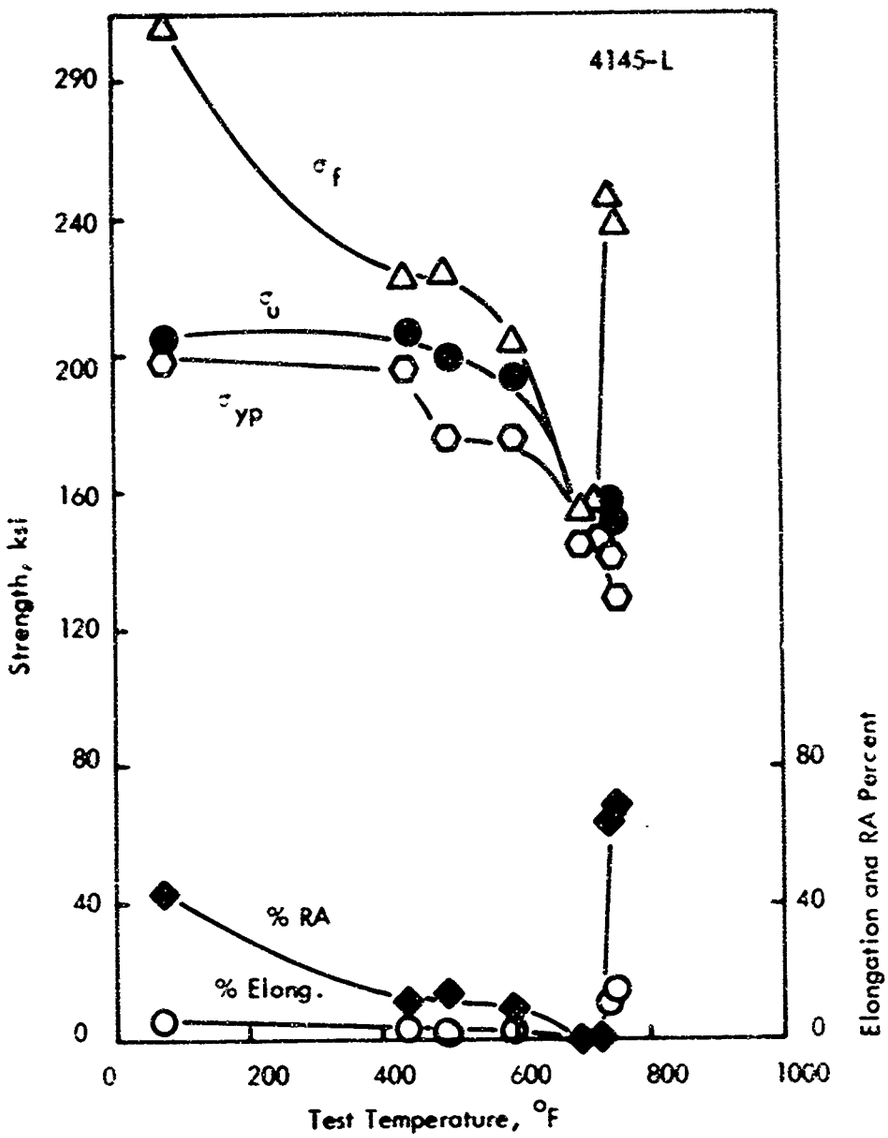

Fig. 64. Elevated Temperature Tensile Properties of Internally Leaded 4145 Steel Heat Treated to 200 ksi Nominal UTS and Prestretch to the UTS, at Room Temperature Prior to Testing.

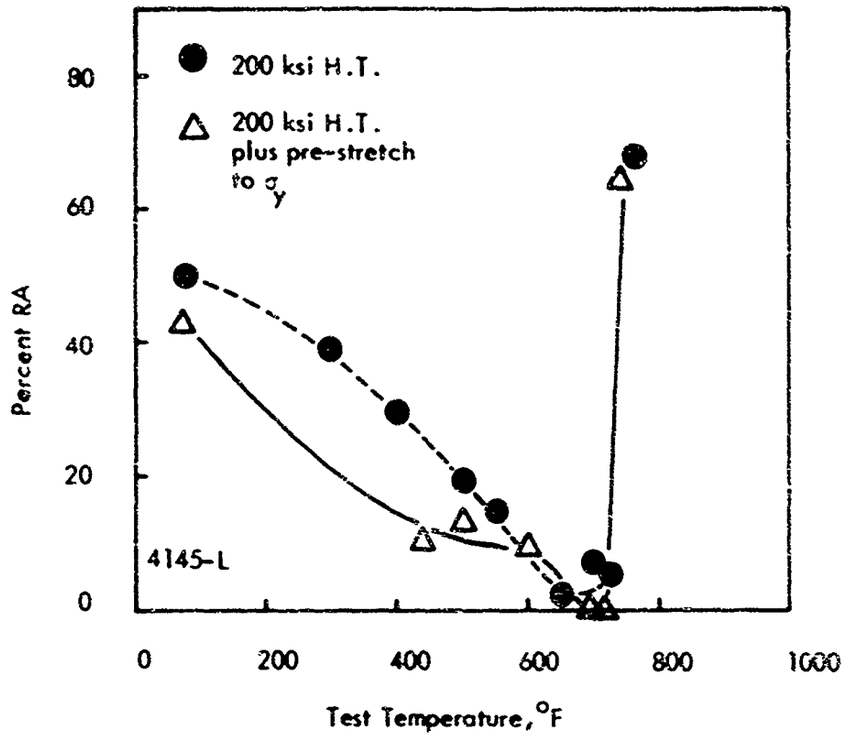

Fig. 65. The Effect of Pre-Stretching on Ductility Properties of Internally Leaded 4145 Steel at 200 ksi Nominal UTS.

REFERENCES

1. W. R. Warke, "The Effect of Composition and Test Conditions on Lead Embrittlement of Steel", Ph.D. thesis, IIT, 1969; also as W. R. Warke and N. N. Breyer, Tech. Rept. on Contract DA-20-113-AMC-10820(T). (AD-701047), 1969.

2. R. Zipp, W. R. Warke and N. N. Breyer, "A Comparison of Elevated Temperature Tensile Fracture in Non-Leaded and Leaded 4145 Steel". Electron Microfractography, ASTM, STP453 (1969), p. 111.

3. W. Rostoker, J. M. McCaughey and H. Markus, "Embrittlement by Liquid Metals", New York, 1960.

4. W. Barclay and F. N. Rhines, unpublished work, Carnegie Institute of Technology, reference in [1].

5. V. A. Labzin and V. I. Likhtman, "The Creep Laws of Single Crystals of Zinc in the Presence of a Surface Active Low-Melting Metallic Melt", Soviet Physics - Doklady, 4, 1959, p. 1282.

6. E.D. Shchukin, L. A. Kochanova and A. V. Pertsov, "The Temperature Transition from Brittleness to Plasticity Under Conditions of Strength-Reducing Absorption Effect". Soviet Physics - Crystallography, 8, 1963, p. 49.

7. M. H. Kamdar and A. P. C. Westwood, "Environment Sensitive Mechanical Behavior", Gordon and Breach, New York, 1966.

8. J. R. Low, Jr., D. F. Stein, A. M. Turkals and R. P. Laforce, "Alloy and Impurity Effects on Temper Brittleness of Steel", Trans. AIME, Vol. 242, (1968), p. 14.

9. C. J. McMahon, Jr., "Temper Brittleness - An Interpretive Review", Temper Embrittlement in Steel, ASTM, STP 407, (1968), p. 127.

10. J. Capus and G. Mayer, "The Influence of Trace Elements on Embrittlement Phenomena in Low Alloy Steels", Metallurgia 62, (1960), p. 133.

11. U. Q. Cabral, A. Hacke and A. Constant, "Mise en evidence de la fragilite de revenu par des essais de corrosion sous tension en presence d' hygrogene", Comptes Rendus, Academic des Sciences, Paris, Vol. 260, (1965), p. 6887.

12. W. Rostoker, J. M. McCaughey and H. Markus, "Embrittlement by Liquid Metals", 162 pp., Reinhold Publishing Corporation, New York, 1960.

13. A. R. C. Westwood, C. M. Preece and M. H. Kamdar, Tech. Rept. RIAS TR-67-8c (First Annual Report on Contract DA-001-AMC-1109(x), 1967; to be published in "Fracture-Engineering Fundamentals and Environmental Effects", (H. Liebowitz, ...), Academic Press, New York.

14. S. Mostovoy and N. N. Breyer, Trans. ASM, 61 (1968) 210.

15. W. R. Warke, Ph.D. Thesis, Illinois Institute of Technology, Chicago, 1969; also as, W. R. Warke and N. N. Breyer, Tech. Rept. on Contract DA-20-113-AMC-10820(T) (AD 701047), 1969, 140 pp.

16. Y. M. Potak and M. Shchlegakov, Zh. Tekhn. Fig., 25 (1955) 897.

17. H. Nichols and W. Rostoker, Trans. ASM, 56 (1963) 494.

18. L. Pauling, "The Nature of the Chemical Bond", 3rd Ed., p. 93, Cornell University Press, Ithaca, 1960.

19. E. T. Teatum, K. A. Gschneidner, Jr., and J. T. Waber, U. S. At. Energy Comm. LA-4003, 1968, 206 pp.

20. W. Rostoker, J. M. McCaughey and H. Markus, "Embrittlement by Liquic Metals", Reinhold, New York (1960), p. 67.

21. H. Nichols and W. Rostoker, "Influence of Thermal-Mechanical History on the Embrittlement of Aluminum Alloys by Mercury", Trans. AIME, 224, (1962), p. 1258.

22. H. Nichols and W. Rostoker, "Mercury Embrittlement of an Al-4-1/2 pct. Mg. Alloy", Trans. AIME, (1964), 251.

23. R. Rosenberg and I. Cadoff, "Fracture of Solids", Interscience, New York (1963).

24. J. V. Rinnovatore, J. D. Corrie and J. D. Meakin, "Effect of Cold Work Upon the Embrittlement of 70:30 Alpha-Brass in 2% Na Amalgam", Trans. ASM, 61 (1968), p. 321.

25. S. Mostovoy, "Embrittlement of Leaded Steel at Intermediate Temperature", Ph.D. Thesis, Ill. Inst. of Tech. (1968).

26. S. Mostovoy and N. N. Breyer, "The Effect of Lead on Micro-Crack Initiation and Propagation in Alloy Steels", Final Report Phase I, Part A, Contract No. DA-20-113-AMC-10820(T), Ill. Inst. of Tech. (1968).

27. S. Mostovoy and N. N. Breyer, "The Effect of Lead on the Mechanical Properties of 4145 Steel", Trans. ASM, 61 (1968) p. 219.

28. W. R. Warke, "The Effect of Composition and Test Conditions on Lead-Embrittlement of Steel", Ph.D. Thesis, Ill. Inst. of Tech., (1969).

Security Classification

DOCUMENT CONTROL DATA - R & D

Security classification of title, body of abstract and indexing annotation must be entered when the overall report is classified

1 ORIGINATING ACTIVITY (Corporate author) Illinois Institute of Technology 3300 South Federal Street Chicago, Illinois 60616	2a REPORT SECURITY CLASSIFICATION Unclassified 2b GROUP

3 REPORT TITLE

"ENVIRONMENTAL SENSITIVITY OF STRUCTURAL METALS: LIQUID METAL EMBRITTLEMENT"

4 DESCRIPTIVE NOTES (Type of report and inclusive dates)

First Annual Technical Progress Report, period covered: 25 June 1969 to 24 June 1970 .

5 AUTHOR(S) (First name, middle initial, last name)

Paul Gordon, Darryl L. Albright, Earl Zwicker, Norman N. Breyer, Lawrence J. Broutman, Russell D. Larsen, James W. Dally, William R. Warke

6 REPORT DATE	7a TOTAL NO OF PAGES	7b NO OF REFS
July 1970	118	28

8a CONTRACT OR GRANT NO	9a ORIGINATOR'S REPORT NUMBER(S)
DAAA-25-69-C0608 b PROJECT NO	55232 - 1ATPR
c	9b OTHER REPORT NO(S) (Any other numbers that may be assigned this report)

10 DISTRIBUTION STATEMENT

This publication or any portion thereof may not be reproduced without specific authorization from the Commanding Officer, Frankford Arsenal, ATTN: Chief Metallurgy Research Laboratory, Philadelphia, Pennsylvania 19137. However, DDC is authorized to reproduce the publication for

11 SUPPLEMENTARY NOTES	12 SPONSORING MILITARY ACTIVITY
	U. S. Army, Frankford Arsenal Tacony and Bridge Streets Philadelphia, Pennsylvania 19137

13 ABSTRACT

This is the first annual technical progress report on a research program on liquid metal embrittlement (LME). The phenomenon of LME is being investigated on levels from the atomic through bulk specimen and structural properties, and is being considered from both experimental and theoretical viewpoints. The research is aimed at elucidating the three important aspects of LME, namely, the mechanism by which embrittlement takes place at a crack, or potential crack, site, the mechanism by which the embrittling species is transported to this site, and the various metallurgical, physical, and mechanical factors which have a significant influence on the severity of the embrittlement.

Eleven specific investigations are underway in various stages of progress, with the first two topics aimed primarily at an understanding of the transport mechanism in LME, the second five at the embrittlement mechanism, and the next three at mechanical and metallurgical factors influencing the embrittlement. The last topic is an effort at a new theoretical approach to LME.

10 Distribution Statement (cont')

U. S. Government purposes. The information in this publication has not been cleared for release to the public. DDC AVAILABILITY NOTICE Qualified requestors may obtain copies of this publication directly from DDC. Foreign announcement and dissemination of this publication by DDC is limited.

DD FORM 1473

Security Classification

Security Classification

14 KEY WORDS	LINK A		LINK B		LINK C	
	ROLE	WT	ROLE	WT	ROLE	WT

DD FORM 1473

Security Classification